

# **UNIVERSITÄTSKLINIKUM HAMBURG-EPPENDORF**

ZMNH, Institut für Molekulare und Zelluläre Kognition

Prof. Dr. Dietmar Kuhl

## **The role of CLN3 in the lysosomal-autophagosomal system**

### **Dissertation**

zur Erlangung des Doktorgrades PhD  
an der Medizinischen Fakultät der Universität Hamburg.

vorgelegt von:

Daniela Wünkhaus (geb. Borchert),  
geboren in Oldenburg

Hamburg 2021

**Angenommen von der  
Medizinischen Fakultät der Universität Hamburg am: 21.12.2021**

**Tag der Disputation: 04.04.2022**

**Veröffentlicht mit Genehmigung der  
Medizinischen Fakultät der Universität Hamburg.**

**Prüfungsausschuss, der/die Vorsitzende: PD Dr. Guido Hermey**

**Prüfungsausschuss, zweite/r Gutachter/in: Prof. Dr. Med. Manuel Friese**

# Table of contents

1. Introduction.....	5
1.1 Lysosomes.....	5
1.1.1 Lysosomal biogenesis.....	6
1.1.2 Lysosomal distribution, fusion and contact sites .....	7
1.1.3 Lysosomes as metabolic signaling centers .....	8
1.1.4 Lysosomal Ca <sup>2+</sup> signaling.....	11
1.2 Autophagy .....	12
1.3 Lysosomal storage diseases.....	15
1.3.1 Neuronal Ceroid Lipofuscinosis.....	15
1.3.2 Juvenile neuronal ceroid lipofuscinosis.....	16
1.4 Aim of the study.....	19
2. Material and Methods .....	20
2.1 Generation and cultivation of cells .....	20
2.1.1 Cultivation of HeLa cells .....	20
2.1.2 Generation and cultivation of ARPE-19 CLN3-KO cells.....	20
2.1.3 Generation, cultivation and quality control experiments of iPSC derived RPE cells.....	21
2.2 High-content confocal imaging with OPERA Phenix.....	23
2.2.1 Transfection and imaging of LC3-GFP-mCherry construct.....	23
2.2.2 DQ-BSA and Cathepsin B – Magic Red Assay .....	24
2.2.3 Immunocytochemistry, colocalization and live cell imaging.....	24
2.2.4 TFEB knockdown using siRNAs .....	26
2.3 Electron microscopy .....	26
2.4 Immunoblotting.....	27
2.5 BMP/LBP analysis using mass spectrometry .....	28
2.6 mRNA expression analysis .....	29
2.7 Lysosomal exocytosis .....	30
2.8 Lysosomal patch clamp analysis.....	31
2.9 Compound treatments.....	31
3. Results .....	33
3.1 CLN3 deficient cell lines to study the role of the CLN3 protein .....	33
3.1.1 Generation of ARPE-19 CLN3-KO cell line .....	34
3.1.2 Differentiation of iPS cells to RPE cells .....	35
3.2 Phenotypic characterization of CLN3 deficient cells .....	36
3.2.1 Altered lysosomal degradation capacity in CLN3 deficient cells.....	36
3.2.2 Increased levels of LAMP1 protein in CLN3 deficient ARPE-19 cells.....	38
3.2.3 Autophagic flux.....	39
3.2.4 Increased lysosomal marker LC3-II in CLN3 deficient HeLa and ARPE-19 cells.....	41
3.2.5 SubC accumulates in ARPE-19 and iPSC derived RPE CLN3-KO cells ...	41
3.2.6 Cell cycle arrest amplifies CLN3-KO phenotypes in ARPE-19 cells .....	42
3.3 Detailed phenotypic characterization of CLN3 deficient ARPE-19 cells .....	45
3.3.1 Accumulation of SubC and Gb3 in ARPE-19 CLN3-KO cells .....	45
3.3.2 Reduced BMP/LBPA levels in ARPE-19 CLN3-KO cells.....	46
3.3.3 Increased lysosomal number and size in ARPE-19 CLN3-KO cells .....	47
3.3.4 Impaired autophagy in ARPE-19 CLN3-KO cells.....	50
3.3.5 Impaired lysosomal enzyme activity in ARPE-19 CLN3-KO cells .....	55
3.4 TRPML1 activation ameliorates lysosomal phenotypes in ARPE-19 CLN3-KO cells.....	57

3.4.1 Increased TRPML1 activity in ARPE-19 CLN3-KO cells.....	57
3.4.2 TRPML1 activation reduces lysosomal number/size in ARPE-19 CLN3-KO cells.....	58
3.4.3 TRPML1 activation reduces lysosomal accumulations of SubC and Gb3 in ARPE-19 CLN3-KO cells.....	59
3.4.4 TRPML1 activation does not elevate BMP/LBPA levels in ARPE-19 CLN3-KO cells.....	61
3.5 Possible mechanisms involved in amelioration of CLN3 associated lysosomal phenotypes.....	62
3.5.1 TRPML1 activation induces TFEB translocation in ARPE-19 CLN3-KO cells.....	62
3.5.2 TRPML1 activation fails to elevate mature CathD and TPP1 enzyme levels	
3.5.3 SubC reduction is mediated by TFEB independent processes.....	64
3.5.4 LC3-II levels increase after activation of TRPML1 in ARPE-19 WT and CLN3-KO cells.....	65
3.5.5 TRPML1 activation induces lysosomal exocytosis in ARPE-19 WT and CLN3-KO cells.....	68
4. Discussion.....	71
4.1 ARPE-19 CLN3-KO cells as cellular model for JNCL disease.....	71
4.2 Detailed phenotypic characterization of ARPE-19 CLN3-KO cells.....	73
4.3 Increased TRPML1 activity in ARPE-19 CLN3-KO cells.....	77
4.4 TRPML1 activation ameliorates lysosomal phenotypes in ARPE-19 CLN3-KO cells.....	77
4.5 Potential mechanisms involved in lysosomal phenotype reduction.....	78
5. Summary/Zusammenfassung.....	81
5.1 Summary.....	81
5.2 Zusammenfassung.....	82
6. Abbreviations.....	83
7. References.....	85
8. Acknowledgements.....	91
9. Lebenslauf.....	93
10. Eidesstattliche Versicherung.....	94

# 1. Introduction

## 1.1 Lysosomes

Since their discovery in the 1950s by Christian de Duve<sup>1</sup>, lysosomes were long thought to be mainly responsible for the degradation of macromolecules, damaged organelles and microbes<sup>2,3</sup>. This view has changed in the last decade: lysosomes are today known as important metabolic signaling hubs within cells (Figure 1).

Lysosomes consist of more than 60 acid hydrolases, various cofactors, ion channels and transporters and receive their cargo for degradation, such as lipids, proteins and polysaccharides via several routes, including endocytic, phagocytic and autophagic pathways<sup>3,4</sup>. The lysosomal lumen is segregated by a single lipid bilayer from the cytoplasm and consists of an acidic pH of 4.5-5.0<sup>4,5</sup>. The acidic environment is maintained by the vacuolar H<sup>+</sup>-ATPase (v-ATPase), which constantly transports H<sup>+</sup> protons across the limiting membrane<sup>5</sup>. Highly glycosylated lysosomal membrane proteins (LMPs) protect the membrane from acidic digestion. LMPs are also involved in protein and nutrient transport across the membrane and fusion of lysosomes with other organelles and the plasma membrane. Lysosome associated proteins 1 and 2 (LAMP1 and 2) and lysosomal integral membrane protein 2 (LIMP2) belong to the most abundant LMPs in mammals<sup>6</sup>. Furthermore, lysosomes are stores for Ca<sup>2+</sup>, Zn<sup>2+</sup> and other ions as well as metabolites including phosphate and ATP<sup>2</sup>. Lysosomal ion homeostasis is regulated by five main channel families, including transient receptor potential channels from the mucolipin subfamily (TRPMLs).

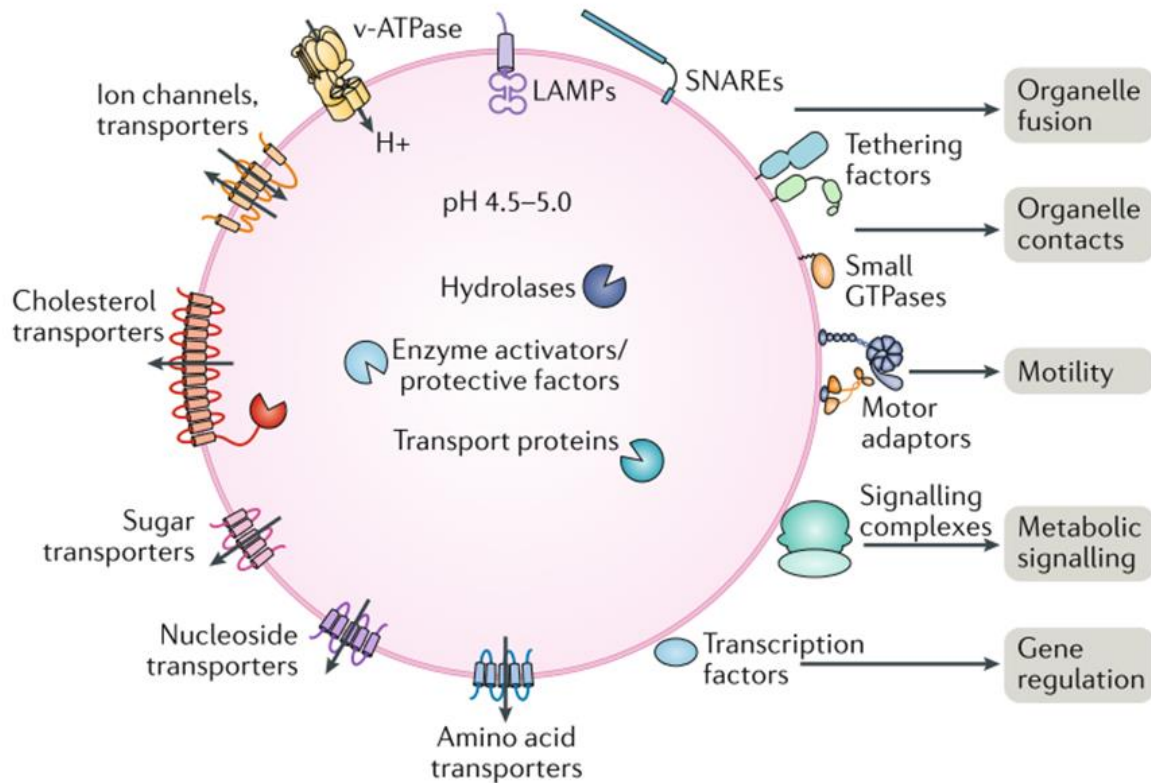


**Figure 1: Lysosomes.** Lysosomes serve with their acidic pH and more than 60 hydrolytic enzymes as the main degradation and recycling organelles of the cell. The lysosomal membrane comprises a variety of integral-membrane and peripherally associated proteins, which regulate import and export of nutrients and ions, contacts and fusion processes to other organelles and is furthermore involved in several metabolic signaling pathways. (Taken from Ballabio and Bonifacio 2019)

### 1.1.1 Lysosomal biogenesis

Lysosomal biogenesis is a complex process involving biosynthetic and endocytic pathways of the cell<sup>6</sup>. The transcription of many lysosomal genes is regulated by the transcription factor EB (TFEB), which induces the expression of genes containing a CLEAR (coordinated lysosomal expression and regulation) sequence<sup>7</sup>. Newly synthesized lysosomal proteins are transported from the ER to *cis*-Golgi compartments, where enzymes add the mannose-6-phosphate (M6P) group to soluble lysosomal hydrolases<sup>8</sup>. In the *trans*-Golgi network (TGN), the M6P groups are recognized by M6P receptors (M6PRs). The enzyme-M6PR complex is then transported via clathrin-coated vesicles to early endosomes<sup>6</sup>, which ultimately develop into mature lysosomes. Due to the acidic pH in this compartments, the M6P receptors dissociate from the enzymes and are transported back to the TGN. Recent studies also identified M6PR-independent transport mechanisms involving lysosomal sorting receptors like Sortilin 1 (SORT1) and LIMP2<sup>7</sup>. In contrast to the soluble hydrolases, the majority of lysosomal membrane proteins (LMPs) contain a

lysosomal signal peptide, consisting of a tyrosine- or dileucine-based motif. LMPs are either directly transported to lysosomes or travel via the secretory pathway to the plasma membrane and subsequently reach lysosomes through endocytic processes.

Via endocytic processes cells are able to take up material from the outside. Furthermore, endocytosis functions as the major membrane recycling and signaling pathway, also enabling the transport of membrane proteins and receptors to lysosomes. Endocytic vesicles are formed by invagination of the plasma membrane (Figure 2)<sup>9</sup>. They fuse with early endosomes (EE), which are characterized by a pH of about 6 and the presence of RAB5 and early endosome antigen 1 (EEA1) protein markers. EEs exhibit a tubular structure, but constantly change their morphology and composition. During maturation they form intraluminal and recycling vesicles (RV) and sort released cargos and receptors into the different types of vesicles. Multivesicular bodies (MVB), which contain intraluminal vesicles are also termed as late endosomes (LE)<sup>10</sup>. Whereas, recycling vesicles move directly back to the plasma membrane, late endosomes, defined by containing RAB7 proteins and a lower pH of 5-6<sup>9</sup>, eventually fuse with acidic lysosomes<sup>10</sup>.

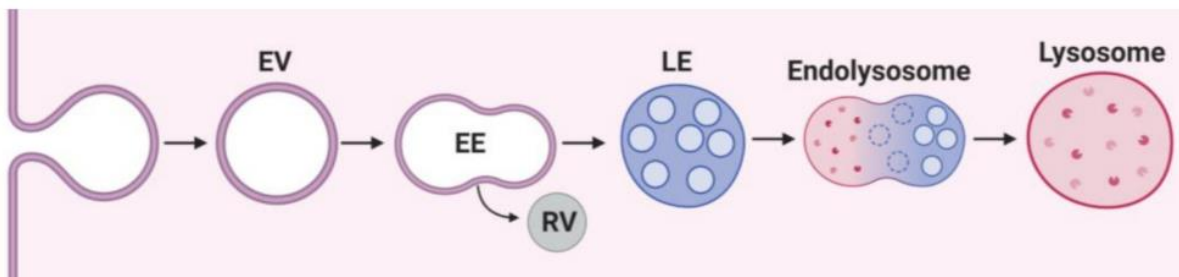


**Figure 2: Lysosomal maturation during endocytosis.** Invaginations of the plasma membrane form endocytic vesicles (EV), which fuse with other early endosomes (EE) to form a 'sorting station'. From here cargo is sorted into recycling vesicles (RV) and intraluminal vesicles for lysosomal degradation. EEs mature to a late endosome (LE), which fuse then with lysosomes. (Taken from Trivedi, Bartlett and Pulinilkunnil 2020)

### 1.1.2 Lysosomal distribution, fusion and contact sites

Mammalian cells contain between 50 and 1000 lysosomes distributed throughout the cytoplasm<sup>3</sup>. Cellular localization of lysosomes depends on the nutrient status of the cell. Under resting conditions, they are scattered around the cytoplasm, whereas nutrient deprivation and autophagy induction is accompanied by lysosomal accumulation in the perinuclear region<sup>11</sup>. Lysosomes move along microtubules in a retrograde and anterograde manner by using the motor proteins dynein and kinesin<sup>12</sup>. Coupling of lysosomes to these motor proteins is mediated by several

adaptor proteins, including RAB7, ALG2, RILP, FYCO1, CORC and ARL8<sup>3</sup>. Also actin microfilaments and myosin motor proteins are involved in the correct positioning and movement of lysosomes, especially in the cell periphery<sup>12</sup>. Lysosome motility is indispensable for the fusion processes with other vesicles, like endosomes, (auto-) phagosomes and the plasma membrane. Fusion events are mediated by the assembly of soluble NSF attachment protein receptor (SNARE) complexes, the release of Ca<sup>2+</sup> from the lysosomal lumen, small GTPases (ARL8, RAB7), several tethering factors (HOPS, EPG5, PLEKHM1, ATG14L), autophagosome docking proteins (LC3, GABARAP) and regulator proteins (SYT7, BORC, UVRAG, Rubicon)<sup>3</sup>. Lysosomes are also staying in non-fusogenic contacts to other organelles like the endoplasmic reticulum (ER), mitochondria, peroxisomes or the Golgi network. Contact to the endoplasmic reticulum (ER) is not only associated with the maturation of endosomes to lysosomes<sup>13</sup>, also, proteins, such as NPC1 and NPC2 regulate the lysosomal export and import of cholesterol at these sites<sup>3</sup>. Recently, mitochondria-lysosome contact sites were found to be coordinated by RAB7. These contacts are hypothesized to mark sites for mitochondrial fission and regulate bidirectional mitochondrial and lysosomal dynamics<sup>14</sup>. In addition to membrane bound organelles, lysosomes were found to interact with RNA granules<sup>3</sup>.

### **1.1.3 Lysosomes as metabolic signaling centers**

In the past years, lysosomes have emerged from their role as main cellular degradative organelles to essential signaling hubs regulating various cellular processes<sup>15,16,14,3</sup>. Proteins on the lysosomal surface are involved in nutrient sensing, Ca<sup>2+</sup> signaling, autophagic cargo sensing and pro-inflammatory response, lysosome-dependent cell death and endolysosomal damage response as well as lipid signaling<sup>3</sup>. The key regulator of biosynthetic cellular pathways is the mechanistic target of rapamycin complex 1 (mTORC1), dynamically associated with lysosomes depending on energy and nutrient status of the cell (Figure 3 A)<sup>3</sup>. In the presence of nutrients and growth factors, mTORC1 is activated and localized to lysosomes. When activated, mTORC1 supports mRNA translation, ribosome biogenesis and lipid synthesis. In contrast, mTORC1 is inhibited and detached from lysosomes under stress conditions. This leads to the activation of catabolic mechanisms such as autophagy<sup>5</sup>. mTORC1 is composed of its core protein mTOR, a large

serine/threonine kinase and several subunits including RAPTOR, PRAS40, DEPTOR and mLST8. RAPTOR is reported to mediate substrate binding, whereas PRAS40 and DEPTOR inhibit intrinsic mTOR kinase activity. The function of mLST8 remains obscure (Figure 3 B)<sup>5</sup>.

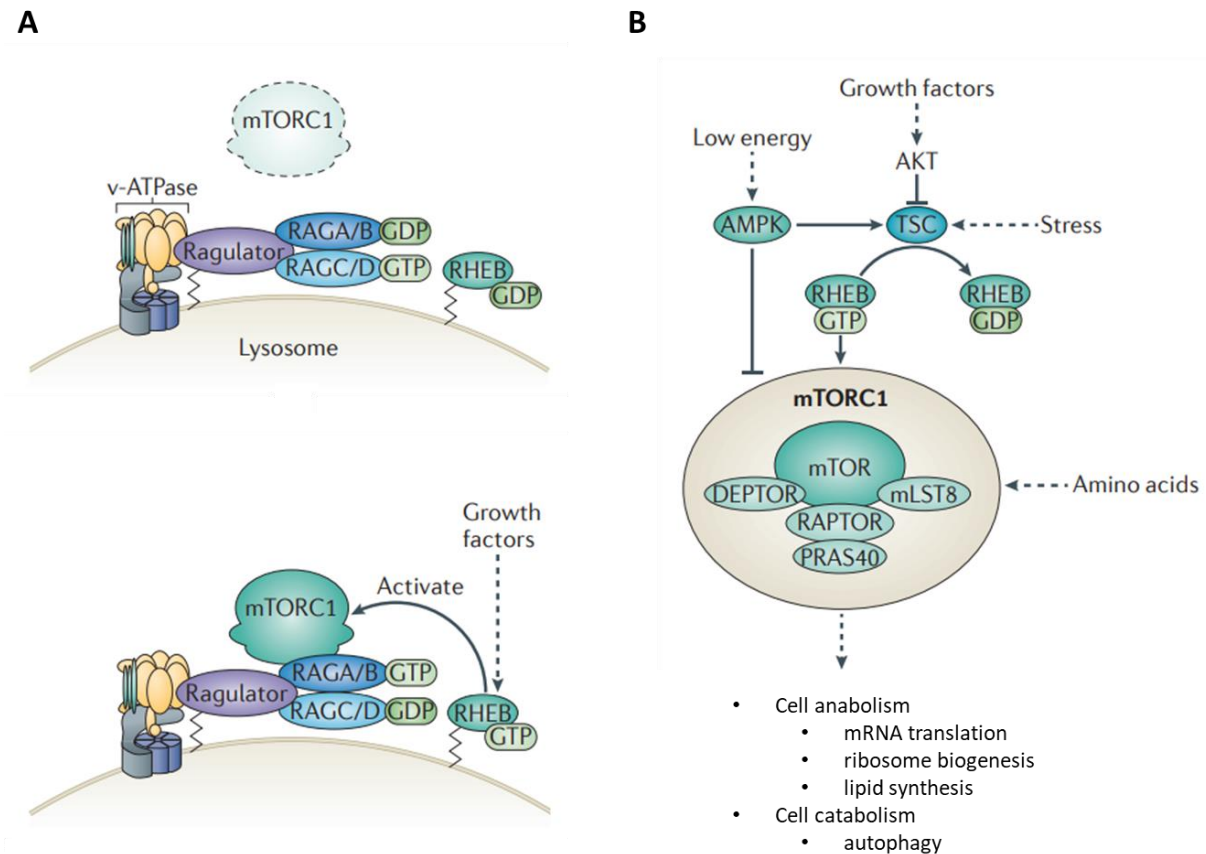


**Figure 3: mTOR activation and signaling pathway.** **A** mTORC1 is dislocated from the lysosome under stressful conditions, but is located to the lysosomal surface under nutrient-rich conditions. **B** Several upstream signals, including energy status, growth factors, stress and amino acid signals lead to activation/inhibition of mTORC1. mTORC1 thereby regulates cell anabolism and catabolism pathways. (Modified from Jewell, Russell and Guan 2013)

mTORC1 activity is influenced by four major upstream signals: growth factors, energy status, oxygen and amino acids (Figure 3 B)<sup>17</sup>. The heterodimer tuberous sclerosis complex (TSC), composed of TSC1 & 2, is one of the most important sensors that negatively regulates mTORC1 activity. Growth factors eventually lead to the inactivation of the TSC1/2 complex and thus activation of mTORC1. The energy status of the cell is monitored by AMP-activated protein kinase (AMPK). In case of energy depletion, mTORC1 activity is reduced, either via TSC2 phosphorylation or directly through RAPTOR phosphorylation by AMPK. In response to oxygen levels, mTORC1 activity is affected by multiple pathways, including AMPK and TSC1/2

sensing mechanisms<sup>17</sup>. Amino acids, especially their entry into lysosomes, were shown to activate and translocate mTORC1 to the lysosomal surface by amino acid-dependent activation of RAG GTPases and their interaction to RAPTOR<sup>3, 5, 17</sup>.

Upon activation, mTORC1 promotes cell anabolism through several pathways. mTORC1 dependent phosphorylation of the eukaryotic initiation factor 4E (eIF4E)-binding protein 1 for example, regulates cap-dependent translation, whereas phosphorylation of the p70 ribosomal S6 kinase 1 (S6K1) induces biogenesis of mRNA and ribosomes<sup>17</sup>. mTORC1 is also known to be involved in lipid synthesis, which is required for cell growth and proliferation<sup>17</sup>. In addition, a link between mTORC1 activity and mitochondrial metabolism as well as biogenesis was found<sup>17</sup>. mTORC1 also specifically enables lysosomal and autophagosomal gene expression by its interaction with the transcription factor TFEB (Figure 4). Under nutrient-rich conditions, active mTORC1 phosphorylates TFEB, leading to its cytoplasmic retention. In contrast, the lack of phosphorylation under starvation due to inactive mTORC1 induces TFEB translocation into the nucleus causing gene expression<sup>18</sup>. Furthermore, active mTORC1 represses autophagy by phosphorylating and thereby repressing UNC51-like kinase 1 (ULK1) and autophagy-related gene (ATG) protein 13 (ATG13) (Figure 4)<sup>17</sup>.

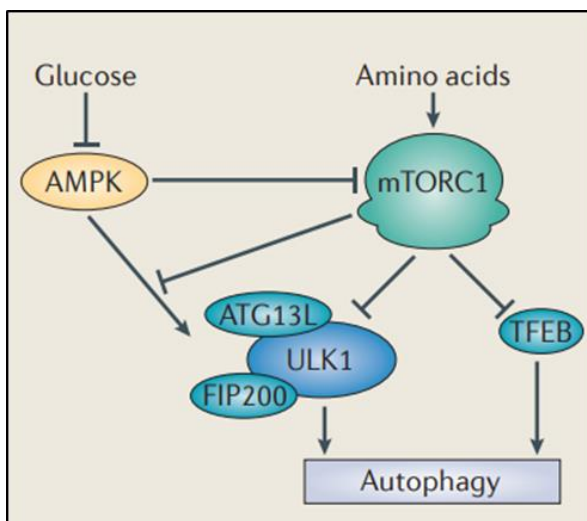


**Figure 4: mTORC1 dependent regulation of autophagy.** mTORC1 is inhibited under starvation conditions by the energy sensor AMPK and by amino acid signaling, leading to activation of autophagy. Under starvation conditions mTORC1 is active and inhibits autophagy. (Taken from Jewell, Russel and Guan 2013).

### 1.1.4 Lysosomal Ca<sup>2+</sup> signaling

Lysosomal Ca<sup>2+</sup> signaling is a key mechanism for various lysosomal and cellular functions. The three main Ca<sup>2+</sup> channel types identified in lysosomes are TRPML channels, two-pore channels (TPC) and P2X purinoceptor 4 (P2X4). TRPML channels (TRPML1, TRPML2, TRPML3) belong to the mucolipin TRP subfamily, localizing to vesicles along the endosomal pathways. The non-selective cation channel TRPML1, also known as mucolipin-1, is the major calcium-release channel of lysosomes<sup>19</sup>. Mutations in *MCOLN1*, the gene encoding TRPML1, lead to the lysosomal storage disorder mucopolipidosis type IV (MLIV), characterized by psychomotor retardation and ophthalmological abnormalities<sup>20</sup>. TRPML1 channels are activated by several stimuli including starvation, reactive oxygen species and the phosphoinositide phosphatidylinositol 3,5-bisphosphate (PtdIns(3,5)P)<sub>2</sub><sup>3</sup>. The Ca<sup>2+</sup> sensor ALG2, directly interacts with TRPML1 upon its activation by PtdIns(3,5)P<sub>2</sub> and thereby promotes dynein mediated retrograde transport of lysosomes towards the microtubule organizing center (MTOC)<sup>11</sup>.

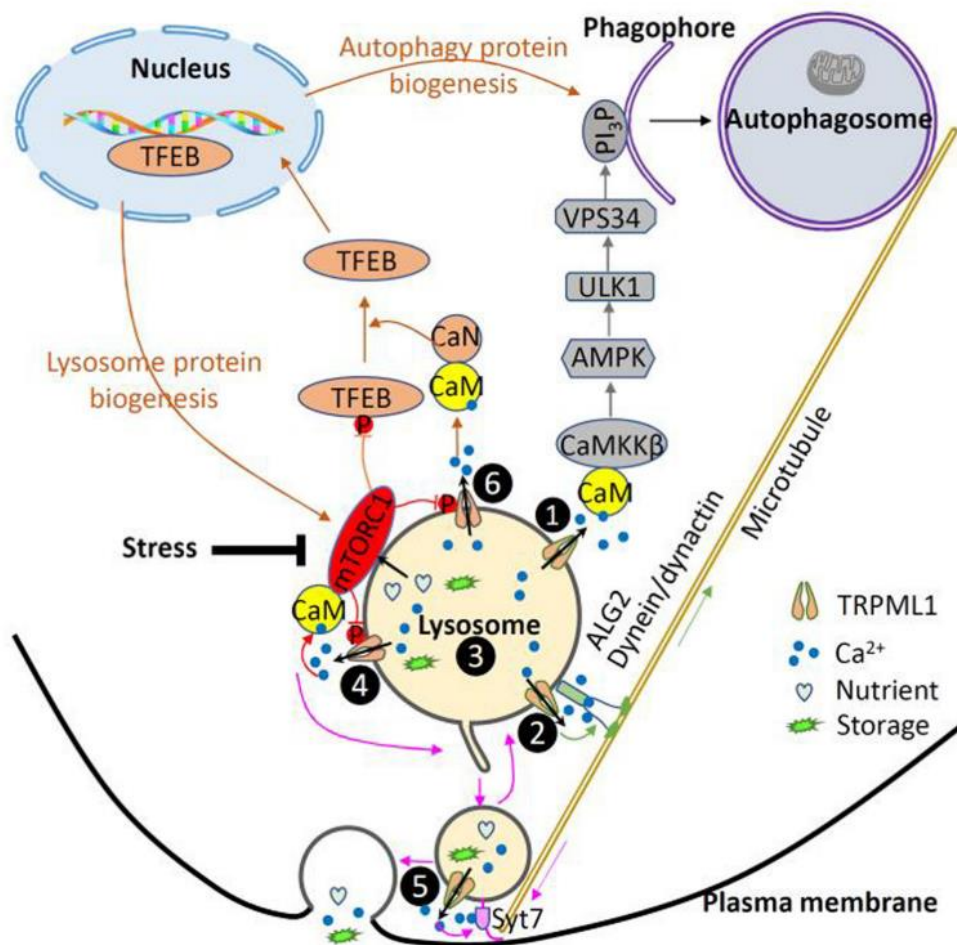


**Figure 5: TRPML1 dependent cellular processes.** 1 CAMKKβ/AMPK-dependent autophagosome formation. 2 ALG2-dependent lysosomal movement. 3 increased lysosomal degradation. 4 CaM-dependent mTORC1 reactivation. 5 Syt7-

dependent lysosomal exocytosis to remove garbage. **6** TFEB translocation inducing lysosomal autophagy-related gene expression. (Taken from Huang *et al.* 2020)

Several membrane fusion processes, such as endosome-lysosome, autophagosome-lysosome and plasma membrane-lysosome fusion, the latter occurring during lysosomal exocytosis, are promoted by  $\text{Ca}^{2+}$  release from lysosomes<sup>21</sup>. In addition, TRPML1 activation and subsequent  $\text{Ca}^{2+}$  release lead to the induction of autophagy. Upon starvation or other stimuli,  $\text{Ca}^{2+}$  release by TRPML1 activates the phosphatase calcineurin which dephosphorylates TFEB, leading to its nuclear translocation and subsequently to increased expression of lysosomal and autophagosomal genes<sup>22</sup>. A TFEB-independent process induces biogenesis of autophagosomes via the CAMKK $\beta$ /AMPK pathway.  $\text{Ca}^{2+}$  released by TRPML1 activates CAMKK $\beta$  and its substrate AMPK, that regulates autophagy through phosphorylation of both ULK1 and Beclin1, and the subsequent induction of the VPS34 complex<sup>19</sup>. Furthermore, a direct link between mTORC1 and TRPML1 has been reported. In nutrient-rich conditions, mTORC1 is active and inhibits TRPML1 through phosphorylation<sup>20</sup>. Starvation leads to inhibition of mTORC1, but activation of TRPML1, which in turn facilitates calmodulin-dependent reactivation of mTORC1. This negative feedback loop is hypothesized to ensure reactivation of mTORC1 during prolonged starvation<sup>23</sup>.

With its various cellular functions, TRPML1 is a promising therapeutic target for several diseases. Recent publications have shown, that activation of TRPML1 decreases lysosomal accumulation material and also has beneficial effects on autophagy in cellular models of Amyotrophic Lateral Sclerosis (ALS), Parkinson's, Niemann-Pick type C and Duchenne Muscular Dystrophy disease<sup>24,25,26,27</sup>.

## 1.2 Autophagy

Cellular homeostasis is maintained by a balance between anabolism and catabolism. The main catabolic pathways in cells are the ubiquitin-proteasome system (UPS) and the autophagy-lysosomal pathway. Whereas UPS specifically targets individual, short-lived proteins, autophagy was long thought to be a bulk process for degradation of long-lived and aggregated proteins as well as organelles<sup>28</sup>. Autophagy is a tightly regulated 'self-eating' process, in which cytoplasmic material is delivered to lysosomes for degradation. There are three different types of autophagy known: Microautophagy, Chaperon-mediated autophagy (CMA) and Macroautophagy (Figure

6 A). In microautophagy, invaginations of the lysosomal membrane directly engulf a portion of the cytoplasm. CMA in contrast, is controlled by chaperones, which selectively transport cytoplasmic proteins with pentapeptide motifs across the lysosomal membrane via the lysosomal associated membrane protein LAMP2A<sup>29</sup>. Macroautophagy, hereafter referred to as autophagy, is a multi-step process that starts with the formation of a double membrane, the so called isolation membrane or phagophore. The phagophore engulfs cytoplasmic material and forms the autophagosome upon closure, which is transported to lysosomes for fusion to an autolysosome, finally leading to degradation of engulfed material (Figure 6 A)<sup>17, 29</sup>.

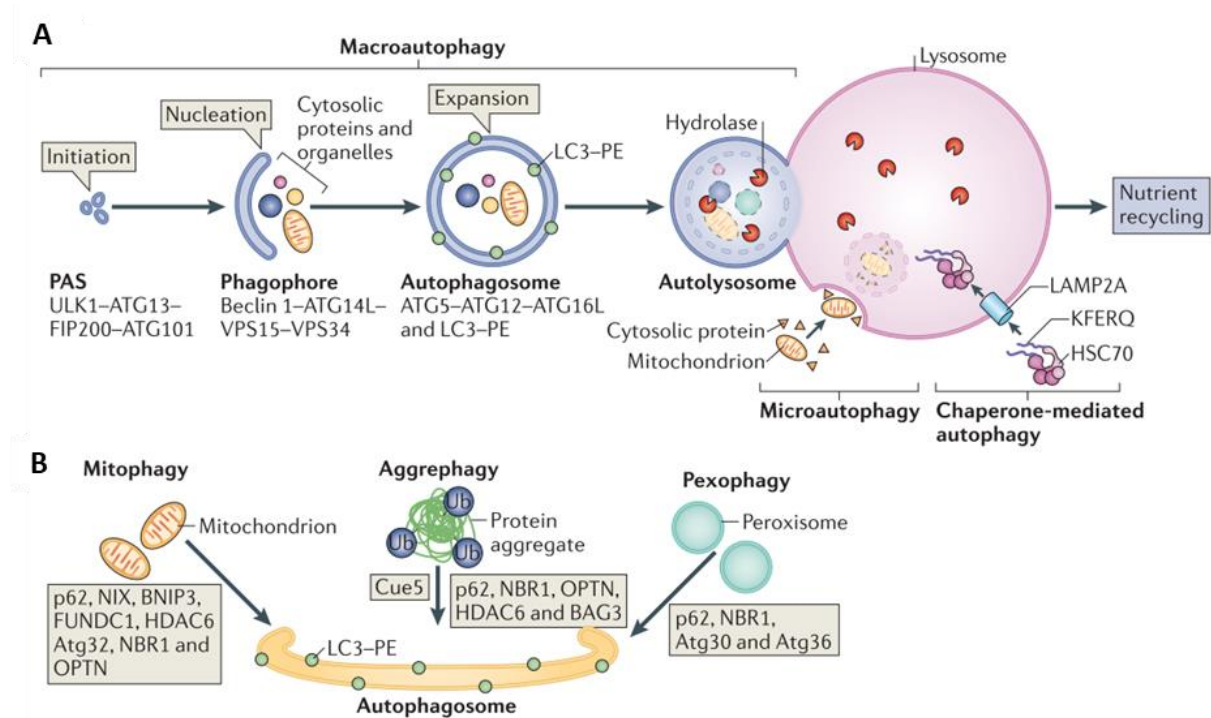


**Figure 6: Overview of autophagy pathways.** A Initiation of macroautophagy begins at the phagophore assembly site (PAS). The membrane formed is termed phagophore and expands to the autophagosome, which engulfs cytoplasmic material. The autophagosome fuses with the lysosome, containing a variety of hydrolases for degradation and recycling of molecules, proteins and organelles. There are two other forms of autophagy: Microautophagy and Chaperone-mediated autophagy. B Different forms of macroautophagy are named by their cargo. Mitophagy leads to degradation of mitochondria, in aggrephagy ubiquitin labeled aggregates are recycled, whereas the autophagy of peroxisomes is called pexophagy (Taken from Kaur and Debnath 2015).

Phagophore assembly is initiated near the ER by the ULK complex at the phagophore assembly site (PAS). The ULK complex contains ULK1, ULK2, ATG13, focal adhesion kinase family-interacting protein of 200 kDa (FIP200) and ATG101, which are amongst others controlled by mTORC1<sup>30</sup>. The activated ULK complex together with the class III PI3K complex, consisting of Beclin 1, vacuolar protein sorting 15 (VPS15), VPS34 and ATG14, promotes the local production of

autophagosome specific PtdIns(3)P<sup>28</sup>. During expansion, the ATG12-ATG5-ATG16 complex is recruited to the autophagosome and facilitates the lipidation of the microtubule-associated protein 1 light chain 3B (LC3B)<sup>28</sup>. LC3B is processed by the ubiquitin-like conjugation system to its cytosolic form LC3-I and then by phosphatidylethanolamine (PE) conjugation to the autophagosomal membrane located LC3-II<sup>31</sup>. Due to its localization to the autophagosomal membrane, LC3(-II) is widely used as a marker for autophagy<sup>32</sup>. In addition to the control of autophagosomal size, LC3 proteins play a key role in the selective recruitment of autophagic cargo to the autophagosomes<sup>33</sup>. Cargo adaptor proteins, such as P62/SQSTM1, link degradation material to LC3-II in the autophagosomal membranes by their ability to simultaneously interact with both, the autophagosomes via the LC3-interacting region (LIR) and with cargo substrates mostly via an ubiquitin-binding domain (UBD). The recognition of cargo via autophagy receptors changed the view of autophagy, which was long thought to be a bulk degradation process and is now more and more seen as a targeted protein and organelle recycling pathway<sup>33</sup>.

Cargo loaded autophagosomes are trafficking along microtubules in a dynein-dependent manner to lysosomes, which are clustered around the nucleus<sup>29</sup>. Autophagosome-lysosome fusion is regulated by a number of proteins, including the BORC complex, ARL8, HOPS, RAB7, PLEKHM1 and EPG5, as well as Rubicon and a subset of SNAREs<sup>3</sup>. The efficiency of autophagosome-lysosome fusion is sensitive to the types and levels of phosphatidylinositol (PI) phosphates in membranes of both autophagosomes and lysosomes. Within the resulting autolysosomes, degradation starts with the disruption of the inner autophagosomal membrane, followed by the degradation of the cargo orchestrated by more than 60 different lysosomal hydrolases. Catabolites generated by autophagic degradation are hypothesized to mostly get exported from lysosomes through various transporters and being reused by the cell<sup>34</sup>.

Selective autophagy processes are named after the cargo they degrade (Figure 6 B). The recycling of mitochondria is for example called mitophagy, aggrephagy names the clearance of protein aggregates and pexophagy is the term for peroxisome degradation<sup>28</sup>.

### **1.3 Lysosomal storage diseases**

Lysosomal storage diseases (LSDs) are rare, metabolic disorders, characterized by a progressive lysosomal accumulation of cellular material, with an overall prevalence of 1:5000<sup>35</sup>. LSDs comprise more than 70 disorders, mostly inherited in an autosomal recessive manner<sup>36</sup>. Onset of LSDs vary from infancy to adulthood. Approximately 70% of LSDs show progressive central nervous system impairments, which are often accompanied by peripheral organ and tissue malfunctions<sup>37</sup>. On the cellular level, the initial accumulation of macromolecules inside endosomal-lysosomal compartments is common to all LSDs, whereas the content of accumulation material depends on the mutation<sup>37</sup>. Many LSDs are monogenic diseases, whereby 50 of them affect enzyme deficiencies, 7 disorders are caused by mutations of integral membrane proteins, 12 are disorders of lysosome-related organelles and 13 disorders involve the production of lipofuscin<sup>36</sup>.

#### **1.3.1 Neuronal Ceroid Lipofuscinosis**

Neuronal ceroid lipofuscinoses (NCLs), or Batten disease, is a group of rare inherited disorders considered to be the most prevalent neurodegenerative diseases in children with an incidence of 1:12 500<sup>38</sup>. The NCL diseases share clinical symptoms including progressive vision loss and cognitive decline, seizures, motor retardation and eventually premature death<sup>38,39</sup>. They are categorized by the age of onset, which varies from congenital, infantile, late infantile, juvenile, adult to late adult<sup>38</sup>. There are in total 14 ceroid-lipofuscinosis neuronal (CLN) proteins with different functions within the cell, all leading to NCL diseases (Figure 7). Whereas CLN1, 2, 5, 10 and 13 are soluble lysosomal proteins, CLN3 and 7 are transmembrane proteins. The other CLN proteins were found in different organelles like endosomes, the ER or as soluble proteins in the cytoplasm<sup>40</sup>. The common hallmark of NCLs, also defining their naming, is the lysosomal accumulation of ceroid and lipofuscin<sup>39</sup>. Ceroid and lipofuscin are autofluorescent and consist of a mixture of incompletely degraded proteins and lipids, showing a 'fingerprint-like' ultrastructure under the electron microscope<sup>41</sup>.

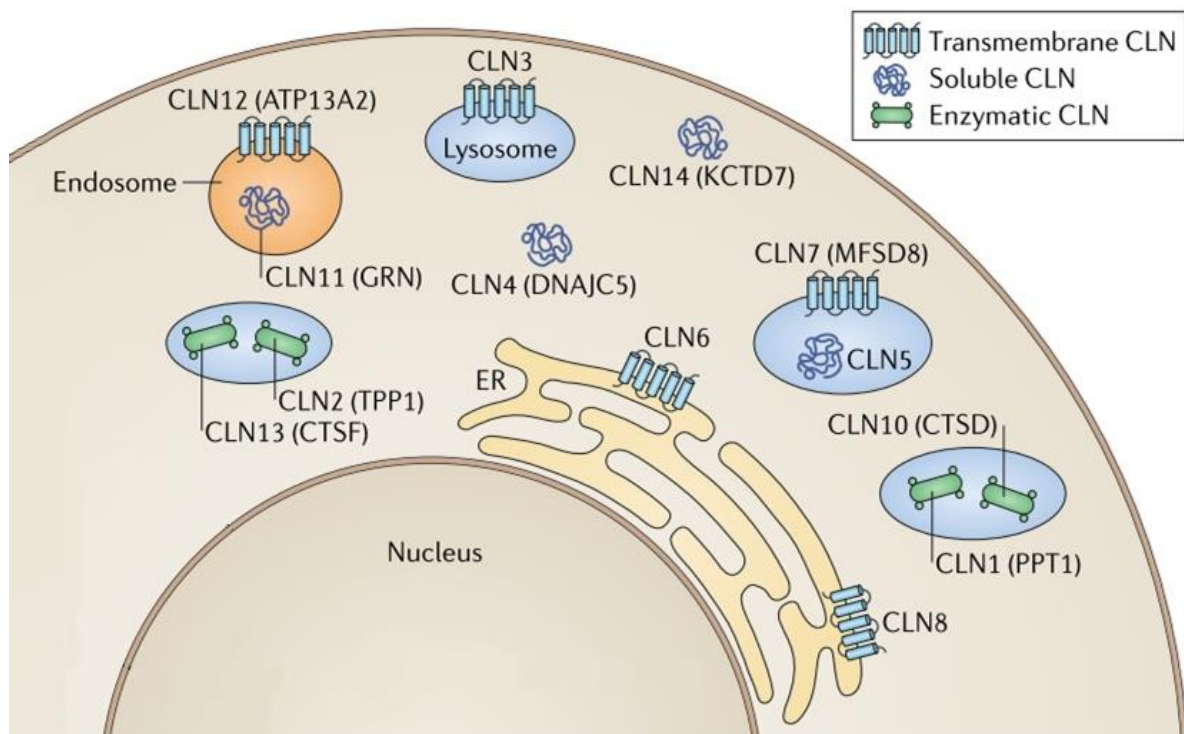


**Figure 7: Cellular localization of NCL causing proteins.** CLN1, 2, 10 and 13 are lysosomal enzymes, CLN5 is soluble lysosomal protein, CLN3 and 7 are lysosomal membrane proteins, CLN11 and 12 are localized to endosomes, CLN6 and 8 are found in ER membranes and CLN4 and 14 are soluble cytosolic proteins. (Modified from Johnson *et al.* 2019)

### 1.3.2 Juvenile neuronal ceroid lipofuscinosis

In the juvenile form of the NCL disease (JNCL), children develop up to school age without obvious impairments. Vision loss is one of the first symptoms, followed by the decline of intellect, loss of motor abilities and death of patients in their twenties to thirties<sup>38</sup>. There is no disease-modifying therapy available so far and current treatment options only address symptoms.

JNCL disease is caused by autosomal recessive mutations in the gene *CLN3*<sup>42</sup>, which is located on chromosome 16. Six transcripts with several splice variants are known for the gene. Most of the isoforms contain between 13 and 16 exons and the longest *CLN3* isoform encodes a protein with a length of 438 amino acids. Various molecules, including TFEB, are involved in regulation of *CLN3* expression. *CLN3* is ubiquitously expressed in multiple tissues and cell types<sup>43</sup> and the protein localizes to the membrane of late endosomes and lysosomes<sup>44</sup>. Several topology models exist, but the most cited one suggests the *CLN3* protein to consist of six transmembrane domains with N- and C-terminus facing the cytoplasm (Figure 8)<sup>45,46</sup>. However, a protein structure with 11 transmembrane domains was recently proposed on the

protein structure database AlphaFold, which is not yet published (<https://alphafold.ebi.ac.uk/entry/Q13286>).

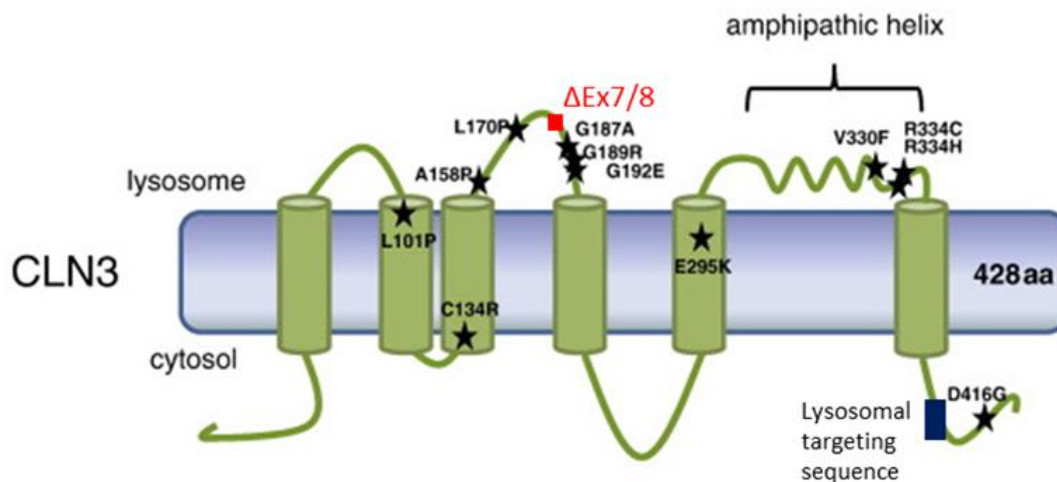


**Figure 8: CLN3 protein topology with most common mutations.** CLN3 protein is located in the lysosomal membrane and is predicted to consist of 6 transmembrane domains, with N- and C-terminus facing the cytoplasm. Mutations are indicated with stars. Most known mutations causing JNCL are located on the luminal part of the protein, including the  $\Delta$ Ex7/8 mutation. (Modified from Kmoch *et al.* 2013)

A nearly 1kb deletion of a genomic fragment including exon 7 and 8 is the most common mutation known for JNCL. It leads to a truncated CLN3 protein lacking the lysosomal targeting sequence and is therefore thought not to reach lysosomes. Other missense mutations are distributed mostly to the luminal side of the protein (Figure 8)<sup>47</sup>.

The low *CLN3* gene expression, its hydrophobic nature and the lack of cellular models that recapitulate the human disease phenotype have restricted analysis of CLN3 localization and function<sup>38,43</sup>. In two studies, performed in CLN3 knockout mice, autofluorescent lipofuscin with the typical fingerprint structure was found<sup>48,49</sup>. Therefore, a CLN3 knockout is regarded as a disease model. Especially, by implementing a knock-in mouse model harboring the exon $\Delta$ 7/8 mutation<sup>50</sup>, generating a cerebellar cell line from this<sup>51</sup> and analyzing patient derived induced pluripotent stem cells (iSPCs)<sup>52</sup>, CLN3 disease phenotypes were confirmed and further investigated. However, the function of CLN3 remains unknown. Proposed CLN3 function include its involvement in endosome to TGN trafficking of lysosomal sorting receptors by an interaction with Rab7A<sup>53</sup> and its regulation of the actin-cytoskeleton by an interaction to myosin-IIb<sup>54</sup>. Various studies suggest a role of CLN3 in the endosomal-lysosomal system (Figure 9)<sup>55,56,52</sup>.

Dysfunctional lysosomes and elevated lysosomal pH are hallmarks of lysosomal storage disorders and have been described for JNCL. Both of them might influence mitochondrial health as well as the autophagy pathway, which are impaired in CLN3 deficient cells<sup>51,55,57,52</sup>. The most prominent phenotype of CLN3 deficient cells is the lysosomal accumulation of lipofuscin<sup>56,58,51</sup>. Furthermore, the mitochondrial ATPase subunit C (SubC)<sup>51</sup> and globotriaosylceramide (Gb3)<sup>59</sup> aggregate in lysosomes. In contrast, bis(monoacylglycerol)phosphate (BMP) also known as lysobisphosphatic acid (LBPA) was found to be reduced in CLN3 deficient cells<sup>60</sup>. It is still unclear which phenotypes are primary and which are secondary causes of CLN3 deficiency.

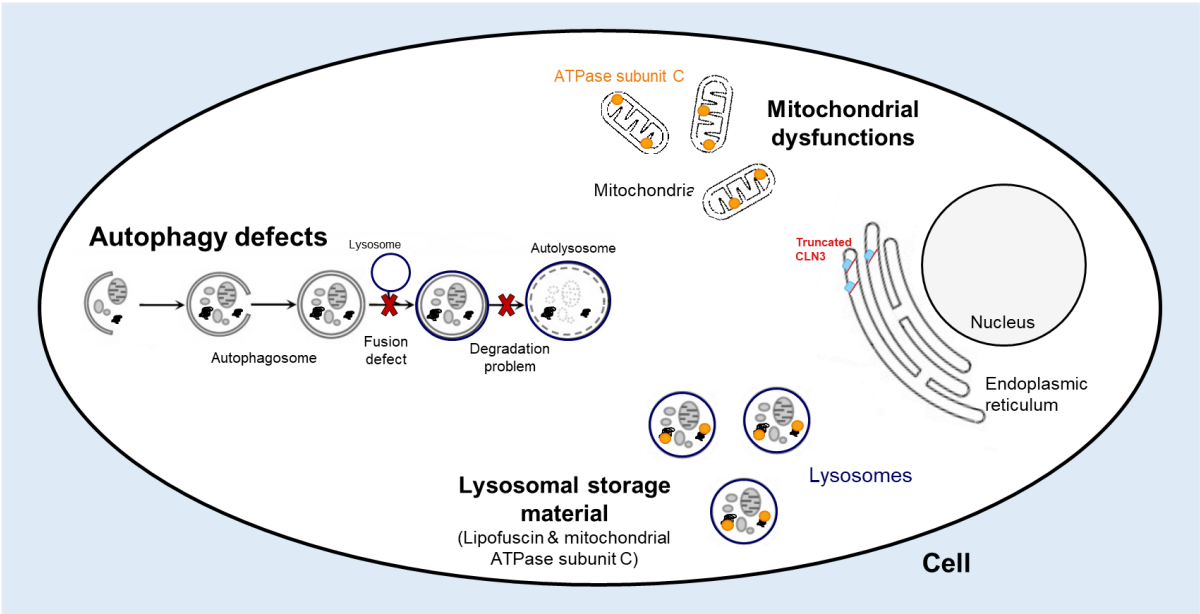


**Figure 9: Main cellular dysfunctions caused by CLN3 mutations.** Truncated CLN3 proteins, due to mutations, are missing the lysosomal targeting sequence, are likely not properly folded and get stuck in the ER. This leads to lysosomal accumulation material such as lipofuscin and mitochondrial ATPase subunit C. Furthermore lysosomal degradation is impaired, autophagy is defective and mitochondria are dysfunctional in CLN3 deficient cells.

## **1.4 Aim of the study**

The aim of this study was to investigate the cellular implications of CLN3 deficiency and elucidate potential therapeutic options for JNCL disease.

JNCL is caused by mutations in the lysosomal membrane protein CLN3. CLN3 deficient cells are mainly characterized by the accumulation of mitochondrial subunit C in lysosomes, lysosomal impairments and autophagy defects. It remains to be elucidated which cellular defects elicit JNCL disease and eventually lead to cell death. Especially lysosomal and autophagy related impairments have been proposed to be primary causes of the disease. Defects in autophagy and lysosomal function in cellular models of several other neurodegenerative diseases were found to be ameliorated by the activation of the lysosomal cation ion channel TRPML1. The effect of TRPML1 activation on CLN3 phenotypes has not been investigated so far.

I hypothesized that lysosomal defects and accumulation material caused by CLN3 deficiency can be reversed by activation of TRPML1 in a cellular model of JNCL.

In a first step, different CLN3 deficient cell lines were characterized with focus on the autophagosomal-lysosomal system to identify a suitable CLN3 cell model.

To determine clear phenotypes of CLN3 deficiency, the lysosomal network of the newly generated and selected cell model was characterized in more detail in the second step.

The third part of the study focused on TRPML1, as a potential therapeutic target for JNCL. Beneficial effects of TRPML1 activation on phenotypes found in the CLN3 deficient cell model were observed. Furthermore, the underlying mechanisms on ameliorated phenotypes were investigated.

## **2. Material and Methods**

### **2.1 Generation and cultivation of cells**

#### **2.1.1 Cultivation of HeLa cells**

HeLa cells were cultivated in MEM Eagle medium (Sigma, M8042) supplemented with 10% FCS (Gibco, 10500) and 2 mM L-Glutamine (Life Technologies, 25030-024). For dissociation, cells were treated for 5 min at 37°C with 0.05 % Trypsin-EDTA (Gibco, 25300-054), resuspended with medium and split according to planned experiments.

#### **2.1.2 Generation and cultivation of ARPE-19 CLN3-KO cells**

CLN3-KO ARPE-19 cells were generated using the CRISPR/Cas9 system. Alt-R-CRISPR\_Cas9 crRNA CLN3 (custom-designed, by IDT, + strand sequence: ATCCCACTGACGAGAACCCG) and Alt-R-CRISPR-Cas9 tracrRNA (IDT, 1072533) were mixed to form crRNA:tracrRNA guide complexes. ARPE-19 cells were transfected with crRNA:tracrRNA duplex and Cas9 nuclease (IDT, 1074182) by electroporation. Single cell clones were expanded and mutations were evaluated by PCR, BioAnalyzer and sequencing. The ARPE-19 CLN3-KO line carries 8 nucleotide deletions in exon 3 on both alleles, leading to a premature stop codon and a truncated protein missing the lysosomal targeting sequence (c.[377-384del+383-390del]). On protein level, these are leading to changes from amino acid 127 onwards and result in a frameshift and a premature stop codon at amino acid 156 (p.[Glu127fs\*156+Gln127fs\*156]).

ARPE-19 cells were cultured in DMEM/F-12 medium (Gibco, 11320-074), supplemented with 2 mM L-Glutamine (Life Technologies, 25030-024) and 10 % heat inactivated FCS (Gibco, 11320-074). For dissociation, cells were treated for 5 min at 37°C with 0.05 % Trypsin-EDTA (Gibco, 25300-054), resuspended with medium and split according to planned experiments. If not otherwise stated, to induce a cell cycle arrest, ARPE-19 cells were treated with 0.3 mM mitomycin C (Merck, 10107409001) for 2 hours and washed with PBS before replating in the required well-format. Cells were kept in culture for 7 days thereafter.

After having the ARPE-19 cells in culture for one year, cells were genotyped to verify the introduced mutations in the CLN3-KO cell line. DNA was isolated using the DNeasy Blood and Tissue Kit (Qiagen, 69504). Using following primers, DNA was

amplified via PCR and sequenced: forward: gagaaaaggcaaccaggacg, reverse: caggagctgagaaaggggag.

### 2.1.3 Generation, cultivation and quality control experiments of iPSC derived RPE cells

iPSC derived RPE cells were generated in cooperation with Nele Schwarz and Katharina Kruszweskis team at Evotec in Göttingen, according to the protocol described by Zhu *et al.* 2013<sup>61</sup>.

For maintenance of differentiated RPE cells, medium was prepared according to the following table:

#### RPE medium (500 ml):

Substance	Supplier	Catalog no.	Amount
DMEM, high Glucose, GlutaMAX	Gibco Life Technologies	31966-21	400 ml
Knockout Serum Replacement	Thermo Fisher Scientific	10828010	100 ml
MEM NEAA (100x)	Thermo Fisher Scientific	11140035	5 ml
3.5 µL β-mercaptoethanol in 2.5 ml L-Glutamine	Sigma	M6250	2.5 ml
L-Glutamine	Gibco Life Technologies	25030-024	

RPE cells were cultivated in transwells (Corning, CLS3460-48EA) and medium was changed every 3 days. For medium change, old medium was first removed from the lower chamber, then from the upper one. Both chambers were washed with RPE medium, then fresh RPE medium containing 10-20ng/mL human Activin A (BioTechne, 338-AC-050) was added. After 20 days in culture RPE cells were passaged to new transwells.

RPE cells were passaged in transwells, but transferred to 384 well plates (Greiner, 781091) for experiments. Both, transwells and 384 well plates were coated with Matrigel (Corning, 356231). Matrigel was defrosted for 30 min on ice and diluted 1:20 in ice-cold DMEM/F-12 medium. Transwells were coated with 300 µl Matrigel and stored for up to one week at 4°C. Old medium was aspirated from both chambers, then 100 µl Trypsin-EDTA (Sigma, T3924) was added to the upper chamber and 400 µl to the lower chamber and transwells were incubated for 10 min at 37°C. After 10 min, cells were dissociated by pipetting inside the transwells until no visible clumps were left over and transferred to tubes containing fresh medium supplemented with 10mg/ml Soybean Trypsin Inhibitor (Sigma, T6522). Tubes were then centrifuged at 180xg for 2 min. Supernatant was discarded and the cell pellet resuspended in RPE

medium containing 10-20 ng/ml activin. Per 1 mm cell pellet 500 µl RPE medium with activin were used. Cell suspension was filtered through a 30 µm cell strainer (Sysmex, 04-004-2326) and washed with 500 µl activin containing RPE medium. Cells were counted using a Neubauer counting chamber. Coating was aspirated before seeding the cells into transwells/384 well plates. Then, 1.5 mio cells diluted in 600 µl RPE medium were seeded per transwell or 33 000 cells diluted in 70 µl medium transferred into one well of a 384 well plate. For seeding, RPE medium was supplemented with 1x Antibiotic-Antimycotic (Thermo Fisher Scientific, 15240062).

### **Quality control assays for iPSC derived cells:**

For quality control, RPE specific markers were stained via immunocytochemistry. Cells were washed with PBS (Gibco, 14190250). For fixation, 50 µl 4% PFA (Science Services, 15714-S) was added for 20 min at room temperature (RT) per well of a 384 well plate. Cells were washed twice with PBS and blocked for 1 h at RT with blocking buffer containing 1% BSA (Miltenyi Biotec, 130-091-376) and 0.3% Triton-X 100 (Sigma, T9284) in PBS. Primary antibodies were diluted in blocking buffer and incubated overnight at 4°C. Cells were then washed for 3 times with PBS. Secondary antibodies in blocking buffer were incubated for 2 h at RT in the dark. After washing 3 times with PBS, cells were incubated with Hoechst (Thermo Fisher Scientific, H3570) diluted 1:2000 in PBS for 30 min at RT in the dark. Cells were washed 3 times with PBS and plates were sealed with an aluminium foil and stored at 4°C in the dark until imaging. For imaging the high-content Operetta instrument from Perkin Elmer was used.

### **Antibodies used for quality control immunocytochemistry:**

<b>Substance</b>	<b>Supplier</b>	<b>Catalog no.</b>	<b>Dilution</b>
Bestrophin (E6-6) (BEST1)	Abcam	Ab2182	1:500
Ezrin (3C12)	SantaCruz	Sc587589	1:200
MERTK (Y323)	Abcam	Ab52968	1:1000
MITF	Abcam	Ab122982	1:500
PMEL17	R&D	NBP2-38185	1:500
RPE65	Neuromics	MO25011-100	1:250
ZO-1	BD	610966	1:200
Phalloidin-Alexa488	Thermo Fisher Scientific	A12379	1:200
Alexa Fluor 488, donkey anti-mouse	Thermo Fisher Scientific	A21202	1:500
Alexa Fluor 488, donkey anti-rabbit	Thermo Fisher Scientific	A21206	1:500

Trans-epithelial resistance (TER) measurements were performed in 3 transwells. As blank a Matrigel coated transwell without cells was used. Before measurement, cells were kept at RT for 5 minutes. Electrodes were sterilized with ethanol and preconditioned in RPE medium afterwards. The resistance in  $\Omega$  was measured across the upper and lower chamber on all three sites of the transwells. Blank was subtracted and resistance multiplied with the growth area of the transwell. Trans-epithelial resistance measurements were performed with the Epithelial Voltohmmeter EVOM<sup>2</sup> from World Precision Instruments.

## **2.2 High-content confocal imaging with OPERA Phenix**

### **2.2.1 Transfection and imaging of LC3-GFP-mCherry construct**

The LC3-GFP-mCherry construct was kindly provided by Guido Hermeij. It was transfected with Lipofectamine 2000 (Invitrogen, 52758) into HeLa cells and using ARPE-19 Cell Avalanche Transfection Reagent (EZ Biosystems, EZT-ARPE-1) into ARPE-19 cells.

For HeLa cell experiments, DNA and Lipofectamine 2000 were prediluted in OptiMEM (Gibco, 11058-021) and mixed in a ratio of 1:2. DNA-Lipofectamine mix were added to T25 flasks (Greiner, 690175) containing medium and cells seeded one day before. Per T25 flask 5  $\mu$ g DNA were added. Cells were incubated for 6 h in the incubator before changing to fresh medium. One day later, cells were reseeded in 96 well plates (Greiner, 655096) coated with Fibronectin (Sigma, F0895). For coating, Fibronectin was diluted 1:100 in Water for Injection (WFI) (Gibco, A1287301), 50  $\mu$ l added per well and incubated for 4 h at 37°C. Before seeding, wells were washed 3 times with WFI. Per well of the 96 well plate, 7000 cells were seeded in 100  $\mu$ l medium.

For transfection of ARPE-19 cells, DNA and ARPE-19 transfection reagent were prediluted in OptiMEM and mixed afterwards. The final DNA-transfection reagent mix contained 0.68  $\mu$ g DNA and 6.4  $\mu$ l transfection reagent in 200  $\mu$ l OptiMEM. This mix was vortexed for 2-3 sec and incubated for 15 min at RT. Different amounts were then added dropwise to the wells. Cells were seeded one day before in 96 well plates and centrifuged at 300xg for 5 min directly after DNA-transfection reagent addition. After the incubation for 5 h at 37°C in the incubator, medium was exchanged.

For compound treatment, cells were treated with 0.3% DMSO (Sigma, D2650), 3.3  $\mu$ M Torin1 (Selleckchem, S2827) and/or 50  $\mu$ M Chloroquine phosphate (Sigma,

PHR1258) 1 day after transfection. After an incubation time of 0.5, 2, 4, 6, 12, 18 and 24 h, medium was aspirated and cells were fixed with 4% PFA (Electron Microscopy Sciences, 15714-S) for 20 min at RT. Cells were washed once with PBS and incubated for 5 min at RT with DAPI (4',6-Diamidino-2-phenylindole dihydrochloride, Sigma, D9542). DAPI was diluted 1:2000 in PBS. Cells were washed 3 times with PBS and stored at 4°C in the dark until imaging. Imaging was performed using the confocal high content OPERA Phenix instrument from Perkin Elmer.

### **2.2.2 DQ-BSA and Cathepsin B – Magic Red Assay**

For the DQ-BSA and Magic Red assays, cells were seeded 1-2 days prior to the experiment in 384 well plates (Greiner, 781091).

DQ-BSA (Thermo Fisher Scientific, D12051) was added in a concentration of 10 µg/ml in trafficking medium. Trafficking medium was composed of DMEM (Gibco, 11960-44) supplemented with 1% FCS (Gibco, 10270-106), 1% NEAA (Gibco, 11140-035), 1% GlutaMax (Gibco, 35050-038) and 1% HEPES (Gibco, 15630-056). Cells were incubated for 1 and 6 h in the incubator after addition of DQ-BSA.

Magic Red – Cathepsin B (ImmunoChemistry Technologies, 938) was diluted in growth medium to a one-fold concentration and incubated with the cells for 30, 180 and 300 min in the incubator.

At the end of the respective incubation times cells were washed once with PBS and stained for 5 min at 37°C with Hoechst (Thermo Fisher Scientific, H1399) 1:1000 diluted in PBS. Cells were washed 3 times with PBS and imaged at the confocal high content OPERA Phenix instrument.

Bafilomycin A1 (BafA) (Sigma, B1793), a known inhibitor of the vacuolar H<sup>+</sup>-ATPase, was used as negative control. 100nM BafA was incubated for 30 min with the cells prior to addition of DQ-BSA/Magic Red dye.

### **2.2.3 Immunocytochemistry, colocalization and live cell imaging**

For immunocytochemistry and colocalization studies cells were fixed in 4% PFA diluted in PBS for 20 min, washed twice and then incubated with 3% BSA (Sigma, A7906), 0.1% Saponin (Sigma, S7900), 0.1% Triton-X-100 (Merck, 108603) in PBS (permeabilization/blocking buffer) for 1h. All following incubation steps were performed in permeabilization/blocking buffer. Cells were incubated with primary antibodies for 1-2 h, followed by secondary antibodies for 1 h. Cell nuclei were stained with DAPI (Sigma, D9542, 1:2000) or Hoechst (Thermo Fisher Scientific,

H1399, 1:5000) in parallel to secondary antibody incubations. In-between incubation steps cells were washed 4 times with PBS.

#### List of antibodies used for immunocytochemistry stainings:

Substance	Supplier	Catalog no.	Dilution
ATPase subunit C	Abcam	ab181243	1:2000
LAMP1	Santa Cruz	H4A3	1:350
LC3	MBL	PM036	1:400
LAMP2	DSHB	H4B4	1:500
NPC1	Abcam	ab134113	1:1000
TFEB	Cell Signaling Technologies	4240	1:100
mTOR	Cell Signaling Technologies	2983	1:200
Goat anti-mouse igG (H+L), CF 647	Sigma	SAB4600182	1:1000
Goat anti-rabbit igG (H+L), CF 568	Sigma	SAB46000085	1:1000

For live cell imaging with LysoTracker green (DND-26, Thermo Fisher, Scientific, L7526), cells were treated with 0.1  $\mu$ M LysoTracker and 1:1000 Hoechst for 5 min at 37°C. Afterwards, cells were washed three times with PBS and imaged directly afterwards.

Shigatoxin B labeled with Cy3 (ShTx-B-Cy3) (from the Institute Curie in Paris) was used to visualize Gb3. Staining with Shigatoxin was performed like a normal immunocytochemistry staining explained above. Cells were incubated with 3  $\mu$ M ShTx-B-Cy3 in parallel to primary antibodies.

Imaging was done with the OPERA Phenix confocal high-content screening system (Perkin Elmer). For most recordings the 20x water objective was used. Laser settings were individual for each experiment, but generally laser power was set between 50 and 100% and exposure time was not exceeding 200 msec.

The image analysis was performed using ACapella 5.1, in a Columbus 2.9 environment via texture thresholding.

Nuclei detection was done on DAPI or Hoechst staining. After intensity based thresholding, the detected objects were further filtered by size, roundness and contrast.

Starting from the detected nuclei, the cell boundary was determined. Cell boundary detection was based on the cytoplasmic background signal of any of the other stainings mentioned above. For colocalization, the intersection of detected texture

masks was calculated. Colocalized objects were used for mean cytoplasm intensity calculations of the corresponding channels. Then, colocalized objects in the cytoplasm were counted and divided by the cell count. The total area covered by colocalized objects divided by the area covered by detected aggregates of one or the other staining was calculated individually.

In case of TFEB, no texture thresholding was done. Instead, a ratio of mean TFEB intensity in the nucleus divided by mean TFEB intensity in the cytoplasm was calculated.

All aggregation methods were performed on a cell, then field, then well-level.

Bar graphs were assembled using Graph Pad Prism and statistically analyzed using the student's t-test or a two-way ANOVA.

Image analysis was done in cooperation with Carina Wollnik.

#### **2.2.4 TFEB knockdown using siRNAs**

Cell cycle arrested ARPE-19 cells were seeded in 384 well plates (Greiner, 781091) and kept in the incubator for 3 days. siRNAs, obtained from Dharmacon (TFEB siRNA: D-009798-03, target sequence: AGACGAAGGUUCAACAUCA and scrambled siRNA: D-001810-10-20, ON-TARGET plus Non-targeting Pool) were transfected using the Lipofectamine RNAiMAX transfection kit (Thermo Fisher Scientific, 13778030). siRNAs and transfection reagent were diluted individually in OptiMEM (Gibco, 11058-021), mixed 1:1, incubated for 5 min at RT and given to the cells. Per well of a 384 well plate 1  $\mu$ M siRNA and 0.1  $\mu$ l transfection reagent were added. Cells were incubated for another 4 days, treated with TRPML1 agonists for 2 days (48 h) and fixed and stained for TFEB, LAMP1 and SubC (see immunocytochemistry for protocol).

### **2.3 Electron microscopy**

Electron microscopy imaging was performed in cooperation with Dr. Michaela Schweizer from the ZMNH. ARPE-19 WT and CLN3-KO cells were fixed with 1% wt/vol glutaraldehyde and 4% paraformaldehyde in 0.1 M PB, pH 7.2 overnight. Thereafter the cells were centrifuged 3 times at 1000xg after each washing step with PBS. The pellets were embedded in 3% agarose (Invitrogen) and small pieces were cut and rinsed three times in 0.1 M sodium cacodylate buffer (pH 7.2–7.4). The cell

pieces were incubated in 1% osmium tetroxide in cacodylate buffer for 20 min on ice. After osmication, the cells were dehydrated using ascending ethyl alcohol concentration steps, followed by two rinses in propylene oxide. Infiltration of the embedding medium was performed by immersing the samples in a 1:1 mixture of propylene oxide and Epon and finally in neat Epon and polymerized at 60°C. Semithin sections (0.5 µm) from cells were prepared for light microscopy mounted on glass slides and stained for 1 min with 1% Toluidine blue. Ultrathin sections (60nm) were examined in an EM902 (Zeiss, Germany). Pictures were taken with a MegaViewIII digital camera (A. Tröndle, Moorenweis, Germany).

For quantification the 'measurement' tool, 'polygon' with the option 'smooth in' from the Image SP software were used. 16 images per condition were analyzed.

## 2.4 Immunoblotting

Cells were dissociated in 0.05% Trypsin-EDTA (Thermo-Fisher, 25300-054), washed with PBS and lysed in RIPA buffer (Sigma, R0278) containing 1x protease and phosphatase inhibitor cocktail (Roche, cOmplete Tablets 04693159001, PhosStop 04906837001). Protein amounts were quantified using the BCA protein assay (Thermo Fisher Scientific, 23227). For LC3 blotting, 16% Tris-Glycine gels, for all other proteins, 4-12% Bis-Tris gels from Thermo Fisher Scientific were used. Protein amounts between 20-30 µg/sample were used for most experiments. Proteins were immunoblotted on 0.2 µm nitrocellulose membranes (GE Healthcare Amersham, 10600006). For blocking and antibody incubation 5% BSA (Sigma, A7906) or 5% milk powder (Heirler, 4010318030305) diluted in TBS-T (Roth, 1061.1) were used. Protein bands were visualized via chemiluminescence using Pierce ECL Western blotting substrate (Thermo Fisher Scientific, 32209) and the Developer (SRX 101A). Protein bands were quantified using Fiji ImageJ.

### List of antibodies used for immunoblots:

Substance	Supplier	Catalog no.	Dilution
LAMP1	Abcam	Ab24170	1:1000
LAMP2	DSHB	H4B4	1:500
NPC1	Abcam	Ab134113	1:2000
LC3	Cell Signaling Technologies	2775	1:500
TFEB	Cell Signaling Technologies	4240	1:500
mTOR	Cell Signaling Technologies	2983	1:800
Phospho mTOR (Ser2448)	Cell Signaling Technologies	2971	1:500

P70S6 kinase	Cell Signaling Technologies	9202	1:500
Phospho p70S6 kinase (T389)	Cell Signaling Technologies	9205	1:200
S6 protein	Cell Signaling Technologies	2217	1:1000
Phospho S6 protein (Ser240/244)	Cell Signaling Technologies	2215	1:500
Cathepsin B	R&D	AF953	1:800
Cathepsin D	Abcam	Ab75852	1:5000
TPP1	Abcam	Ab195234	1:1000
Vinculin	Abcam	Ab129002	1:10 000
GAPDH	Sigma	G9545	1:10 000
Anti-rabbit HRP	Dako	P0448	1:2000
Anti-mouse HRP	Dako	P0447	1:1500
Anti-goat HRP	Dako	P0449	1:2000

## 2.5 BMP/LBP analysis using mass spectrometry

BMP experiments were performed in collaboration with the Proteomics and Metabolomics department at Evotec.

### Sample preparation:

Cells were vortexed 15 sec and sonicated 1 min in 1 ml MeOH: H<sub>2</sub>O 5mM EGTA (2:1). After sonication, samples were transferred in 10 ml borosilicate tubes containing 10 ng of internal standard (BMP 14:0/14:0). 2.5 ml methanol and 2 ml water were added for liquid/liquid extraction followed by the addition of 2.5 ml dichloromethane. In order to avoid emulsion, 80 µl of saturated sodium chloride were added. The homogenate was vortexed for 5 min at RT, then centrifuged at 2500xg for 10 min. The lower organic phase was evaporated under a stream of nitrogen at 37°C. The dried residue was reconstituted in 100 µl methanol with 10 mM ammonium formate. 10 µl of the dissolved reconstitute was used for liquid chromatography and tandem mass spectrometry analysis (LC-MS/MS). A similar extraction protocol was used for analysis of supernatants. The liquid/liquid extraction was performed with 2 ml water.

### Analytical Method:

Samples were directly injected into an ACE3 C18 column (2.1 x 50 mm; 1.7 µm) from AIT (Cormeilles-en-Paris, France) with a water/methanol gradient. Mobile phase A was composed of water with 10 mM ammonium formate, whereas mobile phase B contained methanol with 10 mM ammonium formate. Samples were run with 95%

phase B for 2 min, 95 to 100% phase B for 0.5 min and 100% phase B for 9.5 min. Flow rates were set to 0.4 ml/min from 0 to 2 min and 12.5 to 15 min and changed to 0.2 ml/min from 2.5 to 12 min.

Bis(monoacylglycerol)phosphate species (BMPs) and internal standard (BMP 14:0/14:0) were analyzed on a Quantum Ultra triple quadrupole (Thermo Electron Corporation, San Jose, CA, USA). Positive electrospray was performed on a Thermo IonMax ESI probe. To increase the sensitivity and specificity of the analysis, multiple reaction monitoring was used with following MS/MS transitions: BMP 28:0 MH<sup>+</sup>, 667,5-285,3; BMP 32:0 MH<sup>+</sup>, 723,5-313,5; BMP 32:1 MH<sup>+</sup>, 721,5-313,5; BMP 32:2 MH<sup>+</sup>, 719,5-311,5; BMP 34:0 MH<sup>+</sup>, 751,5-341,6; BMP 34:1 MH<sup>+</sup>, 749,5-339,3; BMP 34:2 MH<sup>+</sup>, 747,5-339,3; BMP 36:0 MH<sup>+</sup>, 779,6-341,6; BMP 36:1 MH<sup>+</sup>, 777,6-339,3; BMP 36:2 MH<sup>+</sup>, 775,5-339,3; BMP 36:3 MH<sup>+</sup>, 773,5-339,3; BMP 36:4 MH<sup>+</sup>, 771,5-337,5; BMP 38:1 MH<sup>+</sup>, 805,6-339,3; BMP 38:2 MH<sup>+</sup>, 803,6-339,3; BMP 38:3 MH<sup>+</sup>, 801,6-339,3; BMP 38:4 MH<sup>+</sup>, 799,5-339,3; BMP 38:5 MH<sup>+</sup>, 797,5-339,3; BMP 38:6 MH<sup>+</sup>, 795,5-337,5; BMP 40:1 MH<sup>+</sup>, 833,6-339,3; BMP 40:2 MH<sup>+</sup>, 831,6-339,3; BMP 40:3 MH<sup>+</sup>, 829,6-339,3; BMP 40:4 MH<sup>+</sup>, 827,6-339,3; BMP 40:5 MH<sup>+</sup>, 825,6-339,3; BMP 40:6 MH<sup>+</sup>, 823,5-339,3; BMP 40:7 MH<sup>+</sup>, 821,5-339,3; BMP 40:8 MH<sup>+</sup>, 819,5-361,5; BMP 40:10 MH<sup>+</sup>, 815,5-385,6; BMP 42:10 MH<sup>+</sup>, 843,5-361,5; BMP 44:10 MH<sup>+</sup>, 871,5-387,6; BMP 44:1 MH<sup>+</sup>, 869,5-387,6; BMP 44:12 MH<sup>+</sup>, 867,5-385,6. The annotation MH<sup>+</sup> is indicating a measurement in positive ion mode, where M corresponds to the mass of the BMP and H to hydrogen. Collision energy for each transition was 30 eV and the tube lens had 170 arbitrary units.

Following spray chamber settings were used: heated capillary, 400°C; spray voltage, 5000 V; sheath gas, 40 arbitrary units; auxiliary gas 10 arbitrary units. Calibration curves were produced by using synthetic BMP 18:1/18:1 and BMP 14:0/14:0 (Avanti Polar Lipid, Alabaster, AL, USA). The amounts of BMP 18:1/18:1 in the samples were determined by using inverse linear regression of standard curves. The relative quantification of the BMP species without analytical standard was performed using BMP 18:1/18:1 calibration curve. Values are expressed as pg per million of cells.

## **2.6 mRNA expression analysis**

Cells were treated as indicated. Dissociation of cells and RNA isolation was done according to manual instructions using RNeasy Mini Kit (Qiagen, 74004). Reverse transcription into cDNA was performed using the SuperScript III First Strand kit

(Invitrogen, 18080-051). For real-time quantitative PCR (RT-qPCR) QuantiTect SYBR Green PCR Kit (Qiagen, 204145) and the LightCycler 480 system II from Roche were used. The LightCycler protocol comprised a denaturation step (95°C for 15 min), the amplification with 40 cycles (95°C for 15 sec, 55°C for 30 sec and 72°C for 30 sec), a melting curve (from 60°C to 95°C in 16 sec) followed by a cool down (37°C for 10 sec). *GAPDH* was chosen as reference gene for analysis of *CLN3* expression, whereas *PPIB* was used as reference gene for all other qPCR experiments. The following primers were used: *CLN3* fw: 5'-GGGTTCTCGTCAGTGGGATT-3', rev: 5'-TAGCGAAGACCACACCACAC-3'; Quantitect primers from Qiagen: Hs\_TFEB\_1\_SG (QT00069951), Hs\_LAMP1\_1\_SG (QT00070994), Hs\_LAMP2\_1\_SG (QT00077063), Hs\_NPC1\_1\_SG (QT00066465), Hs\_CTSB\_1\_SG (QT00088641), Hs\_CTSD\_1\_SG (QT00020391), Hs\_TPP1\_1\_SG (QT00097363), Hs\_MAP1LC3B\_1\_SG (QT00055069), Hs\_PPIB\_1\_SG (QT00067186).

Relative quantification was performed using the  $2^{-\Delta\Delta CT}$  method<sup>62</sup>, except for *CLN3* expression. CT values for *CLN3* mRNA were set in relative relation to CT values of *GAPDH*.

## 2.7 Lysosomal exocytosis

Compound treatment was performed in MEM medium containing 10 mM HEPES. Medium was discarded, cells were washed once with PBS and incubated with Trypsin-EDTA for 5 min at 37°C. Double the amount of cold medium was added and the cell suspension was centrifuged at 200xg for 5 min at 4°C. The cell pellet was resuspended in 1% BSA/PBS containing LAMP1 antibody (Santa Cruz, H4A3, 1:400) and incubated for 20 min on a rotating wheel in the cold room. After centrifugation (200xg, 5 min, 4°C), the cell pellet was resuspended in 1% BSA/PBS containing secondary fluorescence antibody (PE anti-mouse IgG1, BioLegend, 406608) and incubated for 1 h as described above. After an additional centrifugation step, the cell pellet was resuspended in 100  $\mu$ l ice cold PBS. 0.2  $\mu$ l Zombie NIR viability dye (BioLegend, 77184) was added to distinguish between living and dead cells. Cells were kept on ice until their flow cytometry analysis with the FACS Canto II from BD-Biosciences. 40  $\mu$ l of cell samples were analyzed with a flow rate of 1  $\mu$ l/sec. With the forward and sideward scatter (FSC and SSC) size and granularity of cells was measured. Using APC-Cy7 fluorescence, viable cells were detected and PE

fluorescence showed amount of LAMP1 positive cells. To reach a total of 10 000 events (cells) for each condition, gates were set as shown in the results part.

## 2.8 Lysosomal patch clamp analysis

Lysosomal patch clamp experiments were performed by Rachel Tang, from LMU Munich. ARPE-19 cell lines were treated with 1 mM Apilimod (Axon Medchem, 1326) overnight before performing whole-endolysosomal patch-clamp. Currents were recorded using the EPC-10 patch-clamp amplifier (HEKA, Lambrecht, Germany) and PatchMaster acquisition software (HEKA). Data were digitized at 40 kHz and filtered at 2.8 kHz. For application of the TRPML1 agonist (ML-SA1) and antagonist (ML-SI3), cytoplasmic solution was completely exchanged by cytoplasmic solution containing agonists. Cytoplasmic solution contained 140 mM K-MSA, 5mM KOH, 4 mM NaCl, 0.39 mM CaCl<sub>2</sub>, 1 mM EGTA and 10 mM HEPES (pH was adjusted KOH to 7.2). The luminal solution contained 140 mM Na-MSA, 5 mM K-MSA, 2 mM Ca-MSA, 1 mM CaCl<sub>2</sub>, 10 mM HEPES and 10 mM MES (pH was adjusted with methanesulfonic acid to 4.6). 500 ms voltage ramps from -100 to +100 mV were applied every 5 s in all of the patch-clamp experiments. All statistical analysis were evaluated using GraphPadPrism9.0 software.

## 2.9 Compound treatments

For several experiments and assays compound treatments were performed. Many compounds are diluted in DMSO, therefore 0.3% DMSO was used as control treatment. Compound treatment times and concentrations varied between experiments and are indicated in the respective figure legends.

### List of compounds used:

Compound	Supplier	Catalog no.
DMSO	Sigma	D2650
MK6-83	BioTechne	5547
ML-SA1	BioTechne	4746
ML-SA5	Synthesized at Evotec	-
ML-SI3	Enamine	EN300-314172
Torin 1	Tocris	4247
Chloroquine phosphate	Sigma	PHR1258
Bafilomycin A1	Sigma	B1793

Mitomycin C	Merck (Roche)	10107409001
Ionomycin	Cell Signaling Technologies	9995

### 3. Results

#### 3.1 CLN3 deficient cell lines to study the role of the CLN3 protein

To study the role of CLN3 in the lysosomal-autophagosomal system, different CLN3 deficient cell lines and their respective isogenic WT controls were analyzed (Figure 10). Via CRISPR gene editing, the CLN3 protein was knocked out in three cell lines: HeLa, ARPE-19 and iPS cells. HeLa cells are immortalized cervical cancer cells and the oldest, most widely distributed, permanent human cell line used in scientific research<sup>63</sup>. The ARPE-19 cell line originates from a 19 year old donor. Dissected retinal pigment epithelium (RPE) cells were cultivated and spontaneously immortalized. ARPE-19 cells can be cultivated as a monolayer, which still express RPE-specific markers<sup>64</sup>. Induced pluripotent stem cells (iPSCs) are generated from somatic cells of adult tissue. By introducing a set of transcription factors, also known as the 'Yamanaka factors', cells are reprogrammed to pluripotent stem cells and can be differentiated into various kinds of cell types<sup>65</sup>.

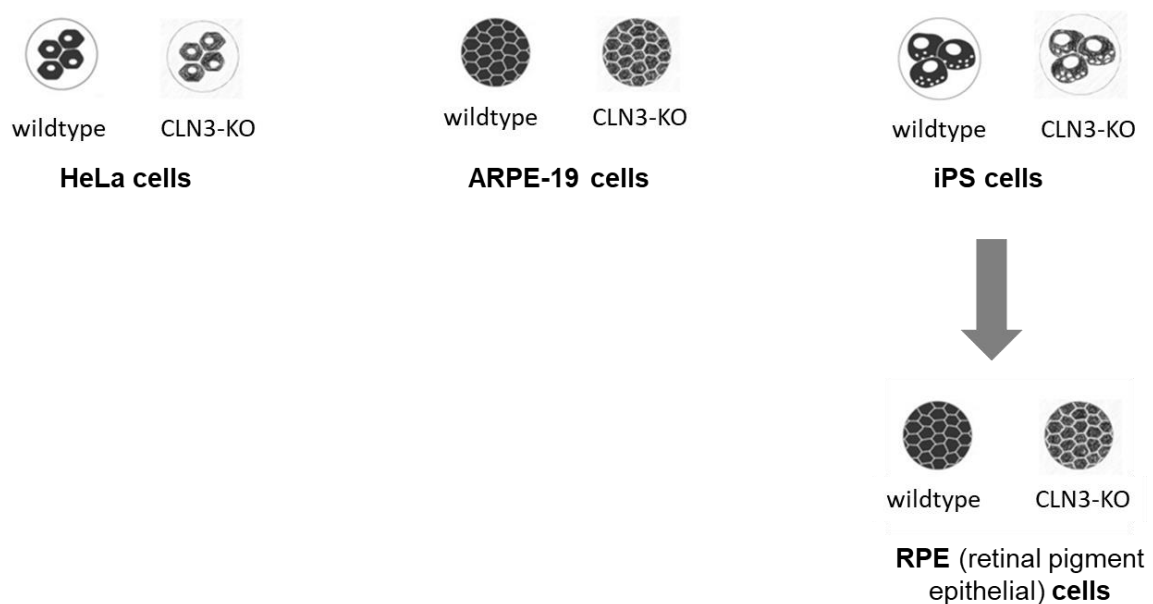


**Figure 10: Available CLN3 deficient cell lines.** Different cell lines from different sources were available for this study. CRISPR gene editing was used to generate isogenic CLN3 knockout clones in HeLa, ARPE-19 and iPS lines. The HeLa CLN3-KO line was provided by Guido Hermey, ARPE-19 CLN3-KO cells were produced at Evotec, the iPS CLN3-KO line was provided by Gemma Gomez-Giro, Luxembourg Centre of Biomedicine. The iPS cells were further differentiated into retinal pigment epithelium cells.

The HeLa CLN3-KO cell line, originating from Guido Hermey's lab at the Zentrum für Molekulare Neurobiologie Hamburg (ZMNH), was generated by Dr. Abuzuar Kaleem and Dr. Sandra Oetjen. The indel mutation introduced by CRISPR gene editing

resulted in a frame shift causing an altered amino acid sequence starting at position 15 and a premature stop codon at position 54 (p.Glu15fs\*45). Sequence variants are described following guidelines from den Dunnen *et al.* 2016, where 'fs' marks a frameshift and '\*' a premature stop codon<sup>66</sup>.

The ARPE-19 CLN3-KO cell line was generated in close collaboration with the CRISPR department at Evotec, which is described below (chapter 3.1.1.).

The iPS cell line was produced by Gemma Gomez-Giro, from Luxembourg Centre for Systems Biomedicine. It carries the transition c.1054C>T on the genomic level, leading to an amino acid exchange and a premature stop codon in exon 13 (p.Gln352\*). WT and CLN3-KO iPS cells were differentiated into retinal pigment epithelium (RPE) cells. The differentiation process as well as quality controls of the RPE cell lines are shown in chapter 3.1.2.

### **3.1.1 Generation of ARPE-19 CLN3-KO cell line**

Using CRISPR gene editing, a CLN3 knockout ARPE-19 cell line (ARPE-19 CLN3-KO) was generated in close collaboration with the CRISPR department at Evotec. Guide RNA corresponds to the genomic sequence in exon 3 (Figure 11 B). The generated CLN3-KO clone carries on genomic level 8 nucleotide deletions on both alleles (g.[377-384del+383-390del]), leading to a frameshift and a premature stop codon at amino acid position 156 (p.[Glu127fs\*156+Gln127fs\*156]). Quantitative RTqPCR showed significant decrease of CLN3 mRNA levels in ARPE-19 CLN3-KO cells (Figure 11 A). Primers to verify the CLN3 knockout on mRNA level were located in exon 6 and 7 (Figure 11 B).

The WT CLN3 protein is predicted to have 6 transmembrane domains and to localize to lysosomal membranes<sup>45,46</sup> (Figure 11 C). Topology studies suggest that the CLN3 protein of the generated ARPE-19 CLN3-KO line only contains the first transmembrane domain (Figure 11 D). This is an even shorter protein, than the 3 transmembrane domain containing protein predicted to remain with the exon 7-8 ( $\Delta$ Ex7/8) deletion, the most frequent CLN3 mutation occurring in JNCL patients (Figure 11 E).

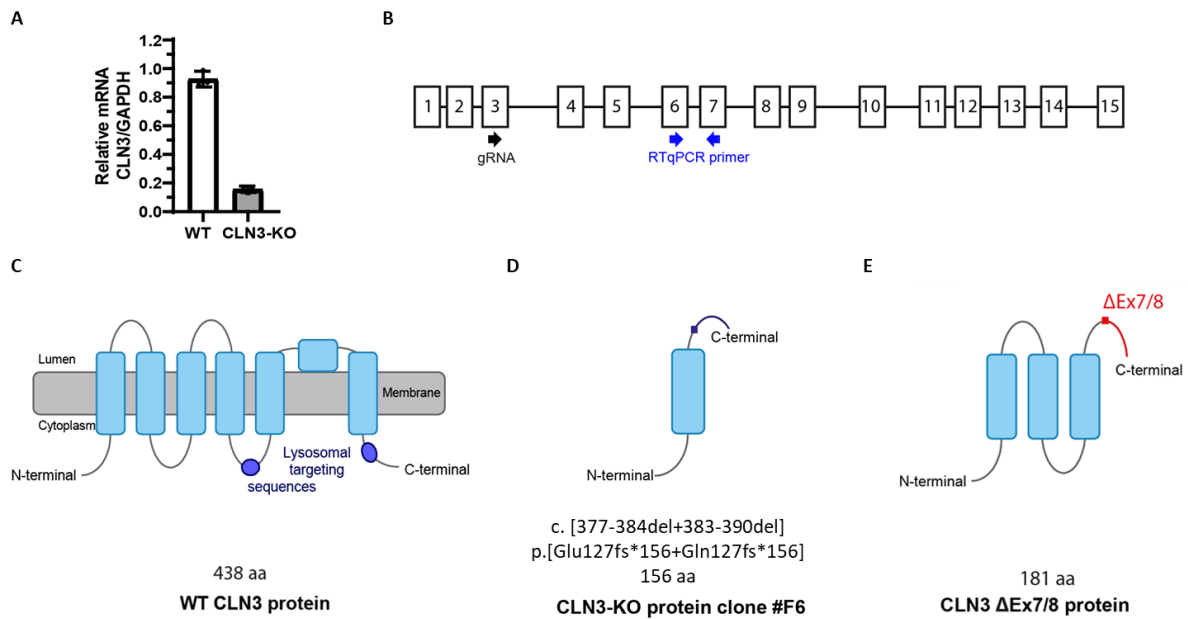


**Figure 11: Generation of ARPE-19 CLN3-KO cell line.** **A** Relative mRNA expression of CLN3, normalized to GAPDH, analyzed by real-time qPCR. Plot summarizes three biological replicates with each three technical replicates from one experiment. **B** CLN3 mRNA scheme, showing guide RNA (gRNA) position used to generate ARPE-19 CLN3-KO cell line via CRISPR technology. qPCR primers to verify knockout are also depicted. **C, D, E** Expected CLN3 protein appearances: WT protein (**C**), generated CLN3-KO clone in ARPE-19 cells (**D**), common CLN3  $\Delta$ Ex7/8 mutant (**E**).

In summary, all available cell lines (HeLa, ARPE-19 and iPS cells) carry mutations in the *CLN3* gene, leading to premature stop codons. These are known to initiate mRNA degradation by nonsense-mediated decay, especially when located upstream of introns<sup>67</sup>. However, if mRNA could escape this mechanism, resulting proteins would lack the lysosomal targeting sequence and get most probably stuck in the ER, which will prevent CLN3 transport to lysosomes. Based on this, all CLN3-KO cells are regarded as suitable cell models to study JNCL disease.

### 3.1.2 Differentiation of iPS cells to RPE cells

The CLN3 deficient iPS cells and the corresponding isogenic WT cell line were differentiated into RPE cells in collaboration with colleagues from the stem cell department of Evotec. After a differentiation period of 65 days (Figure 12 A), pigmented WT and CLN3-KO RPE cells were analyzed for RPE markers, such as Phalloidin, RPE65, ZO-1, EZRIN, BEST1, MITF, MerTK and PMEL17. No differences in RPE expression markers were found between WT and CLN3-KO cells (Figure 12 B, and data not shown). A decreased barrier function of iPSC derived RPE CLN3-KO cells was detected by measuring trans-epithelial resistance (TER) (Figure 12 C).

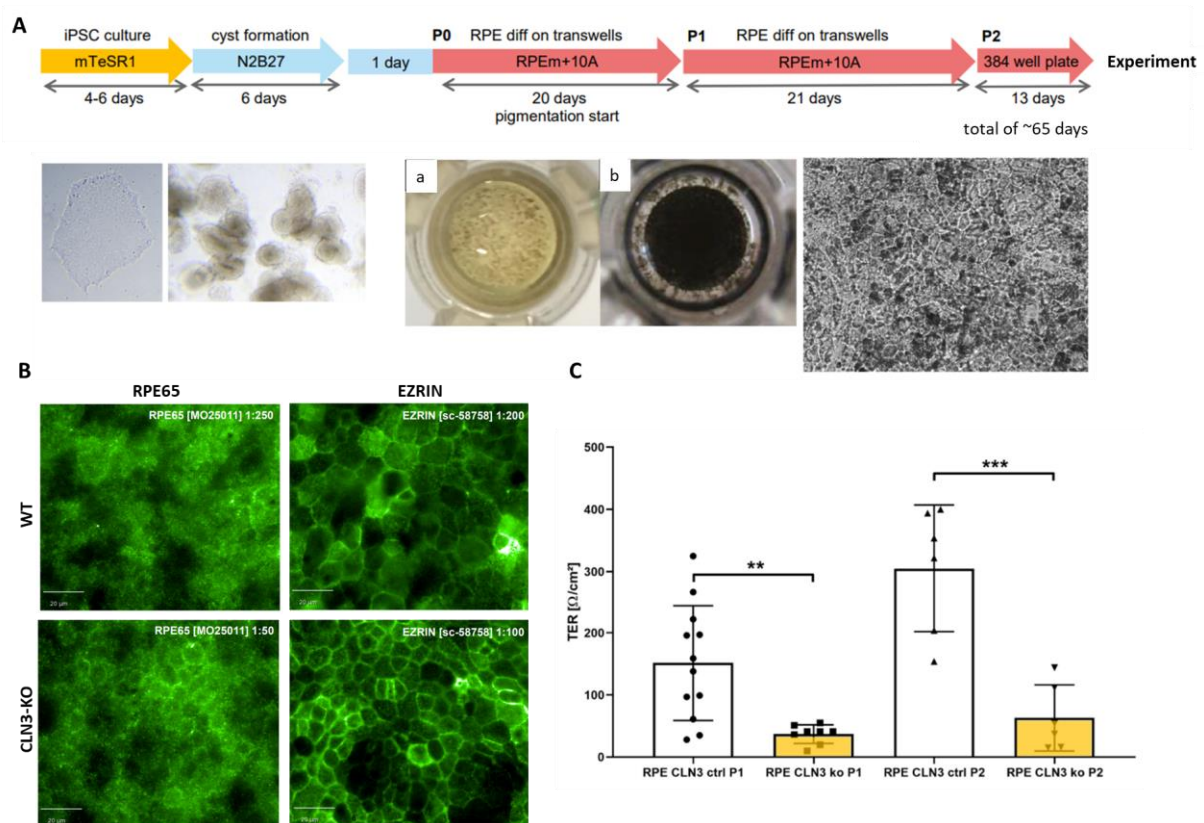


**Figure 12: Quality controls of WT and CLN3-KO iPSC cells differentiated into RPE cells. A** Process of RPE differentiation. a: unpigmented cells, b: pigmented cells. **B** Representative immunocytochemical images of RPE65 and EZRIN stained iPSC derived RPE WT and CLN3-KO cells. Scale bar: 20 μm. **C** Trans-epithelial resistance (TER) measurement of iPSC derived RPE WT and CLN3-KO cells in Passage 1 (P1) and Passage 2 (P2).

## 3.2 Phenotypic characterization of CLN3 deficient cells

The role of the CLN3 protein within the cell is still unknown. However, several cellular dysfunctions have been described for CLN3 deficient cells<sup>55,56,52,51,57,58</sup>. To identify, which of the available cell lines would be a suitable cellular model to study CLN3 disease, the endosomal, autophagosomal and lysosomal systems were investigated in more detail.

### 3.2.1 Altered lysosomal degradation capacity in CLN3 deficient cells

The double-quenched BSA dye (DQ-BSA) enters the cell via endocytosis and serves, after its hydrolysis in lysosomes, as a measure of a functional endocytic pathway and overall lysosomal proteolytic capacity. Low fluorescence intensities in all cell lines and genotypes after 1 hour of incubation with DQ-BSA showed that the dye was not proteolytically cleaved in lysosomes yet and longer incubation times were needed. After 6 hours of incubation, DQ-BSA fluorescence intensity was altered in all three investigated CLN3-KO cell lines (Figure 13). Bafilomycin A1 (BafA) treated cells were

used as negative control, as it is an inhibitor of the vacuolar H<sup>+</sup>-ATPase leading to a decreased lysosomal pH and thus reduced lysosomal enzyme activity as well as impaired lysosomal-endosomal fusion processes<sup>68</sup>.

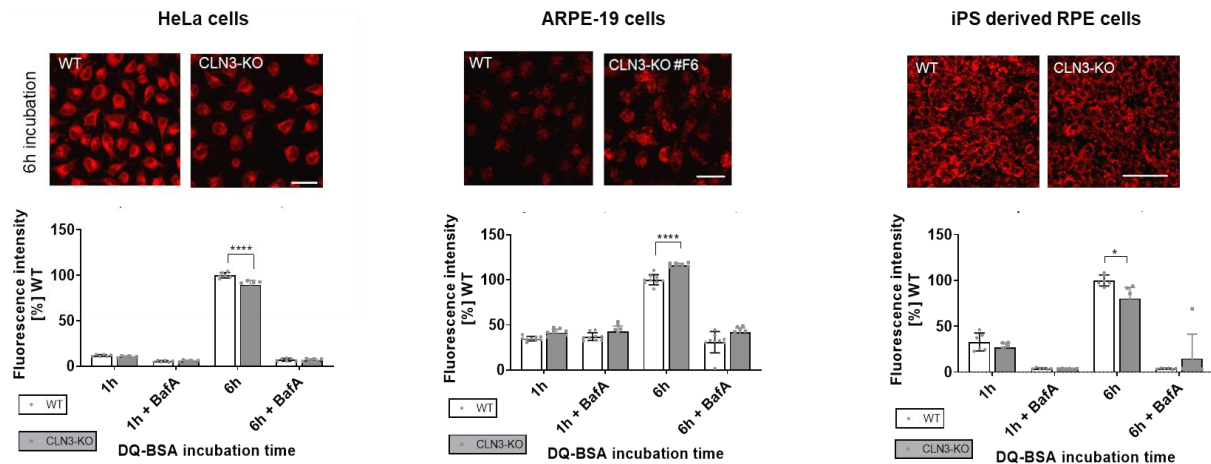


**Figure 13: Impaired endocytic trafficking or altered lysosomal proteolytic capacity in CLN3 deficient cells.** HeLa, ARPE-19 and iPSC derived RPE WT and CLN3-KO cells were incubated with DQ-BSA for 1 and 6 hours. Fluorescence intensity was normalized to WT 6 h condition respectively for each genotype. Bafilomycin A1 (BafA) treatment was used as negative control. High content confocal imaging with number of experiments (n). For each experiment 3 wells per condition and 9 images per well were analyzed. Number of experiments: HeLa cells n=2, ARPE-19 cells n=3, iPSC derived RPE cells n=2. P-values calculated by two-way ANOVA coupled with multiple comparisons using Sidak test. ns nonsignificant<0.1234, \*p-value<0.0332; \*\*p<0.0021, \*\*\*p-value<0.0002, \*\*\*\*p-value<0.0001. Scale bar: 50  $\mu$ m.

CLN3 deficient HeLa and iPSC derived RPE cells showed decreased DQ-BSA signals, whereas ARPE-19 cells exhibited increased fluorescence intensities after 6 h of incubation (Figure 13). To investigate if these differences found between the cell lines are caused by altered lysosomal degradation capacity, the cathepsin B – Magic Red assay was performed.

Cathepsin B – Magic Red dye is a membrane permeable substrate, which liberates a fluorescent cresyl violet fluorophore upon cleavage by cathepsin B within lysosomal compartments. In contrast to DQ-BSA, the Magic Red dye is acting independent of endocytic trafficking, and is therefore a suitable substrate to investigate lysosomal degradation capacity. Treatment of HeLa, ARPE-19 and iPSC derived RPE cells with Magic Red, revealed an altered cathepsin B activity in CLN3 deficient HeLa and ARPE-19 cells (Figure 14).

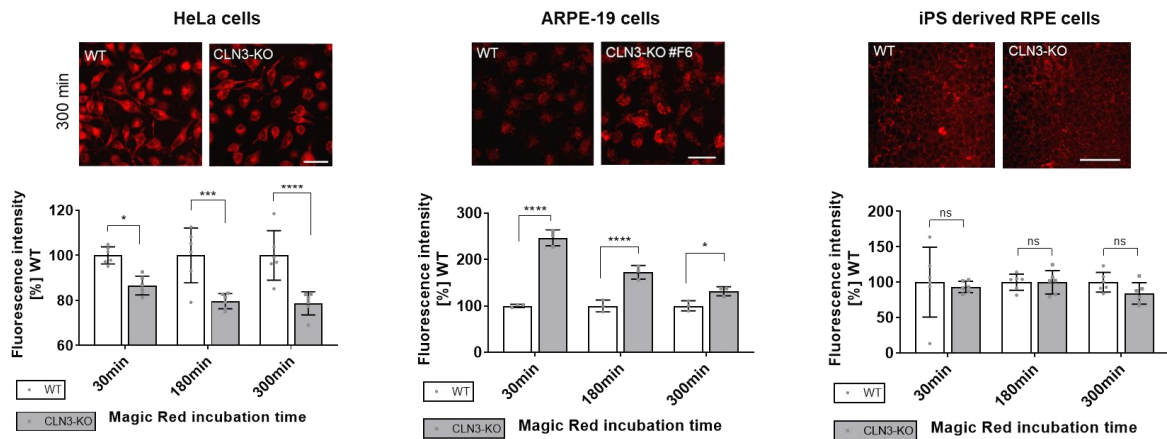


**Figure 14: Altered cathepsin B activity in HeLa and ARPE-19 cells.** HeLa, ARPE-19 and iPSC derived RPE WT and CLN3-KO cells were incubated with cathepsin B – Magic Red dye for 30, 180 and 300 min. Fluorescence intensity was normalized to WT respectively for each incubation time and genotype. High content confocal imaging with number of experiments (n). For each experiment 3 wells per condition and 9 images per well were analyzed. Number of experiments: HeLa cells n=2, ARPE-19 cells n=1, iPSC derived RPE cells n=2. P-values calculated by two-way ANOVA coupled with multiple comparisons using Sidak test. ns nonsignificant<0.1234, \**p*-value<0.0332; \*\**p*<0.0021, \*\*\**p*-value<0.0002, \*\*\*\**p*-value<0.0001. Scale bar: 50  $\mu$ m.

HeLa CLN3-KO cells showed a reduced Magic Red fluorescence intensity compared to WT cells, with the most significant difference between WT and CLN3-KO cells after 300 min incubation. However, in ARPE-19 CLN3-KO cells cathepsin B activity was increased compared to WT cells, with the biggest difference after 30 min incubation time (Figure 14). CLN3 deficient iPSC derived RPE cells showed no alterations in Magic Red staining. These partially contradictory results indicate an altered lysosomal degradation capacity in CLN3 deficient cells. Especially in ARPE-19 CLN3-KO cells, increased levels of DQ-BSA and cathepsin B – Magic Red could also be elicited by differences in lysosomal number or size.

### 3.2.2 Increased levels of LAMP1 protein in CLN3 deficient ARPE-19 cells

To investigate if lysosomal amounts are altered in the different cell lines, lysosomal membrane protein LAMP1 was investigated using immunocytochemistry. LAMP1 immunofluorescence was significantly increased in CLN3-KO ARPE-19 cells, whereas CLN3 deficient HeLa and iPSC derived RPE cells did not show a significant difference to their WT controls (Figure 15).

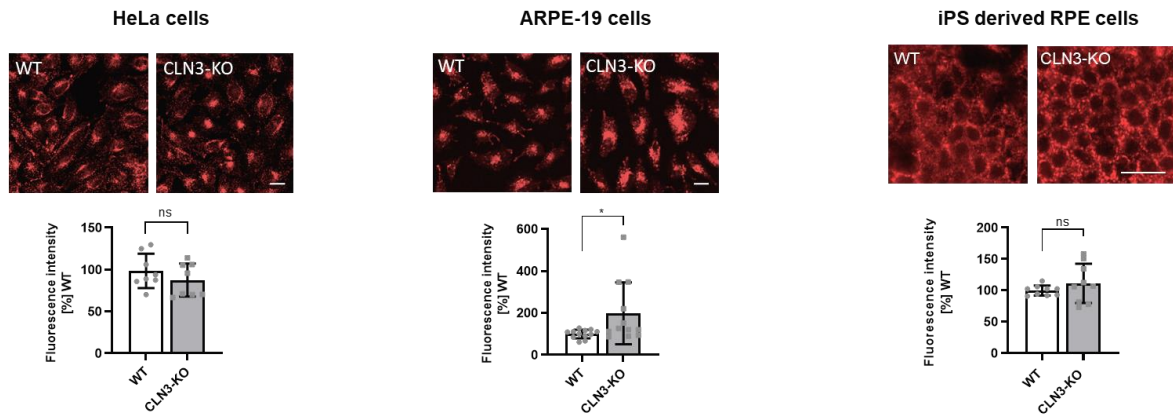


**Figure 15: Increased LAMP1 protein levels in ARPE-19 CLN3-KO cells.** LAMP1 immunofluorescence of HeLa, ARPE-19 and iPSC derived RPE WT and CLN3-KO cells. Fluorescence intensity was normalized to WT respectively for each cell type. High content confocal imaging with number of experiments (n). For each experiment 3 wells per condition and 9 images per well were analyzed. Number of experiments: HeLa cells n=3, ARPE-19 cells n=3, iPSC derived RPE cells n=3. P-values calculated by two-tailed unpaired students t-test. ns nonsignificant<0.1234, \*p-value<0.0332; \*\*p<0.0021, \*\*\*p-value<0.0002, \*\*\*\*p-value<0.0001. Scale bar: 20  $\mu$ m.

Increased LAMP1 protein levels point towards an accumulation of lysosomes in ARPE-19 CLN3-KO cells.

### 3.2.3 Autophagic flux

Several studies have documented defects in the autophagy pathway in CLN3 deficient cells<sup>55,57,52</sup>. Therefore, autophagic flux kinetic was investigated using a tandem fluorescent LC3-GFP-mCherry construct. The lipidated form of LC3, called LC3-II is present on autophagosomes<sup>69</sup> and an established marker for autophagy<sup>32</sup>. Upon fusion of autophagosomes with acidic lysosomes, the fluorescent GFP signal is quenched by the low lysosomal pH, whereas the pH stable mCherry is still detectable. This change in fluorescence levels allows visualization of autophagic flux<sup>70</sup>. The LC3-GFP-mCherry construct was transfected into HeLa and ARPE-19 WT and CLN3-KO cells. iPSC derived RPE cells were due to the high cell numbers needed for transfection optimization excluded from this experiment. Green and red fluorescence intensities of HeLa cells were tracked for a time-course of 24 hours. Under normal conditions (DMSO treatment), no differences in red and green fluorescences were detected between WT and CLN3-KO cells (Figure 16 A). As controls Torin1 and Chloroquine were used. The mTOR inhibitor Torin1 induces autophagy<sup>18</sup>, whereas Chloroquine inhibits fusion of autophagosomes with lysosomes and thereby blocks autophagy<sup>71</sup>. HeLa WT and CLN3-KO cells treated with Torin1 showed increased levels of red fluorescence. By simultaneous treatment

with Torin1 and Chloroquine, in addition to red also green fluorescence intensities were elevated (Figure 16 A). These results confirm a functional autophagy induction and inhibition in CLN3 deficient cells. No difference between WT and CLN3-KO cells could be detected.

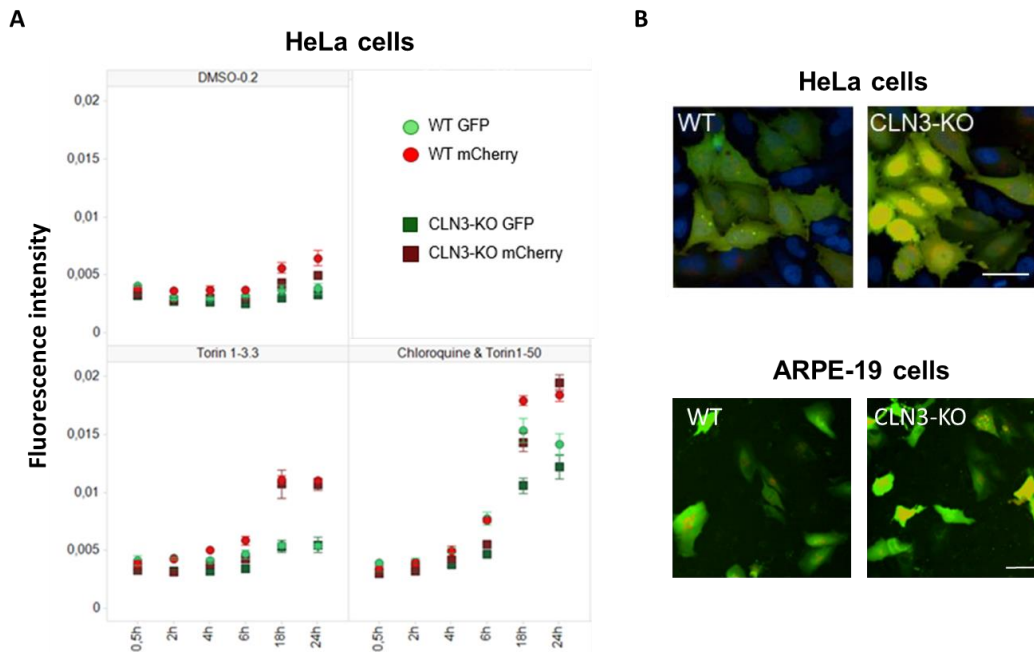


**Figure 16: Autophagic flux kinetics not altered in CLN3 deficient HeLa cells.** HeLa and ARPE-19 WT and CLN3-KO cells were transfected with the LC3-GFP-mCherry construct. **A** Red and green fluorescence intensities of HeLa WT and CLN3-KO cells over a time-course of 24 hours. Cells were treated with DMSO (vehicle), 3.3 $\mu$ M Torin1 and a combination of 50  $\mu$ M Chloroquine with 3.3  $\mu$ M Torin1. **B** Representative fluorescence images of HeLa and ARPE-19 WT and CLN3-KO cells transfected with LC3-GFP-mCherry construct. Scale bar: 50  $\mu$ m.

The LC3-GFP-mCherry construct was transfected into HeLa cells using Lipofectamine 2000 and into ARPE-19 cells by Cell Avalanche ARPE-19 transfection reagent. Transfection efficiency for HeLa cells was about 80-90%, but could not be improved over 40% for ARPE-19 cells despite using a cell line adapted transfection reagent. Furthermore, CLN3-KO cells of both cell lines exhibited an increased number of cells with a high green cytoplasmic background fluorescence (Figure 16 B). Titration of DNA amounts against transfection reagent was not improving this issue. The high cytoplasmic background fluorescence was overlaying the high-fluorescent spots generated by autophagosomes and auto-lysosomes. Therefore, the transfection of LC3-GFP-mCherry construct was not perceived as a suitable technique to study autophagic flux in CLN3 deficient cells. The results with LC3-GFP-mCherry construct shown in Figure 16 A should be considered with caution.

### 3.2.4 Increased lysosomal marker LC3-II in CLN3 deficient HeLa and ARPE-19 cells

Instead of using the LC3-GFP-mCherry construct, autophagy was investigated by immunoblot analysis of the LC3 protein in CLN3 deficient HeLa and ARPE-19 cells. iPSC derived RPE cells were excluded from this analysis, because their differentiation was resulting in a too small number of cells for immunoblot analysis. The LC3 protein localizes in its lipidated form LC3-II to autophagosomes and is therefore often used as a standard marker for autophagy. LC3-II is generated by conjugation of the cytosolic LC3-I to phosphoethanolamine (PE) on the surface of nascent autophagosomes<sup>32,69</sup>. In both cell lines, CLN3 deficient cells showed increased levels of LC3-II (Figure 17).

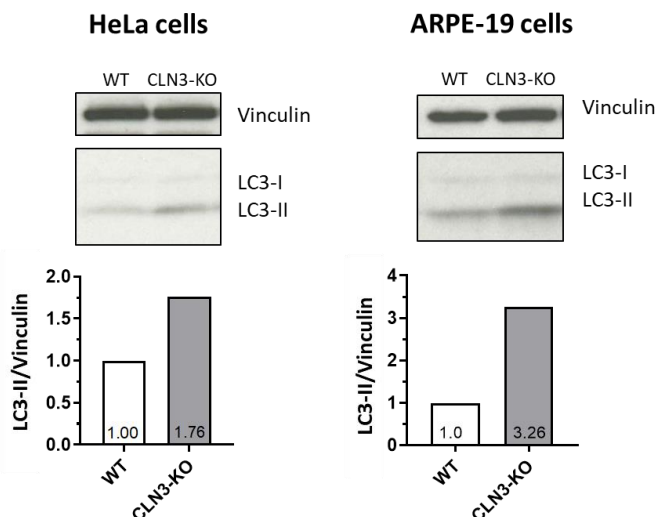


**Figure 17: Increased LC3-II levels in CLN3 deficient HeLa and ARPE-19 cells.** Immunoblot of LC3 protein in HeLa and ARPE-19 WT and CLN3-KO cells. HeLa cells n=1, ARPE-19 cells n=1. For LC3-II quantification protein amounts were normalized to loading control Vinculin and to WT cells.

Elevated LC3-II levels indicate an increased level of autophagosomes in CLN3-KO cells, which points towards an autophagy defect in these cells. It remains to be elucidated where in the autophagic pathway the defect occurs.

### 3.2.5 SubC accumulates in ARPE-19 and iPSC derived RPE CLN3-KO cells

Mitochondrial ATPase subunit C (SubC) is the most commonly described lysosomal storage material for CLN3 disease<sup>42,51,52</sup>. Therefore, HeLa, ARPE-19 and iPSC derived RPE WT and CLN3-KO cells were stained for SubC and LAMP1 by immunocytochemistry. ARPE-19 and iPSC derived RPE cells showed increased levels of SubC in LAMP1 positive vesicles compared to their WT controls (Figure 18).

In ARPE-19 cells autofluorescence was additionally detected. In contrast, CLN3 deficient HeLa cells did neither accumulate any SubC nor showed an increased autofluorescence. Autofluorescence was not investigated in iPSC derived RPE cells.

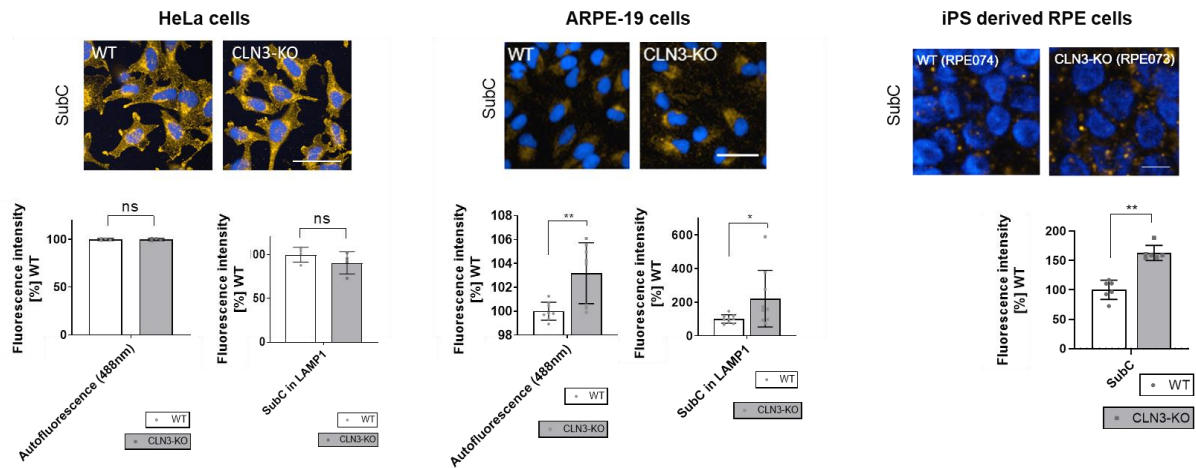


**Figure 18: SubC accumulates in CLN3 deficient ARPE-19 and iPSC derived RPE cells.** SubC immunofluorescence in HeLa, ARPE-19 and iPSC derived RPE WT and CLN3-KO cells. In HeLa and ARPE-19 cells SubC colocalization to LAMP1 is shown. In addition, autofluorescence was investigated in HeLa and ARPE-19 cells. Fluorescence intensity was normalized to WT, respectively for each genotype. High content confocal imaging with number of experiments (n). For each experiment 3 wells per condition and 9 images per well were analyzed. Number of experiments: HeLa cells n=1, ARPE-19 cells n=6, iPSC derived RPE cells n=2. P-values calculated by two-tailed unpaired students t-test. ns non-significant<0.1234, \*p-value<0.0332; \*\*p<0.0021, \*\*\*p-value<0.0002, \*\*\*\*p-value<0.0001. Scale bar: 50  $\mu$ m.

### 3.2.6 Cell cycle arrest amplifies CLN3-KO phenotypes in ARPE-19 cells

HeLa and ARPE-19 cells are, in contrast to iPSC derived RPE cells, proliferating cells. Cell division could enable them to compensate for the cellular defects caused by CLN3 deficiency, especially by passing accumulation material to their daughter cells. Arresting the cell cycle with the chemotherapeutic agent mitomycin C<sup>72</sup>, lead to increased accumulation of SubC in ARPE-19 CLN3-KO cells compared to the non-arrested ARPE-19 CLN3-KO cells (Figure 19). HeLa CLN3-KO cells in contrast did not show increased levels of SubC after cell cycle arrest.

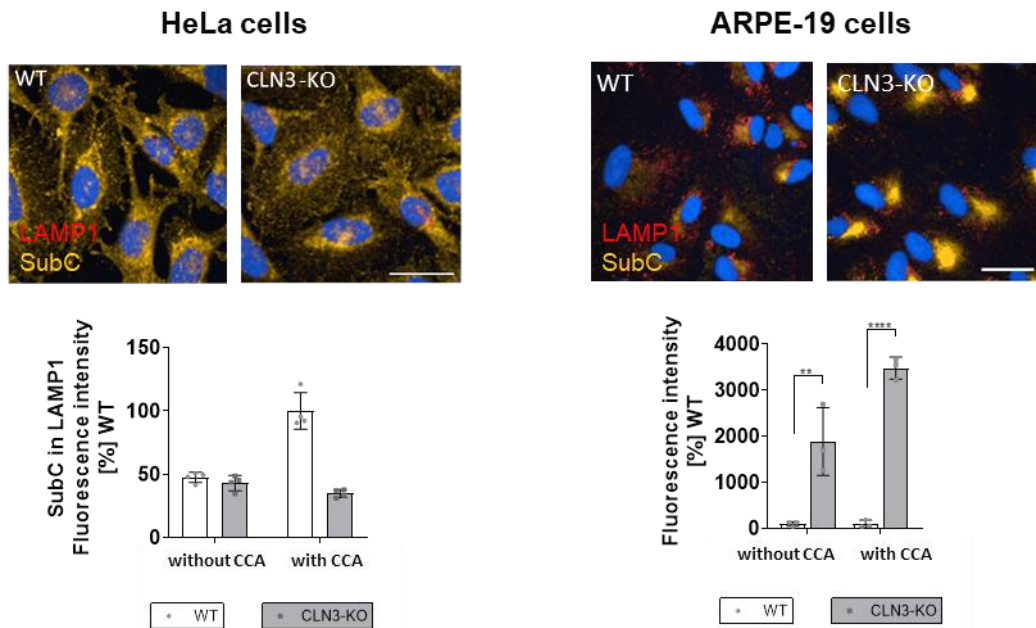


**Figure 19: Cell cycle arrest elevates SubC accumulations in CLN3 deficient ARPE-19 cells.** For cell cycle arrest (CCA), cells were treated for 48 h with 0.1  $\mu$ M mitomycin C, then fixed and stained for SubC and LAMP1. Fluorescence intensity of SubC in LAMP1 was normalized to WT mitomycin C treated condition, respectively for each cell type. High content confocal imaging with number of experiments (n). For each experiment 3 wells per condition and 9 images per well were analyzed. Number of experiments: HeLa cells n=1, ARPE-19 cells n=1. P-values calculated by two-way ANOVA, 0.1234 (ns), 0.0322 (\*), 0.0021 (\*\*), 0.0002 (\*\*\*), <0.0001 (\*\*\*\*).

Different substances, concentrations and incubation times of cell cycle arrest agents were tested based on the cathepsin B – Magic Red assay in ARPE-19 cells. Whereas mitomycin C is known to cross-link DNA<sup>72</sup>, hydroxyurea is most widely believed to target and inactivate ribonucleotide reductase<sup>73</sup> and thereby prevent DNA replication. Both substances, hydroxyurea and mitomycin C increased cathepsin B - Magic Red fluorescence intensity in CLN3-KO cells (Figure 20). Significant amplification of CLN3-KO phenotypes could be induced by low concentrations of mitomycin C. Therefore, mitomycin C was chosen as cell cycle arrest substance for further experiments.

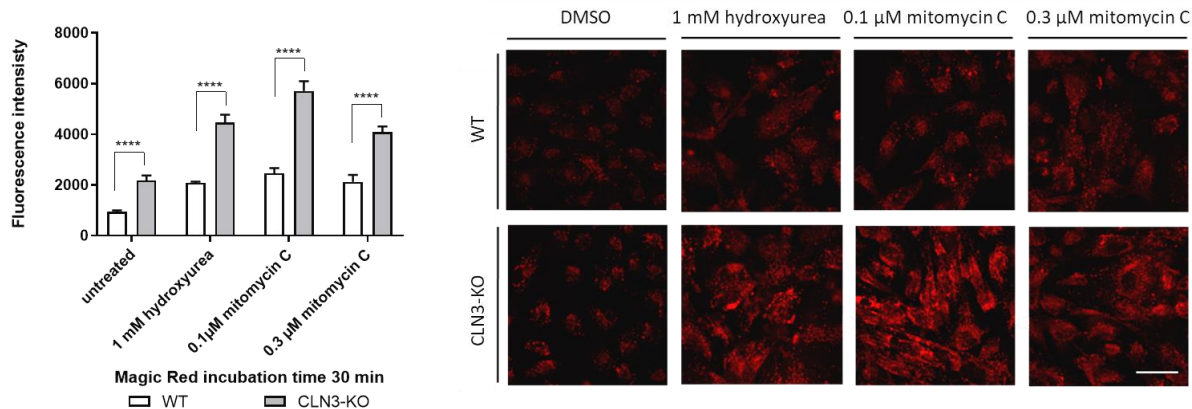


**Figure 20: Cell cycle arrest increases cathepsin B - Magic Red staining in CLN3 deficient ARPE-19 cells.** For cell cycle arrest ARPE-19 WT and CLN3-KO cells were treated for 14 days with different concentrations of hydroxyurea and mitomycin C. Cells were incubated for 30 min with cathepsin B – Magic Red dye. High content confocal imaging with number of experiments (n). For each experiment 3 wells per condition and 9 images per well were analyzed. Number of experiments: n=1. P-values calculated by two-way ANOVA. ns nonsignificant<0.1234, \**p*-value<0.0332; \*\**p*<0.0021, \*\*\**p*-value<0.0002, \*\*\*\**p*-value<0.0001. Scale bar: 50 μm. Scale bar: 50 μm.

Altogether, distinct phenotypes of CLN3 deficient cells were found. HeLa CLN3-KO cells showed decreased lysosomal enzyme activity as well as an autophagy defect. However, lysosomal marker levels of LAMP1 were not altered and no lysosomal storage material was detected. Furthermore, cell cycle arrest had no effect on SubC accumulation in HeLa CLN3-KO cells. In contrast, ARPE-19 CLN3-KO cells exhibited increased fluorescence intensity of cathepsin B - Magic Red and DQ-BSA dye, in line with elevated levels of LAMP1 and SubC accumulation. The Magic Red and SubC phenotype could be increased by cell cycle arrest. Like HeLa cells, CLN3 deficient ARPE-19 cells showed an autophagy defect. In CLN3 deficient iPSC derived RPE cells endocytic trafficking was altered, whereas LAMP1 levels and enzyme activity were not changed. Comparable to ARPE-19 cells, SubC storage material was found in iPSC derived RPE CLN3-KO cells.

ARPE-19 CLN3-KO cells showed a consistent CLN3 phenotype, which could be amplified by cell cycle arrest. Their fast and easy proliferation offers enough cellular material for additional studies. Furthermore, their origin from retinal pigment epithelial cells classifies them as a highly disease relevant cell type. ARPE-19 cells were therefore selected for the following studies.

### **3.3 Detailed phenotypic characterization of CLN3 deficient ARPE-19 cells**

ARPE-19 CLN3-KO were investigated with focus on storage material, lysosomes and autophagic flux. For this, cell cycle arrest (CCA) was further optimized. For all following experiments 0.3 mM mitomycin C was added for 2 h to the cells. After washing with PBS, cells were seeded into the required final experimental format and incubated for 7 days with regular medium changes.

#### **3.3.1 Accumulation of SubC and Gb3 in ARPE-19 CLN3-KO cells**

In previous experiments, ARPE-19 CLN3-KO cells were found to accumulate SubC. After repeating immunocytochemistry of SubC for several times, its accumulation could not always be confirmed under normal cell culture conditions. However, using the optimized cell cycle arrest protocol (CCA) always yielded in increased SubC levels in CLN3 deficient ARPE-19 cells (Figure 21 A). SubC fluorescence intensity colocalizing to LAMP1 and area of SubC-LAMP1 colocalization were found to be increased.

Globotriaosylceramide (Gb3), mostly known to accumulate in Fabry's disease<sup>74</sup> was recently shown to accumulate in CLN3 deficient cells<sup>59</sup>. As a receptor for Shiga toxins, Gb3 can be assessed with fluorescently labeled Shiga toxin (Sh-Tx-B-Cy3)<sup>75</sup>. Investigating Gb3, elevated fluorescence intensities of ShTx-B-Cy3 colocalizing with LAMP1 were found in ARPE-19 CLN3-KO cells (Figure 21 B). However, area of Sh-Tx-B-Cy3 – LAMP1 colocalization was not increased in CLN3 deficient cells. Gb3 accumulation was only studied under cell cycle arrest conditions.

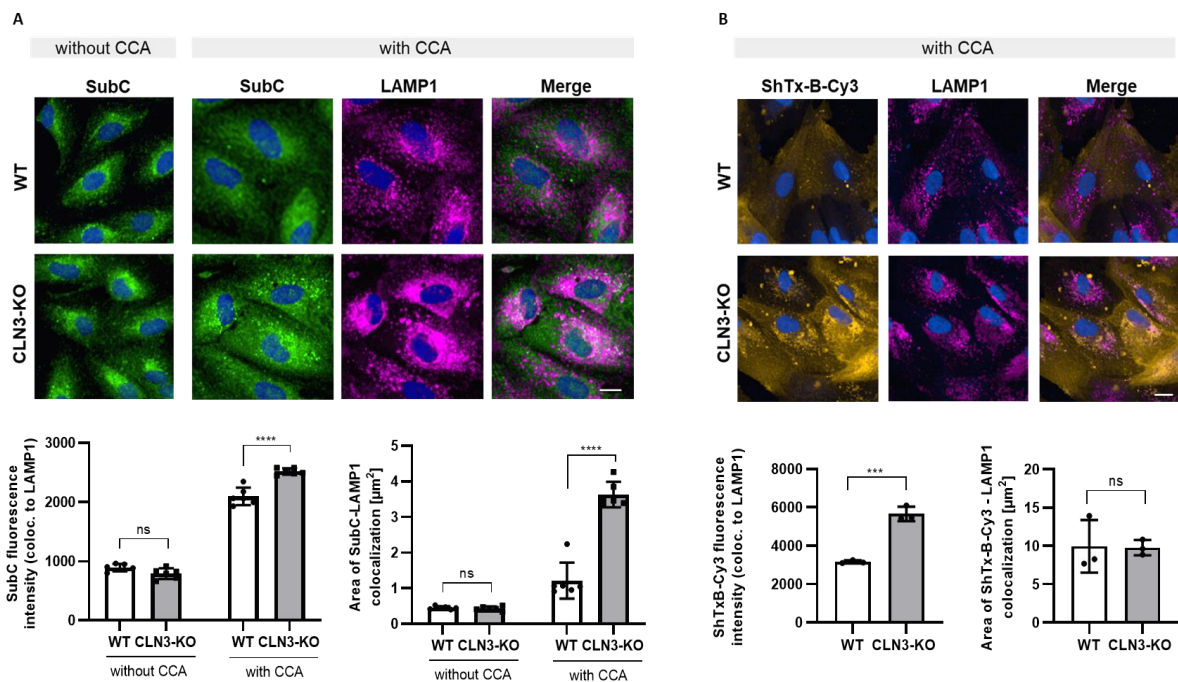


**Figure 21: ARPE-19 CLN3-KO cells accumulate SubC and Gb3 under cell cycle arrest (CCA) conditions.** Immunofluorescence staining of ARPE-19 cells with and without cell cycle arrest. **A** Immunofluorescence staining of mitochondrial ATPase subunit C (SubC) and LAMP1 with quantification of SubC fluorescence intensity colocalizing to LAMP1 and area of SubC-LAMP1 colocalization. **B** Labeling of globotriaosylceramide (Gb3) using Shiga toxin (ShTx-B-Cy3) and LAMP1 with quantification of ShTx-B-Cy3 fluorescence intensity colocalizing to LAMP1 and area of ShTx-B-Cy3 - LAMP1 colocalization. For cell cycle arrest, cells were treated for 2 h with 0.03 mM mitomycin C, washed with PBS and cultured for further 7 days. High content confocal imaging. Quantifications summarize data from one experiment. In total three independent experiments were performed. Per experiment 3 wells per condition and 9 images per well were analyzed. Values are means  $\pm$  SD. Scale bar: 20  $\mu\text{m}$ .

### 3.3.2 Reduced BMP/LBPA levels in ARPE-19 CLN3-KO cells

Intralysosomal vesicle (ILV) membranes are enriched with a typical anionic lipid known as bis(monoacylglycerol)phosphate (BMP) also named lysobisphosphatic acid (LBPA). BMP/LBPA accounts for 15-20 Mol% of total phospholipids in the late endosomal/lysosomal compartment and is not detected in other cellular compartments<sup>76,77</sup>. BMP/LBPA located in the internal membranes of lysosomes interacts with activator proteins necessary for lipid degradation<sup>78,79</sup>. BMP/LBPA levels are reduced in some lysosomal storage diseases including CLN3 disease<sup>60</sup>, and increasing BMP/LBPA levels have been shown to ameliorate storage phenotypes such as cholesterol overload in *NPC1*<sup>-/-</sup> cells<sup>80,81</sup>. Therefore, BMP levels in cell lysates and supernatants of ARPE-19 WT and CLN3-KO cells were analyzed (Figure 22). Experiments were performed in close collaboration with the Translational Proteomics and Metabolomics department at Evotec. Using mass spectrometry, 8 different BMP species were detected in cell lysates and 3 BMP species in cell supernatants. Whereas in supernatants no differences were found between WT and CLN3-KO cells, all 8 BMP species were reduced in cell lysates of CLN3-KO cells. BMP 40:7 and BMP 44:12 were especially abundant and showed significant differences with cell cycle arrest.

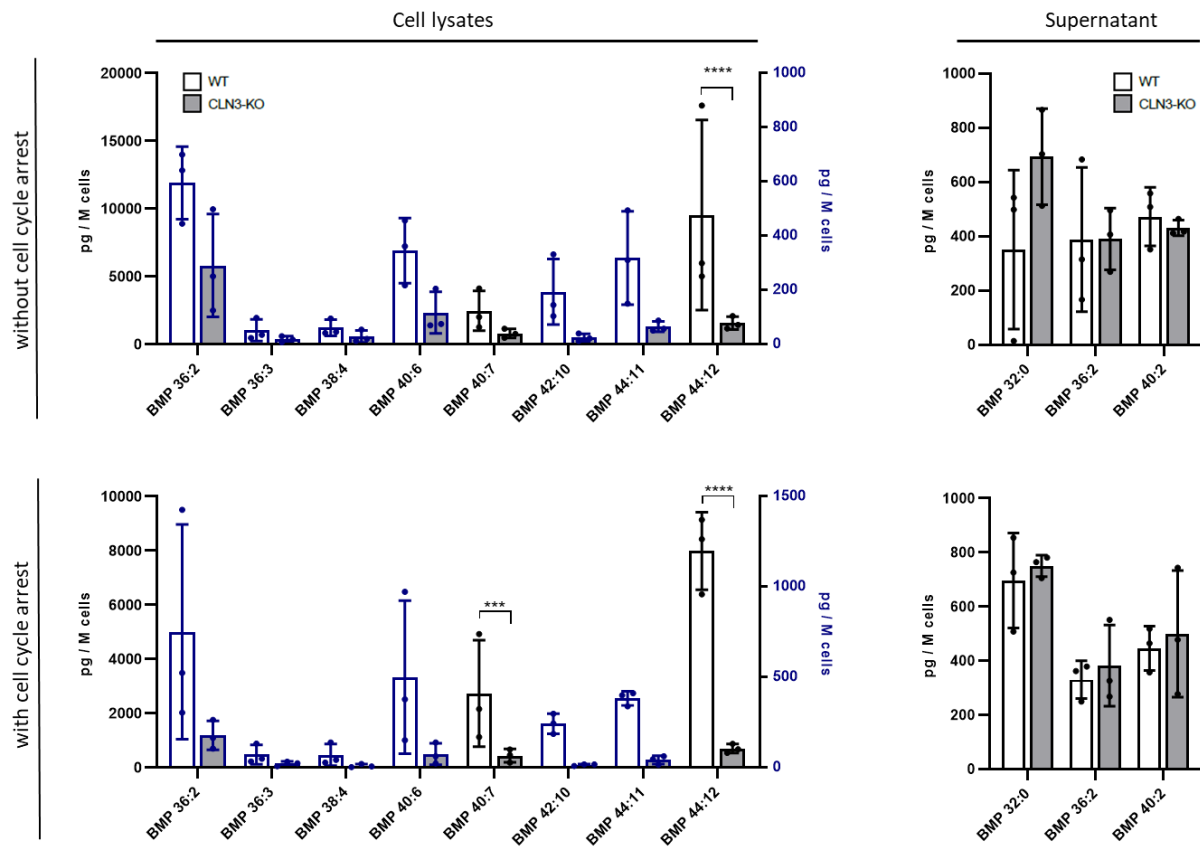


**Figure 22: Reduced BMP levels in cell lysates of ARPE-19 CLN3-KO cells.** BMP species in cell lysates and supernatants of ARPE-19 WT and CLN3-KO cells with and without cell cycle arrest were analyzed using mass spectrometry. BMP levels were quantified in picogram per million of cells from 3 independent cell samples, measured in one LC-MS/MS run. For cell lysates, black samples are associated with left Y-axis, whereas blue sample quantities are based on the right Y-axis. P-values calculated by two-way ANOVA coupled with multiple comparisons using Sidak test. ns nonsignificant<0.1234, \* $p$ -value<0.0332; \*\* $p$ <0.0021, \*\*\* $p$ -value<0.0002, \*\*\*\* $p$ -value<0.0001.

### 3.3.3 Increased lysosomal number and size in ARPE-19 CLN3-KO cells

The effect of CLN3 deficiency on lysosomes was analyzed in more detail using different lysosomal marker proteins, including LAMP1, LAMP2 and NPC1. Additionally, cells were stained with LysoTracker, a pH sensitive dye often used to label lysosomes and late endosomes. Lysosomes of ARPE-19 cells were investigated with and without cell cycle arrest. Quantification of immunofluorescence and immunoblot analysis demonstrated increased levels of lysosomal marker proteins in CLN3-KO compared to WT cells (Figure 23). Consistently, LysoTracker staining was significantly enhanced in CLN3-KO cells. Cell cycle arrest amplified differences between WT and CLN3-KO cells on immunofluorescence and immunoblot level.

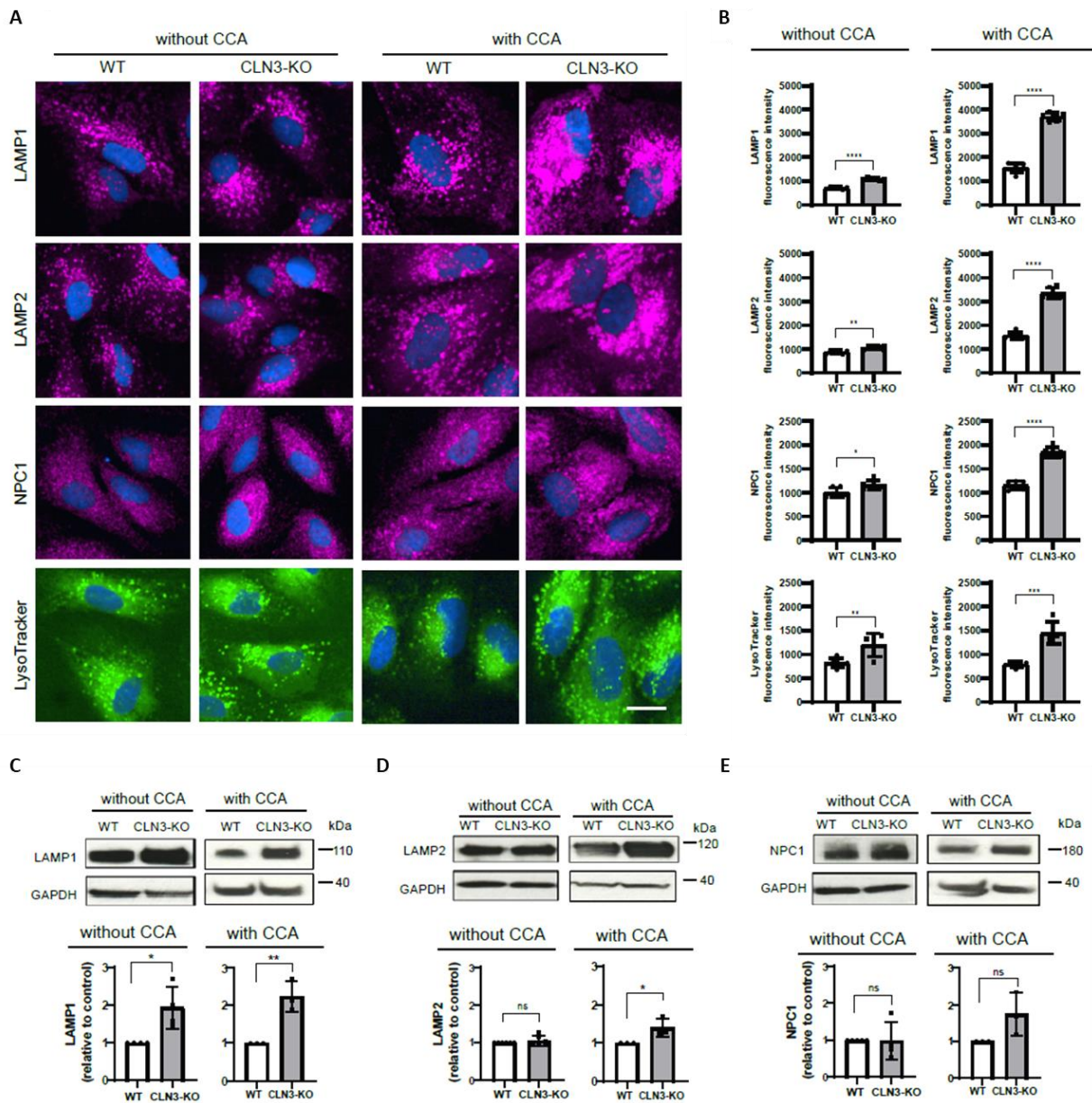


**Figure 23: Lysosomal marker analysis on protein level with and without cell cycle arrest.** **A** Representative immunocytochemical images of LAMP1, LAMP2, NPC1 (magenta) and LysoTracker (green) in ARPE-19 WT and CLN3-KO cells with and without cell cycle arrest (CCA). Scale bar: 20 $\mu$ m. **B** High content confocal imaging. Quantifications summarize data from one experiment. In total three independent experiments were performed. Per experiment 6 wells per condition and 9 images per well were analyzed. Values are means  $\pm$  SD. **C, D, E** Representative images of immunoblot analysis of LAMP1 (**C**), LAMP2 (**D**) and NPC1 (**E**) with and without CCA. Plots show quantification of LAMP1, LAMP2 and NPC1 protein levels, normalized to GAPDH. Values are means  $\pm$  SD,  $n=3$  independent experiments.

To elucidate whether the elevated levels of lysosomal proteins are resulting from an increased lysosomal number and/or size, electron microscopy images of ARPE-19 cells under cell cycle arrest conditions were analyzed. Quantification revealed that CLN3-KO cells exhibit an increased number and size of lysosomes (Figure 24).



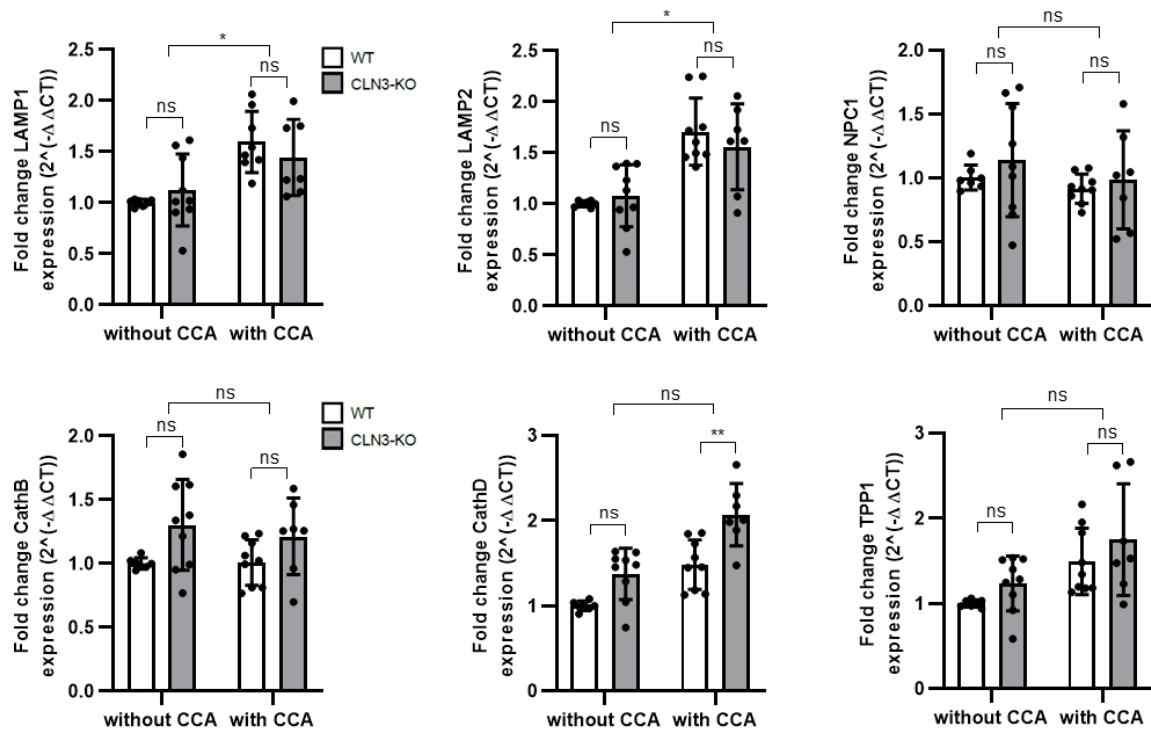


**Figure 25: Expression levels of lysosomal genes in ARPE-19 WT and CLN3-KO cells with and without cell cycle arrest.** mRNA expression levels of lysosomal membrane proteins (LAMP1, LAMP2 and NPC1) and lysosomal enzymes (CathB, CathD and TPP1), normalized to PPIB. Values are means  $\pm$  SD,  $n=3$  independent experiments.  $P$ -values calculated by unpaired two-tailed Student's  $t$ -test and two-way ANOVA coupled with multiple comparisons using Sidak test. ns nonsignificant  $<0.1234$ , \* $p$ -value  $<0.0332$ ; \*\* $p$ -value  $<0.0021$ , \*\*\* $p$ -value  $<0.0002$ , \*\*\*\* $p$ -value  $<0.0001$ .

The expression of the here analyzed lysosomal genes is not significantly altered in ARPE-19 CLN3-KO compared to WT cells. Cell cycle arrest is significantly increasing expression of LAMP1 and LAMP2 in WT and CLN3-KO cells to similar extent.

### 3.3.4 Impaired autophagy in ARPE-19 CLN3-KO cells

Autophagy is a mechanism, that removes defective organelles and aggregates of misfolded proteins via lysosomal degradation<sup>82</sup>. Impaired lysosomal function might therefore directly affect autophagic flux. Furthermore, as above mentioned, autophagic defects are often described in CLN3 mutated cells<sup>55,57,52</sup>. Using immunoblotting and immunocytochemistry, autophagy was investigated in more detail in ARPE-19 WT and CLN3-KO cells. Investigating LC3 with immunoblot technique revealed slightly increased LC3-II levels in ARPE-19 CLN3-KO compared to WT cells with and without cell cycle arrest (Figure 17 and Figure 26 A-B). Upon treatment with the vacuolar ATPase and autophagy inhibitor Bafilomycin A1 (BafA)<sup>68</sup>, LC3-II levels increased in WT and CLN3-KO cells, with and without CCA. Autophagy was also observed by immunolabelling of LC3 and LAMP1 (Figure 26 C-D). LC3 and LC3-LAMP1 colocalizing structures/cell were not altered between WT and CLN3-KO

cells, but significantly increased in both genotypes to the same extent after inhibiting autophagy with BafA or Chloroquine (CQ), indicating that autophagy induction and autophagosome-lysosome fusion are not altered in ARPE-19 CLN3-KO cells.

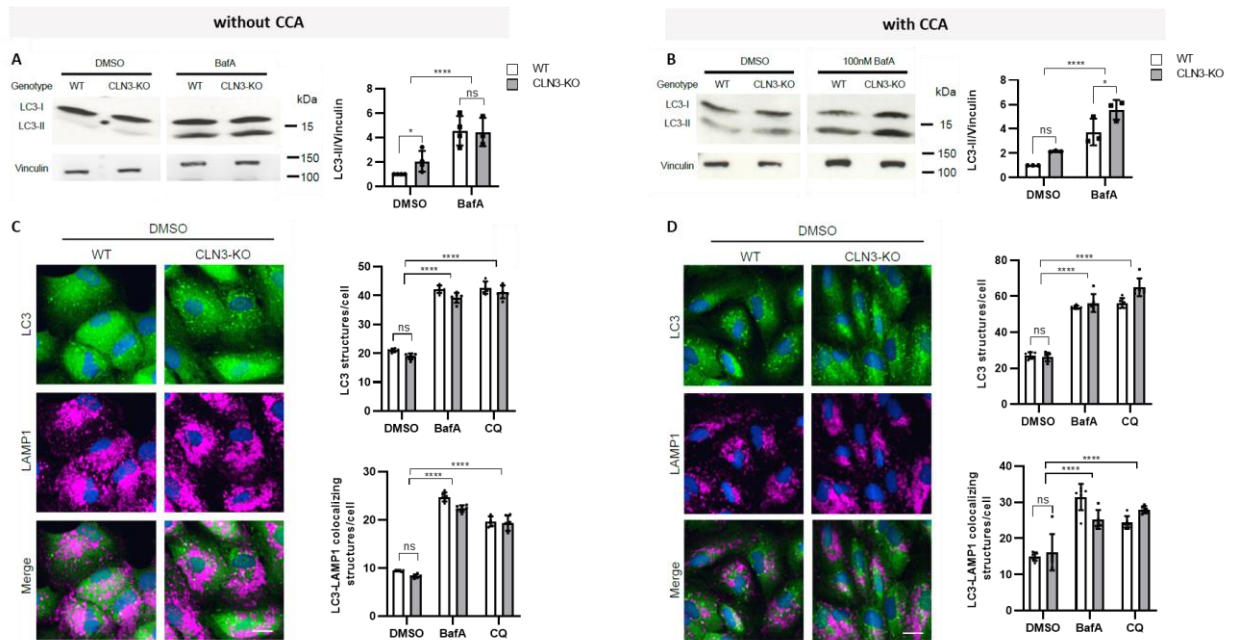


**Figure 26: Elevated LC3-II levels in ARPE-19 CLN3-KO cells.** **A, B** Immunoblot analysis of LC3. ARPE-19 WT and CLN3-KO cells with **(A)** and without **(B)** cycle arrest were treated for 3 h with 100 nM Bafilomycin A1 (BafA). For quantification LC3-II levels were normalized to Vinculin, n=3 independent experiments. **C, D** Representative immunocytochemical images of LC3 and LAMP1 localization in ARPE-19 WT and CLN3-KO cells with **(C)** and without **(D)** cell cycle arrest. Scale bar: 20  $\mu$ m. Plots represent the number of LC3 structures/cell and LC3-LAMP1 colocalizing structures/per cell. Cells were treated with BafA for 3 h. High content confocal imaging. Quantifications summarize data from one experiment. In total three independent experiments were performed. Per experiment 6 wells per condition and 9 images per well were analyzed. Values are means  $\pm$  SD. P-values calculated by two-way ANOVA coupled with multiple comparisons using Tukey test. ns nonsignificant <math>p > 0.1234</math>, \*

To evaluate if increased LC3-II levels found in ARPE-19 cells are caused by an altered upstream regulation of autophagy, gene expression levels of LC3 and transcription factor EB (TFEB) were analyzed. TFEB is a known master regulator of lysosomal biogenesis and expression of lysosomal and autophagy-related genes.<sup>83</sup> LC3 and TFEB mRNA expression levels were comparable between ARPE-19 WT and CLN3-KO cells (Figure 27 A-B). Cell cycle arrest was not influencing expression of LC3, whereas TFEB expression was significantly increased in both genotypes. TFEB translocation from the cytoplasm into the nucleus is regulated by its phosphorylation status, mainly under the control of mTOR. The mTOR inhibitor Torin1 diminishes phosphorylation of TFEB, which results in the translocation of the dephosphorylated protein into the nucleus<sup>15</sup>. In immunocytochemistry experiments, no difference of TFEB nucleus/cytoplasm ratio was found between WT and CLN3-KO

cells, with and without CCA (Figure 27 C-D). Torin1 treatment led to the same amount of TFEB translocation in both cell types and CCA conditions. Additionally, the dephosphorylation of TFEB was visualized as a downward shift of TFEB on immunoblot. No differences were detected between WT and CLN3-KO cells and both conditions (Figure 27 E-F). A significant difference in TFEB protein levels between WT and CLN3-KO cells was neither detected in immunofluorescence nor in immunoblot experiments.

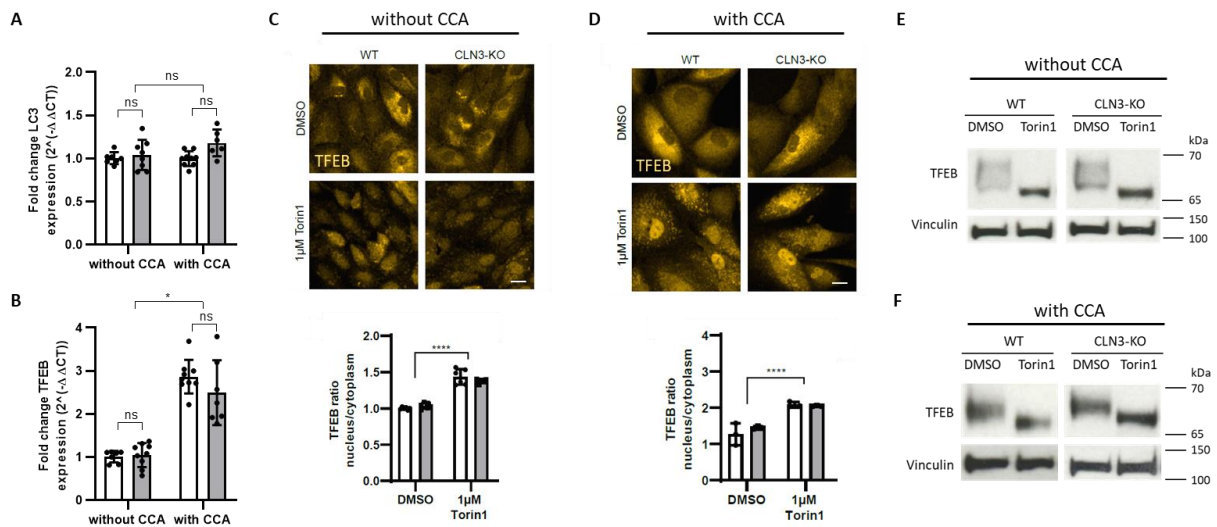


**Figure 27: Upstream regulation of autophagy by TFEB is not altered in ARPE-19 CLN3-KO cells.** **A, B** mRNA expression levels of LC3 (**A**) and TFEB (**B**), normalized to PPIB. Values are means  $\pm$  SD, n=3 independent experiments. **C, D** Representative immunocytochemical images showing TFEB nuclear translocation after treatment of ARPE-19 WT and CLN3-KO cells without (**C**) and with (**D**) cell cycle arrest for 2 h with Torin1. Scale bar: 20  $\mu$ m. Plots show TFEB nuclear/cytoplasm ratio. High content confocal imaging. Quantifications summarize data from one experiment. In total three independent experiments were performed. Per experiment 6 wells per condition and 9 images per well were analyzed. **E, F** Representative immunoblot of total cellular TFEB levels. ARPE-19 WT and CLN3-KO were treated with mTORC-inhibitor Torin1 for 2 h. Treatment leads to TFEB dephosphorylation and nuclear translocation, which is reflected by a size shift. In total 3 independent experiments were performed. *P*-values calculated by unpaired two-tailed Student's *t*-test and two-way ANOVA coupled with multiple comparisons using Sidak test. ns nonsignificant<0.1234, \**p*-value<0.0332; \*\**p*<0.0021, \*\*\**p*-value<0.0002, \*\*\*\**p*-value<0.000

TFEB is involved in the transcriptional regulation of autophagy. Direct induction of phagophore formation can also be induced via TFEB-independent pathways<sup>82</sup>. Especially mTORC1, as a sensor for amino acid and energy status in the cell activates and inhibits pathways affecting autophagosome formation. In the presence of nutrients mTORC1 is activated and recruited to lysosomes, and thereby inhibits autophagy<sup>84,85</sup>. mTOR protein levels and its localization to lysosomes was investigated by immunocytochemistry. mTOR fluorescence intensity was significantly increased in CLN3 deficient ARPE-19 cells without CCA, whereas mTOR colocalization to lysosomes (LAMP1) was comparable in WT and CLN3-KO cells (Figure 28 A-C). Upon inhibition of mTORC1 by serum starvation (STV), Torin1 and

Rapamycin (Rap.) treatment, mTOR fluorescence intensity increased, whereas colocalization to LAMP1 decreased in both genotypes to a similar extent. These results indicate a functional inhibition of mTORC1 in CLN3 deficient cells. The mTORC1 complex is composed of several subunits, which are phosphorylated/dephosphorylated and thereby activated/inhibited separately. Activity of the mTOR complex 1 is therefore difficult to interpret by focusing on mTOR protein alone, which is only one part of the multi-protein complex. Phosphorylation of a direct downstream target of mTOR, the p70S6 kinase and its downstream target the S6 protein, was used to analyze activity status of mTORC1<sup>17</sup>. mTOR, p70 S6 kinase and S6 protein levels were comparable in ARPE-19 WT and CLN3-KO cells without cell cycle arrest (Figure 28 D-I). mTOR and its downstream targets were not investigated under cell cycle arrest conditions. However, phosphorylated levels of these proteins were elevated in CLN3-KO cells, indicating an increased mTOR activity in CLN3 deficient ARPE-19 cells.

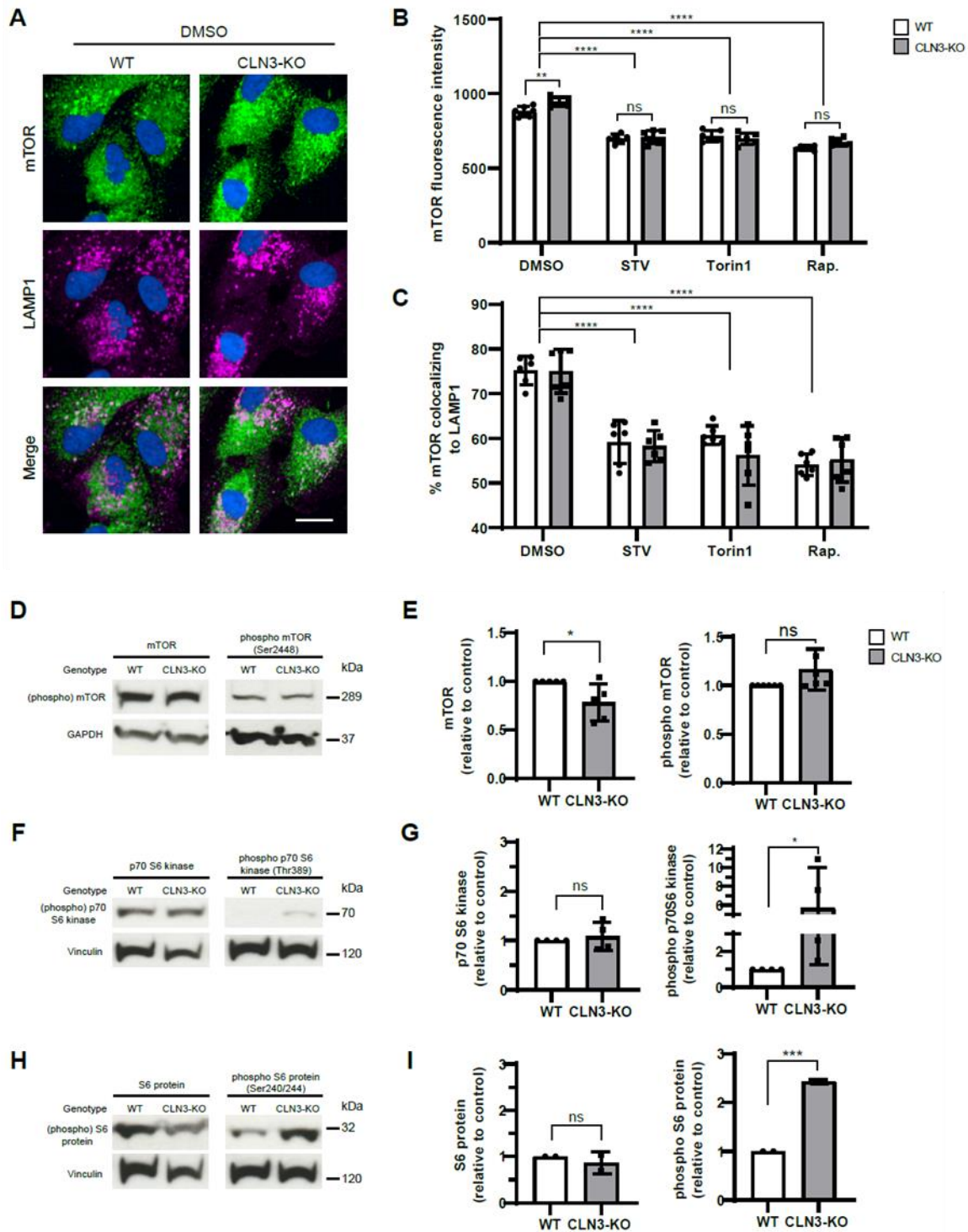


**Figure 28: mTOR activity is increased in ARPE-19 CLN3-KO cells.** **A** Representative immunocytochemical images of mTOR and LAMP1 colocalization in ARPE-19 WT and CLN3-KO cells without cell cycle arrest. Cells held for 30 min under serum starvation (STV) or treated for 30 min with 3  $\mu$ M Torin1 and 20  $\mu$ M Rapamycin (Rap.). Scale bar: 20  $\mu$ m. **B, C** Plots show mTOR fluorescence intensity (**B**) and %mTOR colocalizing to LAMP1 (**C**) of one representative experiment. High content confocal imaging. Quantifications summarize data from one experiment. In total three independent experiments were performed. Per experiment 6 wells per condition and 9 images per well were analyzed. **D, F, H** Representative immunoblots with quantification of (phospho-) mTOR  $n=3$  (**D, E**), (phospho-) p70 S6 kinase  $n=3$  (**F, G**) and (phospho-) S6 protein  $n=2$  (**H, I**) in ARPE-19 WT and CLN3-KO cells without cell cycle arrest. *P*-values calculated by unpaired two-tailed Student's *t*-test and two-way ANOVA coupled with multiple comparisons using Tukey test. ns nonsignificant  $<0.1234$ , \**p*-value  $<0.0332$ , \*\**p*-value  $<0.0021$ , \*\*\**p*-value  $<0.0002$ , \*\*\*\**p*-value  $<0.0001$ .

In summary, although increased mTORC1 activity in ARPE-19 CLN3-KO cells was detected, TFEB mRNA expression, protein or translocation levels were not altered. Additionally, mRNA expression levels of LC3 are comparable to WT cells, whereas LC3 protein levels are increased in CLN3 deficient cells. Furthermore, immunofluorescence analysis of LC3 and LAMP1 indicate that induction of autophagy as well as autophagosome-lysosome fusion is not impaired in ARPE-19 CLN3-KO cells.

### **3.3.5 Impaired lysosomal enzyme activity in ARPE-19 CLN3-KO cells**

Based on the results, autophagy defects found in CLN3 deficient ARPE-19 cells are not assumed to be caused by altered autophagy induction or impaired autophagosome-lysosome fusion. Subsequently, after autophagosome-lysosome fusion, delivered material is degraded by lysosomal enzymes. As stated above (chapter 3.2.1), DQ-BSA and cathepsin B - Magic Red assays revealed increased levels of DQ-BSA degradation capacity and lysosomal cathepsin B activity in ARPE-19 CLN3-KO cells without CCA. However, immunoblot analysis enables the detection of pre-, intermediate and mature enzyme forms. Most pre-enzymes are known to be inactive and become active after proteolytic cleavage in lysosomes. Immunoblot analysis was performed to investigate different enzyme forms of cathepsin B (CathB), cathepsin D (CathD) and TPP1. CathB was selected as comparison to the cathepsin B - Magic Red assay. CathD and TPP1 have been reported to play a role in SubC degradation<sup>86,87</sup>. Whereas pre- forms of all three enzymes were elevated in CLN3 deficient cells, mature/active forms were comparable between ARPE-19 WT and CLN3-KO cells without cell cycle arrest, when normalized to the housekeeper vinculin (Figure 29 **Fehler! Verweisquelle konnte nicht gefunden werden.** A-F). Note, these quantifications were without normalization for differences in lysosomal number/size in WT as compared to CLN3-KO cells. Moreover, CathD and TPP1 were analyzed under cell cycle arrest conditions. Here, quantifications were normalized additionally to lysosomal number/size (LAMP1), revealing comparable or reduced levels of pre-enzymes and significantly decreased levels of mature CathD and TPP1 in ARPE-19 CLN3-KO cells (Figure 29 G-I), leading to the assumption that mature enzyme levels per lysosome are decreased in ARPE-19 CLN3-KO cells.

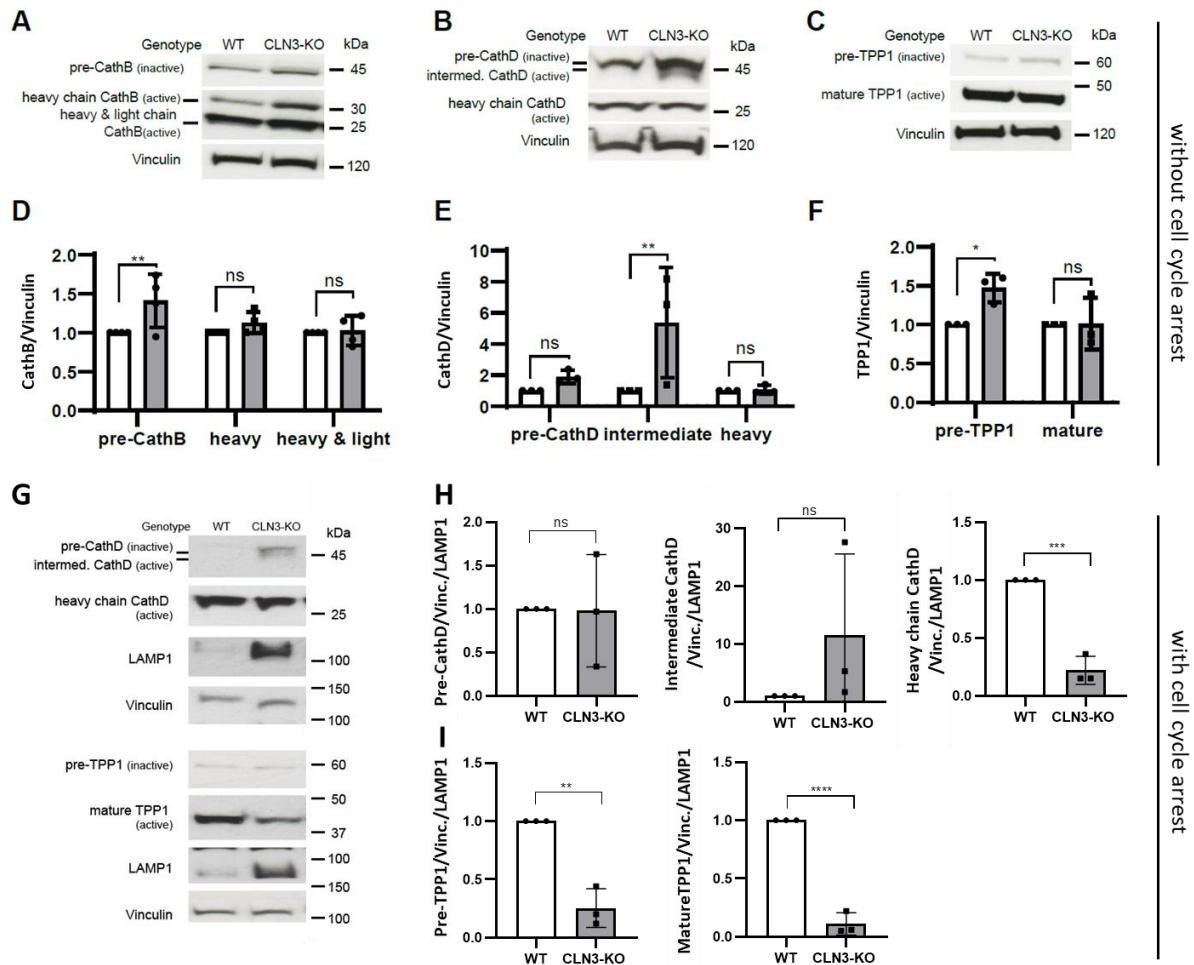


**Figure 29: Defective processing of lysosomal enzymes in ARPE-19 CLN3-KO cells.** **A, B, C** Immunoblot analysis of Cathepsin B (CathB) (**A**), Cathepsin D (CathD) (**B**) and TPP1 (**C**) protein in ARPE-19 WT and CLN3-KO cells without cell cycle arrest. **D, E, F** Quantifications of CathB (**D**), CathD (**E**) and TPP1 (**F**) protein levels, normalized to Vinculin, in ARPE-19 WT and CLN3-KO cells without cell cycle arrest. **G** Immunoblot analysis of CathD, TPP1 and LAMP1 protein in ARPE-19 WT and CLN3-KO cells with cell cycle arrest. **H, I** Quantifications of CathD (**H**) and TPP1 (**I**) protein levels, normalized to Vinculin and thereafter to LAMP1, in ARPE-19 WT and CLN3-KO cells with cell cycle arrest. Data are from three independent experiments. Values are means  $\pm$  SD. P-values calculated by students t-test and two-way ANOVA coupled with multiple comparisons using Tukey test. ns nonsignificant  $<0.1234$ , \* $p$ -value  $<0.0332$ ; \*\* $p$ -value  $<0.0021$ , \*\*\* $p$ -value  $<0.0002$ , \*\*\*\* $p$ -value  $<0.0001$ .

Altogether, the experiments on lysosomal enzyme activity propose a decreased lysosomal enzyme activity in CLN3 deficient ARPE-19 cells, possibly caused by enzyme processing defects.

### **3.4 TRPML1 activation ameliorates lysosomal phenotypes in ARPE-19 CLN3-KO cells**

TRPML1 is an important regulator of various calcium-dependent processes, such as vesicle trafficking, membrane fusion/fission, lysosome biogenesis, reformation and exocytosis, autophagy induction, and lysosomal and autophagy-related gene expression controlled by the transcription factor EB (TFEB)<sup>11,19,83,88</sup>. Recent publications have shown that activation of the endolysosomal Ca<sup>2+</sup> channel TRPML1 decreases lysosomal accumulation material and has beneficial effects on autophagy impairments in several lysosomal storage disorders (LSDs) and neurodegenerative diseases<sup>24,25,26,27</sup>. However, effects of TRPML1 activation on CLN3 disease-related phenotypes have not been evaluated so far.

#### **3.4.1 Increased TRPML1 activity in ARPE-19 CLN3-KO cells**

To ensure that ARPE-19 CLN3-KO cells express TRPML1 and are able to respond to TRPML1 agonists, TRPML1 mRNA levels and currents were determined. Similar mRNA expression levels were detected in WT and CLN3-KO cells (Figure 30 A). TRPML1 currents were detected by lysosomal patch clamp, which was performed in collaboration with Rachel Tang from the LMU Munich. By opening the channel with known TRPML1 agonists, such as ML-SA1<sup>89</sup>, TRPML1 currents were detected in ARPE-19 WT and CLN3-KO cells. Surprisingly, larger currents were found in lysosomes of ARPE-19 CLN3-KO as compared to WT cells under both cell cycle arrest conditions. In both WT and CLN3-KO cells, these currents were fully blocked by treatment with the TRPML1 antagonist ML-SI3<sup>90,91</sup> (Figure 30 B-G).

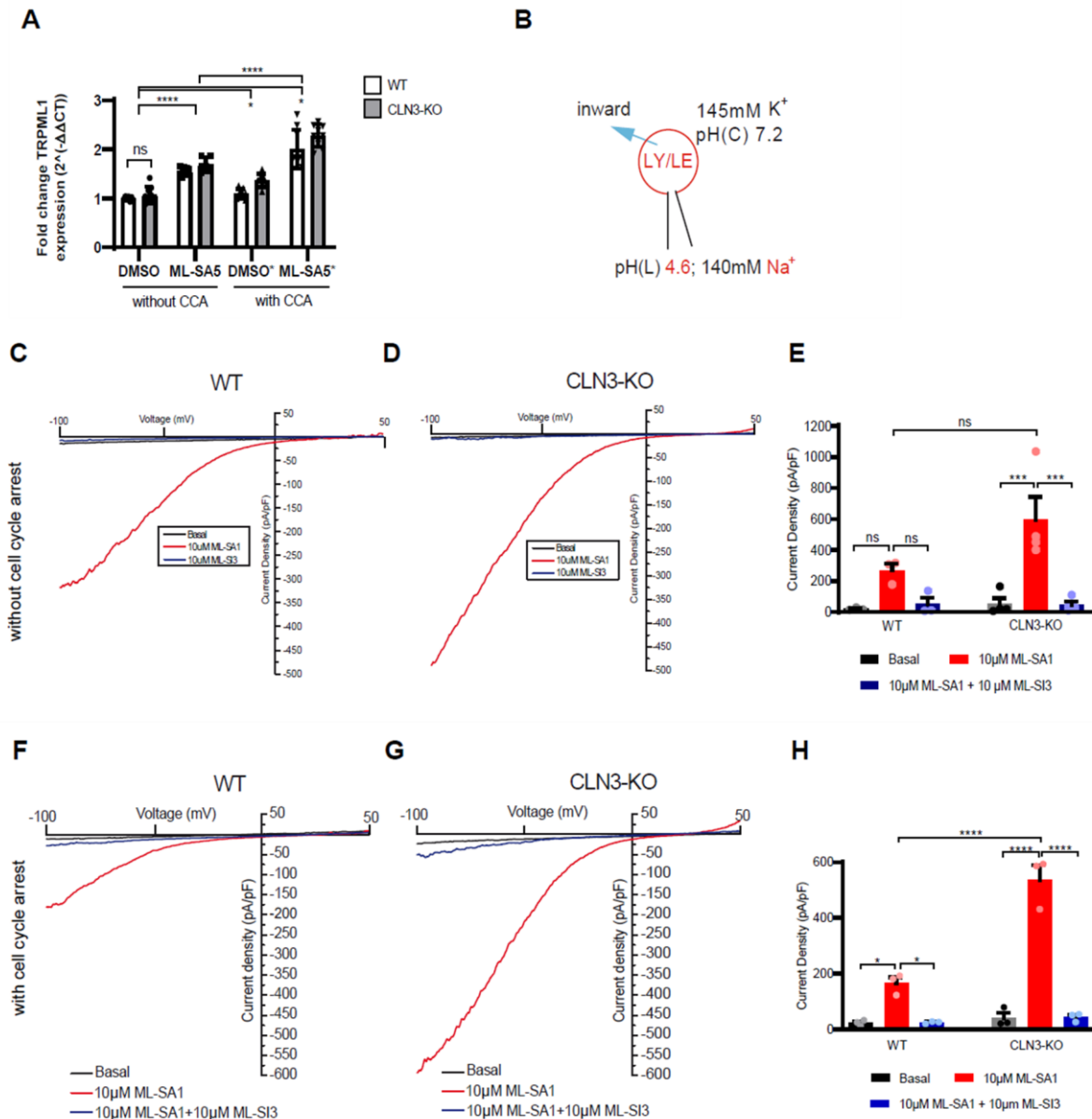


**Figure 30: Increased TRPML1 currents in ARPE-19 CLN3-KO cells.** **A** Relative mRNA expression levels of TRPML1, normalized to PPIB. Cells were treated for 24 h with 30 μM ML-SA5, with and without cell cycle arrest (CCA). Values are means ± SD, *n*=3 independent experiments. **B** Scheme of lysosomal patch clamp technique, showing main buffer components. **C, D** Representative TRPML1 currents with agonist ML-SA1 and antagonist ML-SI3 treatment in non-cell cycle arrested ARPE-19 WT (**C**) and CLN3 KO (**D**) cells, measured with whole endolysosomal patch clamp technique. **E** Plot shows current densities of three independently patched lysosomes from ARPE-19 WT and CLN3-KO cells without CCA. **F, G** Representative TRPML1 currents with agonist ML-SA1 and antagonist ML-SI3 treatment of cell cycle arrested ARPE-19 WT (**F**) and CLN3 KO (**G**) cells, measured with whole endolysosomal patch clamp technique. **H** Plot shows current densities of three independently patched lysosomes from ARPE-19 WT and CLN3-KO cells with cell cycle arrest.

### 3.4.2 TRPML1 activation reduces lysosomal number/size in ARPE-19 CLN3-KO cells

To test effects of TRPML1 agonists on CLN3 disease phenotypes in ARPE-19 cells, a more potent TRPML1 agonist, ML-SA5, was used<sup>27</sup>. mRNA expression levels of LAMP1 were found to be significantly increased upon ML-SA5 treatment (Figure 31 A), whereas LAMP1 protein levels investigated by immunofluorescence were slightly decreased (Figure 30 B, corresponding images can be found in Figure 31 A).

Electron microscopy (EM) analysis revealed that the number and size of lysosomes was slightly reduced upon TRPML1 activation, but total lysosomal area per cell was significantly diminished with ML-SA5 treatment in ARPE-19 CLN3 deficient cells (Figure 31 C-D).

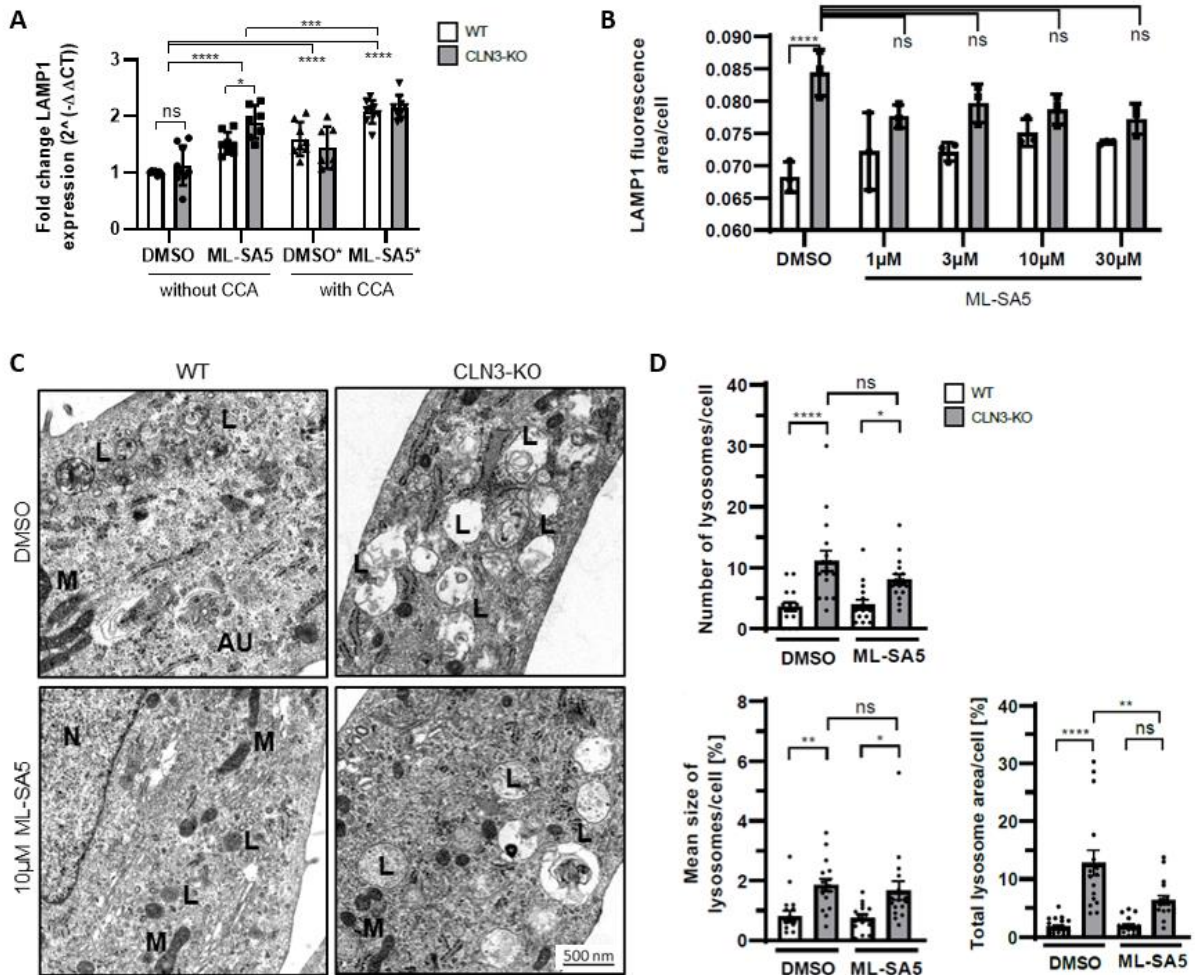


**Figure 31: TRPML1 activation reduces total lysosomal area in ARPE-19 CLN3-KO cells.** **A** Relative mRNA expression levels of LAMP1 normalized to PPIB. With and without cell cycle arrest. Cells were treated for 48h with 30 μM ML-SA5. Values are means ± SD, n=3 independent experiments. **B** Plots show LAMP1 fluorescence area/cell of cell cycle arrested cells treated for 48 h with DMSO/ML-SA5. Corresponding fluorescence images can be found in Figure 32 A. Summarized data from one experiment. In total three independent experiments were performed. Values are means ± SD. **C** Representative electron microscopy images of ARPE-19 CLN3-KO cells under cell cycle arrest. Cells were treated with 10 μM ML-SA5 for 48 h. AU, autophagosomes; L, lysosomes; M, mitochondria; N, nucleus. **D** Plots show quantification of lysosomal number, mean lysosomal size and total lysosome area per cell from 16 electron microscopy images. Values are means ± SEM. *P*-values were calculated by unpaired two-way ANOVA coupled with multiple comparisons using Sidak or Tukey test. ns nonsignificant < 0.1234, \**p*-value < 0.0332; \*\**p* < 0.0021, \*\*\**p*-value < 0.0002, \*\*\*\**p*-value < 0.0001.

### 3.4.3 TRPML1 activation reduces lysosomal accumulations of SubC and Gb3 in ARPE-19 CLN3-KO cells

SubC and Gb3 accumulate in ARPE-19 CLN3-KO cells under cell cycle arrest conditions (chapter 3.3.1). Treatment with ML-SA5 for 48 h significantly decreased

SubC accumulation in CLN3-KO cells in a concentration dependent manner (Figure 32 A-C). Similar to SubC, ML-SA5 decreased Shiga toxin labeled Gb3, colocalizing with LAMP1, in ARPE-19 CLN3-KO cells (Figure 32 D-E).

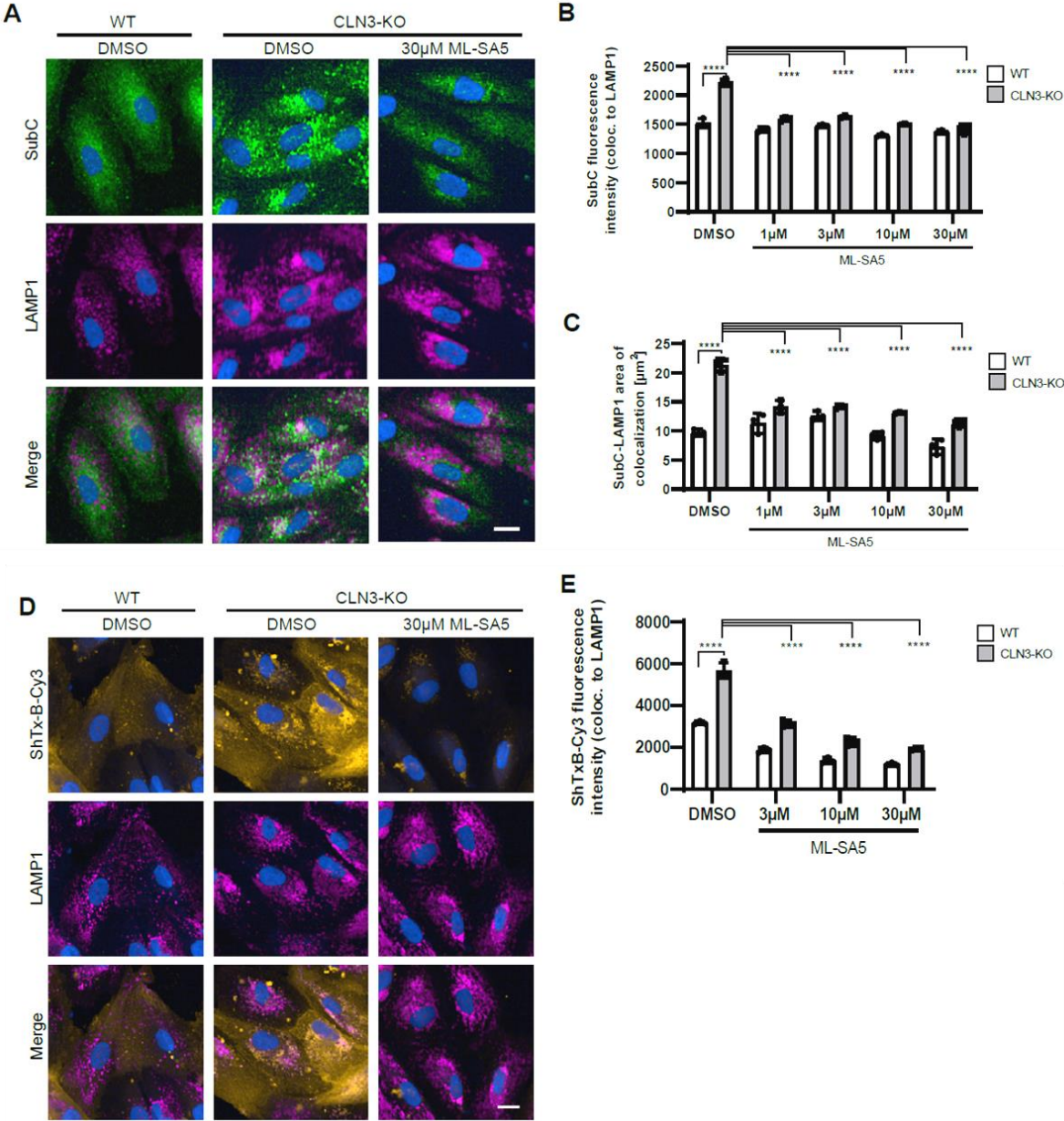


**Figure 32: TRPML1 activation reduces lysosomal accumulation of SubC and Gb3 in ARPE-19 CLN3-KO cells. A** Representative immunocytochemical images of SubC and LAMP1 in cell cycle arrested ARPE-19 WT and CLN3-KO cells. ML-SA5 was added for 48h, 7 days after induction of CCA. Scale bar: 20 µm. **B, C** Quantification of immunocytochemical images shown in A, where **(B)** shows SubC fluorescence intensity and **(C)** area of SubC-LAMP1 colocalization. Representative plots from one experiment. In total three independent experiments were performed. Values are means ± SD. **D** Representative immunocytochemical images of Gb3 labeling using ShTx-B-Cy3 (yellow) and LAMP1 (magenta) in cell cycle arrested ARPE-19 WT and CLN3-KO cells. Cells were treated with ML-SA5 for 48 h. Scale bar: 20 µm. **E** Quantification of ShTx-B-Cy3 fluorescence intensity (images shown in **D**) using data from one experiment. In total three independent experiments were performed. Values are means ± SD. . P-values calculated by two-way ANOVA coupled with multiple comparisons using Tukey test. ns nonsignificant<0.1234, \**p*-value<0.0332; \*\**p*<0.0021, \*\*\**p*-value<0.0002, \*\*\*\**p*-value<0.0001.

### 3.4.4 TRPML1 activation does not elevate BMP/LBPA levels in ARPE-19 CLN3-KO cells

In 2007, BMP/LBPA levels were already described to be reduced in CLN3 deficient cells<sup>60</sup>, which was confirmed in ARPE-19 CLN3-KO cells (chapter 3.3.3). As seen in previous experiments, TRPML1 activation diminished lysosomal storage materials in these cells, raising the question if TRPML1 activation would show any effects on BMP/LBPA levels. ML-SA5 treatment significantly increased BMP 36:2 and slightly increased other BMP species in WT, but not in CLN3-KO cells (Figure 33), raising the assumption that CLN3 may have a key role in BMP/LBPA synthesis.

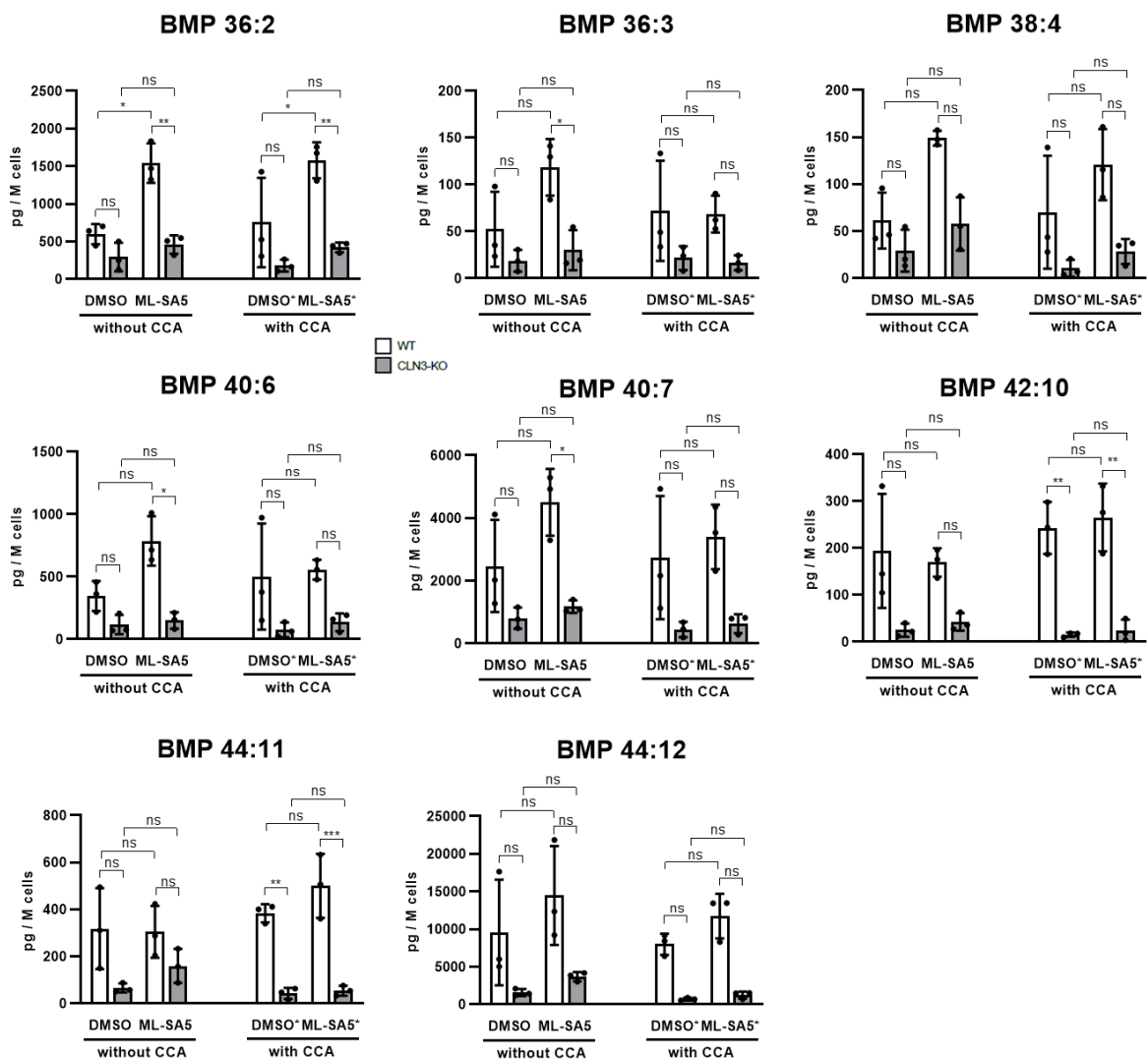


**Figure 33: TRPML1 activation did not elevate BMP levels in ARPE-19 CLN3-KO cells.** BMP species in cell lysates of ARPE-19 WT and CLN3-KO cells without and with cell cycle arrest were analyzed using mass spectrometry. Cells were treated with 3  $\mu$ M ML-SA5 for 48 h. BMP levels were quantified in picogram per million of cells from 3 independent cell samples, measured in one LC-MS/MS run. P-values calculated by two-way ANOVA coupled with multiple comparisons using Sidak test. ns nonsignificant<0.1234, \* $p$ -value<0.0332; \*\* $p$ <0.0021, \*\*\* $p$ -value<0.0002, \*\*\*\* $p$ -value<0.0001.

### **3.5 Possible mechanisms involved in amelioration of CLN3 associated lysosomal phenotypes**

In previous experiments activation of TRPML1 was found to ameliorate increased number/size of lysosomes and storage materials in ARPE-19 CLN3-KO cells. As a next step possible TRPML1 dependent mechanisms involved in the reduction of CLN3 associated phenotypes were investigated. A number of roles have been described for TRPML1 in regulating endolysosomal vesicle homeostasis, including TFEB-dependent lysosomal biogenesis, induction of autophagy, CaMKK $\beta$ /VPS34-dependent and TFEB-independent induction of phagophore formation, lysosomal exocytosis, as well as vesicle fusion. Most of these require its function as a key lysosomal calcium release channel<sup>188,11,19,83</sup>.

#### **3.5.1 TRPML1 activation induces TFEB translocation in ARPE-19 CLN3-KO cells**

TRPML1-mediated lysosomal calcium release triggers dephosphorylation and nuclear translocation of TFEB<sup>83</sup>. To investigate whether TRPML1 agonists induce TFEB translocation in ARPE-19 CLN3-KO cells, cells were stained for TFEB upon stimulation with the TRPML1 agonists ML-SA5, ML-SA1 and MK-83. Comparable levels of TFEB nuclear translocation were detected in WT and CLN3-KO cells, as reflected by similar increases in the ratio of nuclear/cytoplasmic TFEB protein staining (Figure 34 A-C). For reference, the mTORC1 inhibitor Torin1 elicits TRPML1-independent TFEB nuclear translocation and showed comparable effects (Figure 34 A-C). TFEB-dephosphorylation in immunoblot is reflected by a downward molecular weight shift of the protein in the gel. All TRPML1 agonists shifted TFEB to a lower molecular weight, but no differences were detected between WT and CLN3-KO cells (Figure 34 D). TFEB mRNA expression levels were similar in WT and CLN3-KO cells. These did not change following ML-SA5 treatment (Figure 34 E). Note that TRPML1 agonists and Torin1 also induced TFEB nuclear translocation in ARPE-19 cells before CCA, but to a smaller extent than in cells after CCA, which could be explained by the increased TFEB expression levels under CCA.

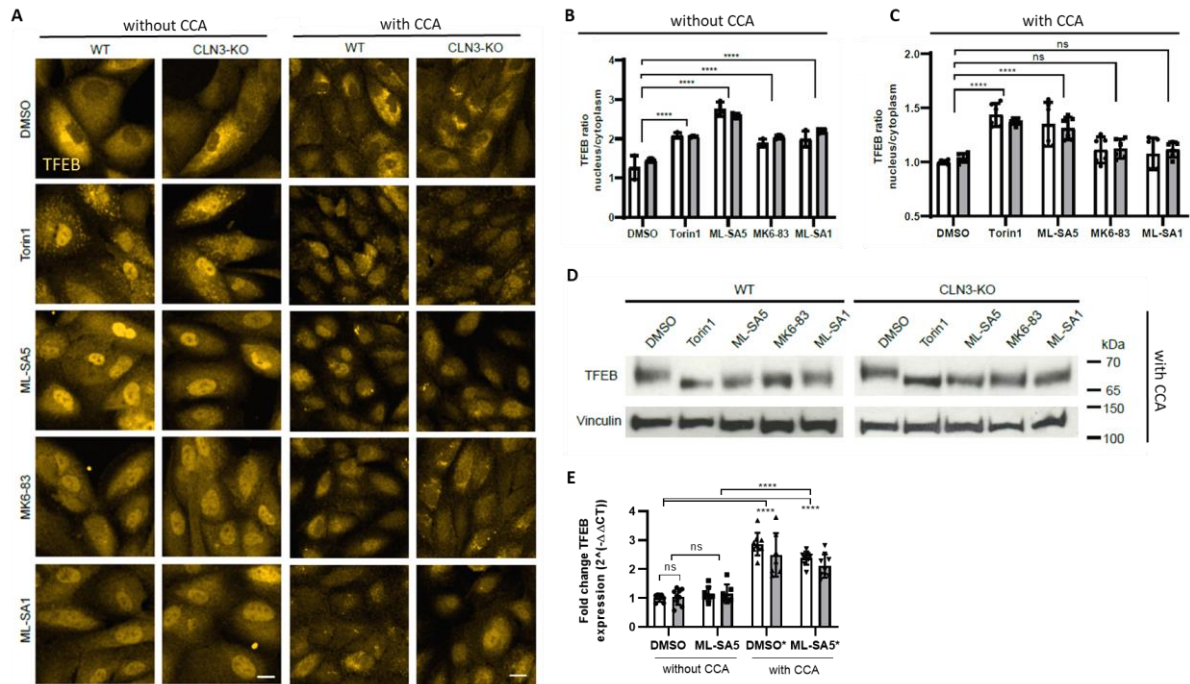


**Figure 34: Effect of TRPML1 activation on TFEB expression and nuclear translocation in WT and CLN3-KO cells.** **A** Representative immunocytochemical images showing TFEB nuclear translocation after treatment with 30  $\mu$ M TRPML1 agonists ML-SA5, ML-SA1 and MK6-83 and 1  $\mu$ M of control compound Torin1 for 2 h, without and with cell cycle arrest in ARPE-19 WT and CLN3-KO. Scale bar: 20  $\mu$ m. **B, C** Quantification of images shown in A. Plot shows TFEB nuclear/cytoplasm ratio. High content confocal imaging. Quantifications summarize data from one experiment. In total three independent experiments were performed. Per experiment 6 wells per condition and 9 images per well were analyzed. Values are means  $\pm$  SD. **D** Immunoblot analysis of total cellular TFEB levels. Cell cycle arrested ARPE-19 WT and CLN3-KO were treated with mTORC-inhibitor Torin1 and TRPML1 agonists for 2 h. Treatment leads to TFEB dephosphorylation and nuclear translocation, which is reflected by a size shift. **E** Relative mRNA expression levels of TFEB, normalized to PPIB without and with CCA. Cells were treated for 24 h with 30  $\mu$ M ML-SA5. Values shown are means  $\pm$  SD,  $n=3$  independent experiments. P-values calculated by a two-way ANOVA coupled with multiple comparisons using Tukey test. ns nonsignificant <0.1234, \* $p$ -value <0.0332; \*\* $p$  <0.0021, \*\*\* $p$ -value <0.0002, \*\*\*\* $p$ -value <0.0001.

### 3.5.2 TRPML1 activation fails to elevate mature CathD and TPP1 enzyme levels

As cathepsin D and TPP1 are described to be involved in SubC degradation<sup>86,87</sup>, their protein expression was analyzed. Experiments revealed increased levels of the pre- and intermediate forms but decreased levels of mature CathD protein in ARPE-19 CLN3-KO compared to WT cells (Figure 35 A, B, C). Treatment with ML-SA5 increased the levels of the pre- and intermediate CathD protein forms, but failed to increase the levels of the mature CathD protein in CLN3-KO cells. Unlike CathD, inactive pre- and active mature TPP1 protein forms were both decreased in CLN3-KO cells. TRPML1 activation increased pre-TPP1 levels but decreased mature TPP1 protein levels in both WT and CLN3-KO cells. Note, these quantifications were done by normalization to LAMP1, which is significantly increased in CLN3-KO cells (see LAMP1 analysis, Figure 35 A). In contrast, ML-SA5 treatment did result in similar increases of CathD and TPP1 mRNA levels in WT and CLN3-KO cells (Figure 35 D, E). However, this enhanced expression fails to compensate for the reduced levels of

mature CathD and TPP1 protein in lysosomes, and therefore unlikely explains the enhanced clearance of SubC observed after treatment with ML-SA5.

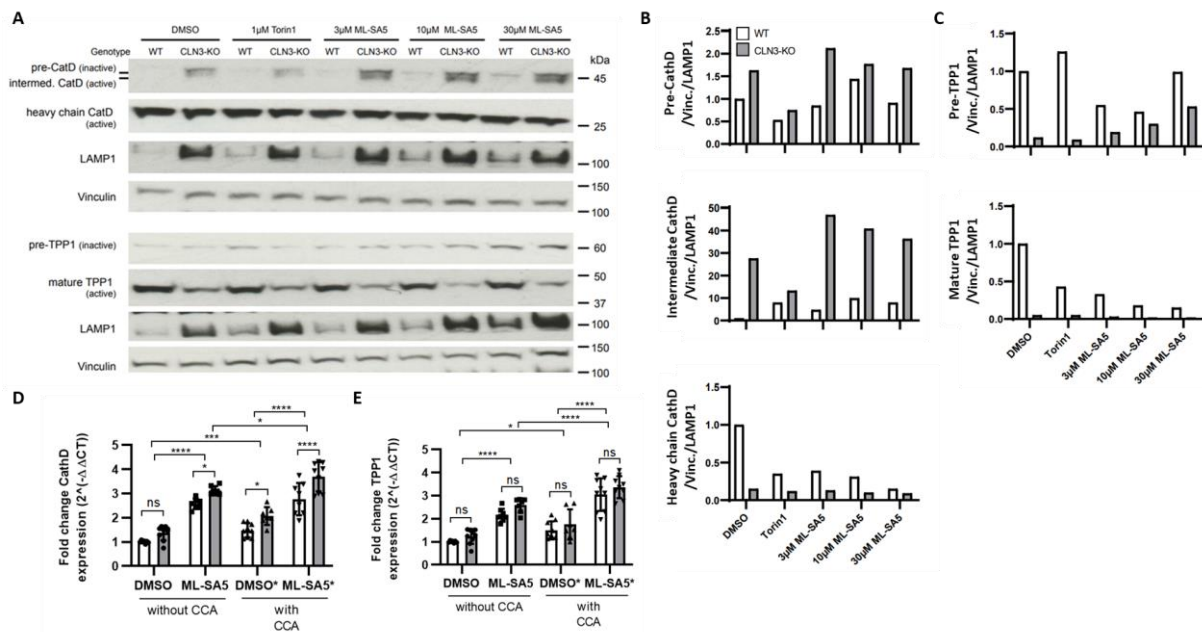


**Figure 35: Effect of TRPML1 activation on lysosomal enzyme activity in WT and CLN3-KO cells. A** Immunoblot analysis of Cathepsin D (CathD), TPP1 and LAMP1 protein. Cell cycle arrested ARPE-19 WT and CLN3-KO cells were treated with 3, 10 and 30  $\mu$ M ML-SA5 for 48 h. **B, C** Quantifications of pre-CathD, the intermediate processed form of CathD, and heavy chain mature CathD (**B**) as well as pre-TPP1 and its mature form (**C**). The data are from one representative experiment. In total three independent experiments were performed. Values are means  $\pm$  SD. **D, E** Relative mRNA expression levels of CathD (**D**) and TPP1 (**E**), normalized to PPIB. Cell cycle arrested cells were treated for 24 h with 30  $\mu$ M ML-SA5. Values are means  $\pm$  SD,  $n=3$  independent experiments. P-values calculated by two-way ANOVA coupled with multiple comparisons using Tukey test. Ns nonsignificant  $<0.1234$ , \* $p$ -value  $<0.0332$ ; \*\* $p$   $<0.0021$ , \*\*\* $p$   $<0.0002$ , \*\*\*\* $p$   $<0.0001$ .

### 3.5.3 SubC reduction is mediated by TFEB independent processes

The transcription factor TFEB is regulating various lysosomal and autophagy related genes. This raised the question, whether TRPML1 activation would also reduce lysosomal accumulation material in the absence of TFEB. To knockdown TFEB protein, siRNAs were transfected in cell cycle arrested ARPE-19 WT and CLN3-KO cells. Knockdown of TFEB was confirmed by immunocytochemistry and immunoblot analysis (Figure 36 A-C). TFEB knockdown was followed by addition of TRPML1 agonist ML-SA5 for 48 hours and subsequent SubC & LAMP1 immunofluorescence staining. ML-SA5 treatment reduced SubC-LAMP1 area of colocalization to same levels in cells without siRNA and with TFEB knockdown (Figure 36 D-E), strongly suggesting that the SubC reduction is mediated by TFEB independent processes.

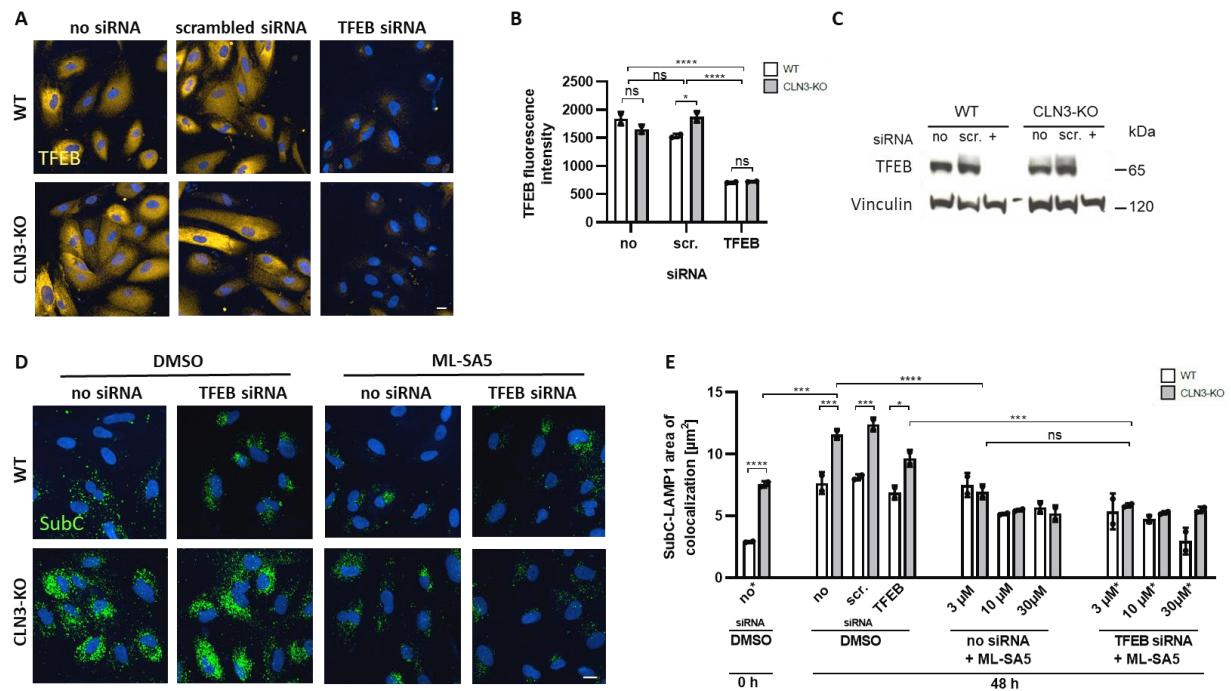


**Figure 36: SubC reduction in CLN3-KO cells is mediated by TFEB independent processes.** **A** Representative immunocytochemical images showing TFEB knockdown with siRNAs in cell cycle arrested ARPE-19 WT and CLN3-KO cells. Scale bar: 20  $\mu\text{m}$ . **B** Quantification of images shown in **A**. Plot shows TFEB fluorescence intensity of one representative experiment. High content confocal imaging. Quantifications summarize data from one experiment. In total three independent experiments were performed. Per experiment 2 wells per condition and 9 images per well were analyzed. Values are means  $\pm$  SD. **C** Immunoblot analysis of total cellular TFEB levels. Cell cycle arrested ARPE-19 WT and CLN3-KO were treated with no, scrambled (scr.) and TFEB (+) siRNAs. **D** Representative immunocytochemical images showing SubC immunofluorescence with siRNA & 3  $\mu\text{M}$  ML-SA5 treatment in cell cycle arrested ARPE-19 WT and CLN3-KO cells. Cells were treated for 48 hours with ML-SA5. Scale bar: 20  $\mu\text{m}$ . **E** Quantification of images shown in **D**. Plot shows SubC-LAMP1 area of colocalization in  $\mu\text{m}^2$ . High content confocal imaging. Quantifications summarize data from one experiment. In total three independent experiments were performed. Per experiment 2 wells per condition and 9 images per well were analyzed. Values are means  $\pm$  SD. Values. P-values calculated by a two-way ANOVA coupled with multiple comparisons using Tukey test. ns nonsignificant < 0.1234, \**p*-value < 0.0332; \*\**p* < 0.0021, \*\*\**p*-value < 0.0002, \*\*\*\**p*-value < 0.0001.

### 3.5.4 LC3-II levels increase after activation of TRPML1 in ARPE-19 WT and CLN3-KO cells

Several studies have documented defects in the autophagy pathway in CLN3 deficient cells<sup>55,57,52</sup>, which were also found in ARPE-19 CLN3-KO cells (chapter 3.2.5 and 3.3.5). It has been reported, that TRPML1 activation leads to early and late effects in the autophagy pathway. An early effect includes an induction of phagophore formation through activation of CaMKK $\beta$ /VPS34<sup>19</sup>. A later effect involves the TFEB-mediated upregulation of CLEAR genes and lysosomal biogenesis<sup>92</sup>. To detect TRPML1-mediated effects on autophagy, the main focus was on LC3 protein.

A brief treatment (30 min) with ML-SA5 increased LC3-II levels in both WT and CLN3-KO cells as shown by immunoblot analysis (Figure 37 A-B). However, LC3 mRNA expression was not changed upon ML-SA5 treatment for 24 hours (Figure 37

C). Immunofluorescence analysis (Figure 37 E-D) showed a rapid increase of LC3 puncta. For reference, increases in LC3-II protein and LC3 puncta were also observed after a 3 h treatment with the vacuolar ATPase and autophagy inhibitor Bafilomycin A1. Treatment with ML-SA5 also significantly increased the number of LC3 puncta colocalizing with LAMP1 and representing autolysosomes (Figure 37 A-B, D-F). Cells without CCA showed similar results (not shown here).

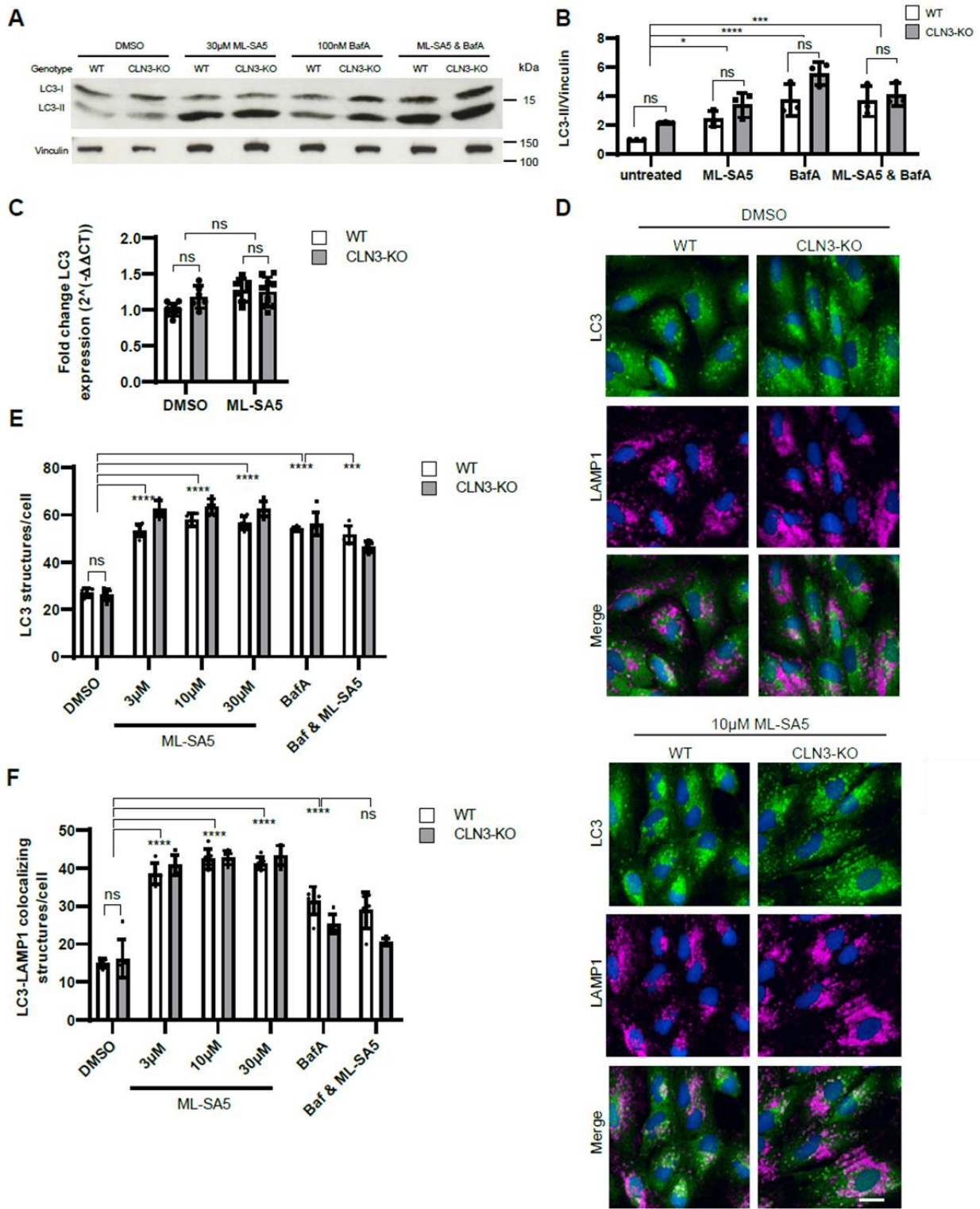


**Figure 37: TRPML1 activation increases LC3-II levels in WT and CLN3-KO cells.** **A** Immunoblot analysis of LC3. Cell cycle arrested ARPE-19 WT and CLN3-KO cells were treated for 30 min with 30  $\mu$ M ML-SA1 and/or for 3 h with 100 nM Bafilomycin A1 (BafA). **B** Quantification of LC3-II levels normalized to Vinculin,  $n=3$  independent experiments. **C** Relative mRNA expression of LC3 normalized to PPIB. Cell cycle arrested ARPE-19 cells were treated for 24 h with 30  $\mu$ M ML-SA5. Values are means  $\pm$  SD,  $n=3$  independent experiments. **D** Representative immunocytochemical images of LC3 and LAMP1 localization in cell cycle arrested ARPE-19 WT and CLN3-KO cells. Scale bar: 20  $\mu$ m. **E**, **F** Plots represent the number of LC3 structures/cell (**E**) and LC3-LAMP1 colocalizing structures/per cell (**F**). Cells were treated with ML-SA5  $\pm$  BafA. BafA was added for 3 h, ML-SA5 for 30 min (**D-F**). High content confocal imaging. Quantifications summarize data from one experiment. In total three independent experiments were performed. Per experiment 3 wells per condition and 9 images per well were analyzed. Values are means  $\pm$  SD. P-values calculated by two-way ANOVA coupled with multiple comparisons using Tukey test. ns nonsignificant  $<0.1234$ , \* $p$ -value  $<0.0332$ ; \*\* $p$ -value  $<0.0021$ , \*\*\* $p$ -value  $<0.0002$ , \*\*\*\* $p$ -value  $<0.0001$ .

Taken together, these data show that TRPML1-mediated effects on phagophore formation and autolysosome formation are similar in WT and CLN3-KO cells and therefore not significantly perturbed by CLN3 deficiency.

### **3.5.5 TRPML1 activation induces lysosomal exocytosis in ARPE-19 WT and CLN3-KO cells**

TRPML1 activation can also trigger lysosomal exocytosis in both fast TFEB-independent and slower TFEB-dependent modes<sup>93,94</sup>. During lysosomal exocytosis, the lysosomal membrane fuses with the plasma membrane. This enables membrane repair, which was proposed to underlie therapeutic effects of ML-SA5 in a Duchenne muscular dystrophy mouse model<sup>27</sup>. It also enables lysosomes to release their content and clear storage materials into the extracellular space. The fusion of the lysosomal membrane with the plasma membrane is calcium-dependent. It can be elicited by TRPML1-mediated lysosomal calcium release, and further facilitated by TFEB activation<sup>93</sup>. To investigate TRPML1-induced lysosomal exocytosis, detection by flow cytometry of a lysosomal luminal LAMP1 epitope that becomes exposed on the cell surface after lysosomes fuse with the plasma membrane was used. To elicit TFEB-independent lysosomal exocytosis events, treatment times with TRPML1 agonists for 90 min were chosen. For reference, cells were treated with the ionophore ionomycin, which triggers a massive increase of cytoplasmic calcium levels inducing TRPML1-independent lysosomal exocytosis<sup>95</sup>.

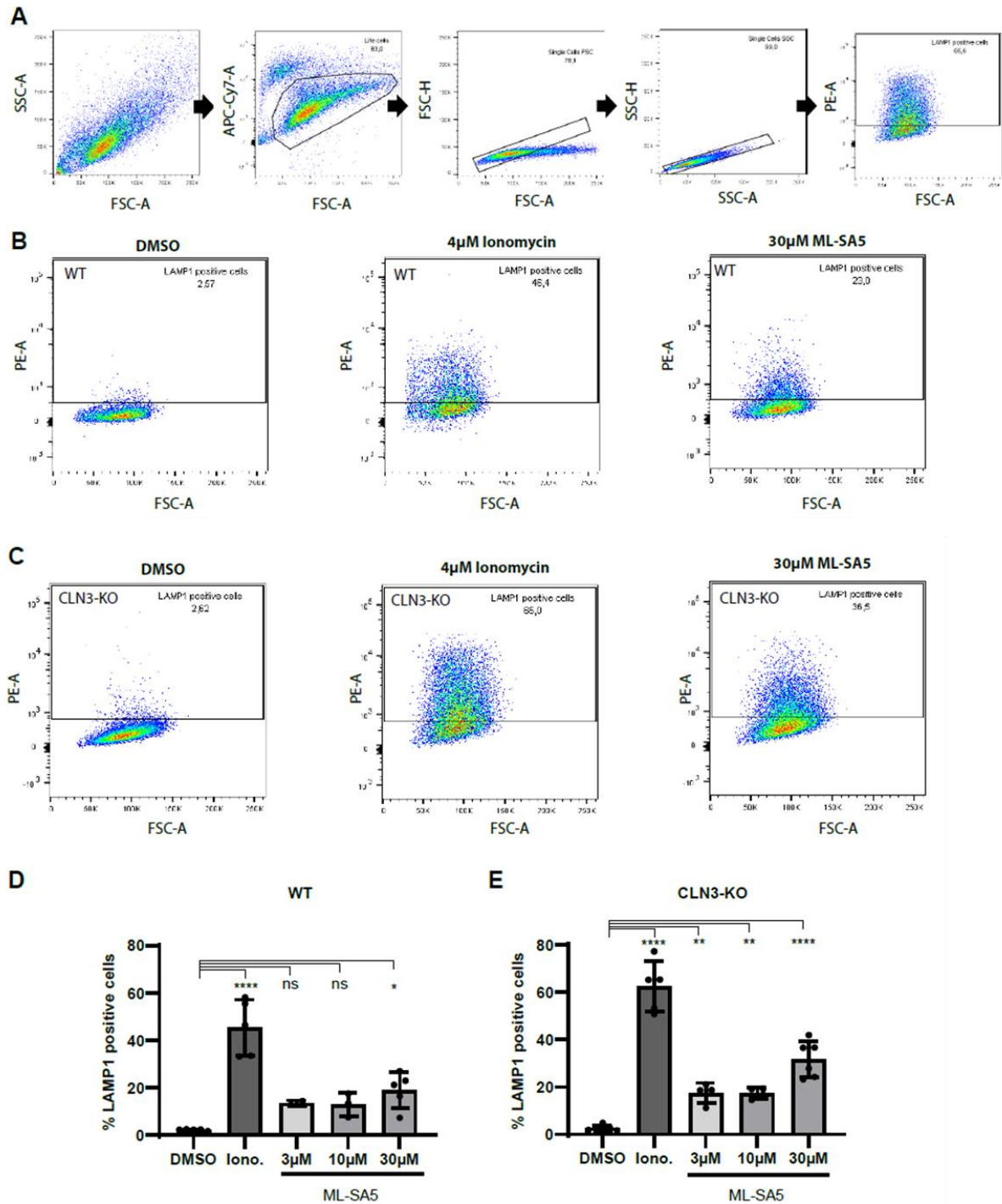


**Figure 38: TRPML1 activation induces lysosomal exocytosis in WT and CLN3-KO cells.** **A** Gating strategy used to identify LAMP1 positive cells by flow cytometry. **B, C** Exemplary flow cytometry plots in cell cycle arrested ARPE-19 WT (**B**) and CLN3-KO (**C**) cells. **D, E** Plots represent the percentage of cell cycle arrested ARPE-19 WT (**D**) and CLN3-KO (**E**) cells showing plasma membrane LAMP1 staining. For reference, cells were treated for 15 min with Ionomycin. ML-SA5 treatment was performed for 90 min. Shown are individual values from single experiments  $\pm$  SD of all experiments,  $n$  ranges from 3-6 independent experiments. P-values calculated by one-way ANOVA coupled with multiple comparisons using Dunnett test. ns nonsignificant<0.1234, \* $p$ -value<0.0332; \*\* $p$ <0.0021, \*\*\* $p$ -value<0.0002, \*\*\*\* $p$ -value<0.0001.

TRPML1 activation by ML-SA5 induced lysosomal exocytosis in WT and CLN3-KO cells under CCA conditions in a concentration-dependent manner. At a concentration of 3  $\mu$ M, approximately 20% of cells showed cell surface exposure of the luminal LAMP1 epitope in CLN3-KO cells (Figure 38 A-E). These levels did not further

increase significantly at 10  $\mu\text{M}$ , but did slightly increase at 30  $\mu\text{M}$ . In general, CLN3-KO cells show increased lysosomal exocytosis compared to WT cells.

In conclusion, TRPML1-mediated lysosomal exocytosis occurs in ARPE-19 CLN3-KO cells and therefore might be one of the key mechanisms by which TRPML1 agonists clear lysosomal storage in CLN3-deficient cells.

In summary, different cellular models for JNCL disease were investigated and the most promising model, the ARPE-19 CLN3-KO cell line, was characterized in more detail with focus on lysosomal and autophagy related impairments. Activating TRPML1, a potential therapeutic target for JNCL, reduced lysosomal phenotypes including lysosomal number/size and lysosomal storage materials SubC and Gb3. TFEB activation, autophagy induction and lysosomal exocytosis were analyzed as possible TRPML1 mechanisms of action (Figure 39).

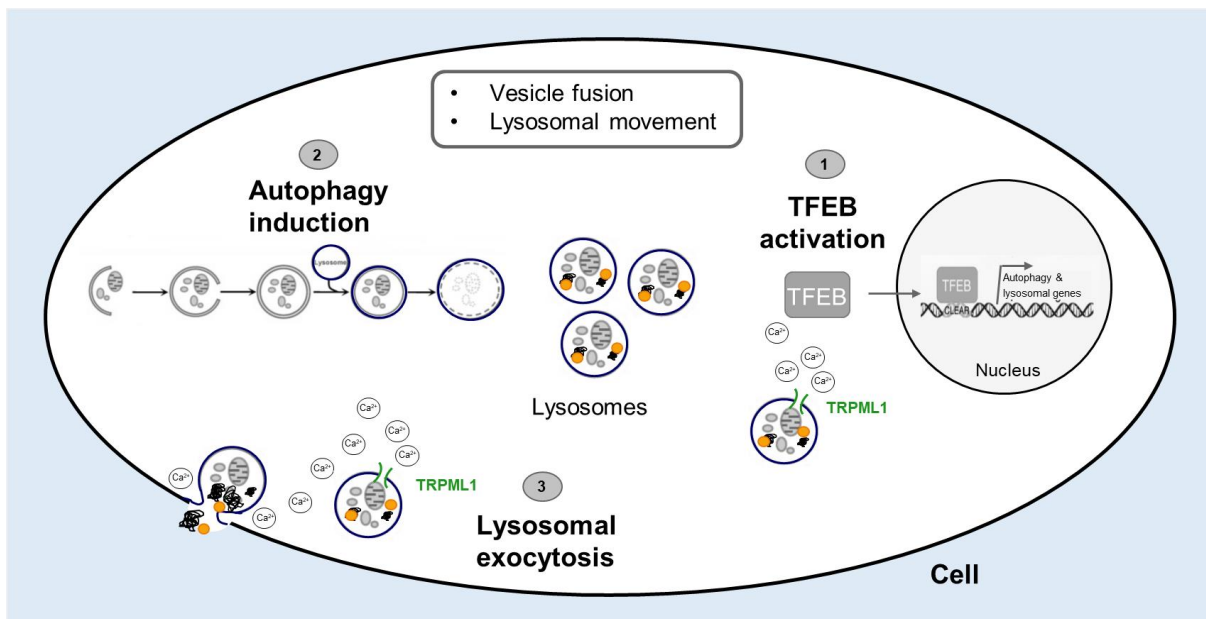


**Figure 39: Investigated mechanisms involved in TRPML1 mediated amelioration of CLN3 phenotypes.** TRPML1 regulates several cellular functions including vesicle fusion and lysosomal movement. Three TRPML1 dependent mechanisms were investigated in more detail, which are TFEB activation, autophagy induction and lysosomal exocytosis.

All three processes were initiated upon activation of TRPML1 in ARPE-19 WT and CLN3-KO cells, indicating a contribution to the reduction of lysosomal phenotypes. However, despite TFEB knockdown, TRPML1 activation still led to reduced SubC levels in CLN3 deficient cells, increasing the role of autophagy and lysosomal exocytosis in lysosomal clearance upon TRPML1 activation.

## 4. Discussion

Mutations in CLN3 cause JNCL, a neurodegenerative disease affecting children<sup>38</sup>. Whereas the function of CLN3 protein is still unknown, a prominent localization to late endosomes and lysosomes is most likely<sup>44</sup>. In agreement, on cellular level, CLN3 mutations are associated with lysosomal impairments, storage material and autophagy defects<sup>55,52,51,57</sup>.

This study aimed to get further insights into alterations in the lysosomal-autophagosomal system of CLN3 deficient cells, for a better understanding which cellular processes are specifically affected. Recently, rescuing effects of lysosomal-autophagosomal defects by activating the lysosomal ion channel TRPML1 were shown for several neurodegenerative disease models<sup>24,25,26,27</sup>. A further aim of this study was therefore to investigate the effects of TRPML1 activation on lysosomal phenotypes and the underlying mechanisms in CLN3 deficient cells.

### 4.1 ARPE-19 CLN3-KO cells as cellular model for JNCL disease

HeLa, ARPE-19 and iPSC CLN3 deficient cells and their respective isogenic WT controls were used to investigate cellular implications of CLN3 mutations. The introduced mutations caused premature stop codons in all three cell lines. This is in accordance with the exon $\Delta$ 7/8 mutation, which induced a frameshift and a premature stop codon in exon 9<sup>43</sup>. As premature stop codons are likely to be degraded by nonsense mediated decay of the mRNA<sup>67</sup> and topology models suggest the absence of the lysosomal targeting sequences, this could prevent mutated CLN3 to be transported to the lysosome. These two independent mechanisms are presumed to prevent correct protein translation and localization of mutated CLN3, making the emergence of a functional CLN3 protein very unlikely. Different studies confirmed this hypothesis. For example, mRNA levels of the CLN3 exon $\Delta$ 7/8 mutant were decreased compared to CLN3 WT mRNA levels<sup>50</sup> and truncated CLN3 protein was published to colocalize with ER markers<sup>43</sup>. In line with this, a reduction of about 80% of CLN3-mutated compared to WT mRNA was found in ARPE-19 cells. Due to the lack of good and specific anti-human CLN3 antibodies<sup>43</sup>, CLN3 protein amount and localization could not be studied on protein level. Previous studies in cell lines deriving from JNCL patients, CLN3 knock-in and knockout mice revealed comparable cellular CLN3 phenotypes<sup>50,51,52</sup>. Therefore, the three generated CLN3 knockout cell lines are regarded as suitable and promising cellular models to study JNCL disease.

HeLa and ARPE-19 cells are mature cell lines and were not further differentiated. In contrast, iPSC cells were differentiated into RPE cells. Fully differentiated RPE cells reflected the RPE-typical features, such as pigmentation, hexagonal morphology, formation of tight junctions and expression of RPE specific proteins<sup>61</sup>. One additional quality criterion of RPE cells is the measurement of the trans-epithelial resistance (TER), which was found to be significantly reduced in CLN3-KO cells. The TER measurement is used to assess the barrier function of epithelial cells. Specific tight junction proteins and the physical structures and properties of the cellular membrane are known to influence the TER<sup>96</sup>. Therefore, a difference in these factors might be causing a reduction of TER in iPSC derived RPE CLN3-KO cells. In contrast, in a study with RPE cells harboring the common  $\Delta$ ex7-8 mutation no difference in TER was found<sup>97</sup>.

To elucidate the ideal cell system to study JNCL disease, endocytic uptake, lysosomal enzyme activity, lysosomal quantity, the accumulation of JNCL typical storage material and the autophagic marker LC3 were investigated. In HeLa and iPSC derived CLN3 deficient RPE cells reduced or equal intensities for nearly all endosomal/lysosomal parameters compared to WT cells were found. In contrast, ARPE-19 CLN3-KO cells showed significantly increased levels of all investigated parameters. Compared to a number of previously published studies, a decreased endocytic uptake and an impaired or reduced lysosomal enzyme activity would have been expected in CLN3 deficient cells<sup>51,57,98</sup>, which fits to the data of HeLa and iPSC derived RPE CLN3-KO cells. Especially in CLN3 deficient ARPE-19 cells, the elevated LAMP1 immunofluorescence indicating an increased number/size of lysosomes, could be an explanation for all the other increased parameters. The elevated DQ-BSA and Magic Red staining are therefore hypothesized not to be caused by an increased endocytic uptake and a higher lysosomal enzyme activity, but rather by a higher lysosomal number/size in this cell type. Accumulation of SubC was not found in HeLa, but in RPE and ARPE-19 CLN3-KO cells and could be further increased in ARPE-19, but not in HeLa cells, with cell cycle arrest. As RPE cells are non-proliferating cells, they were excluded from this analysis. The accumulation of the mitochondrial ATPase subunit C is a common feature of JNCL and observed in different CLN3 deficient cells<sup>51,98,99</sup>. In accordance with previous studies<sup>52,57,100,99</sup>,

elevated LC3-II levels suggest an altered autophagy in HeLa and ARPE-19 CLN3-KO cells. Due to high cell numbers needed for immunoblot analysis, LC3-II levels were not investigated in iPSC derived RPE cells.

Depending on the cell type, lysosomal activity, as well as the amount of phagocytosis and the rate of autophagy is varying. Interestingly, RPE cells are the most highly phagocytosing cells of the body<sup>101</sup>. Lysosomal function and the autophagic pathway are directly influenced by this and most probably regulated differently in RPE cells compared to HeLa cells. Deviating lysosomal activities and the absence of SubC accumulations in HeLa cells might therefore be well explained by this.

Taken together, CLN3 deficient ARPE-19 cells represented the most stable phenotype. Due to their origin from the eye, they are of high relevance to JNCL, where visual impairments can be seen in the early phases of the disease. In addition, their immortalization enables easy proliferation and cost-saving culture conditions compared to iPSC derived RPE cells. ARPE-19 CLN3-KO were therefore chosen for a detailed phenotypic characterization.

## **4.2 Detailed phenotypic characterization of ARPE-19 CLN3-KO cells**

Working with ARPE-19 cells, cell cycle arrest (CCA) was found to elevate not only storage material in the CLN3-KO cells, but also lysosomal levels and lysosomal enzyme activities. Therefore, CCA was implemented as a tool for all following experiments to facilitate detection of phenotypes in CLN3-KO cells. To the best of my knowledge, so far this is the first survey studying CLN3 KO cells under cell cycle arrest. This allows the transformation of various proliferating cell types to non-proliferating cells with enhanced CLN3 phenotypes and might promote elucidating the cellular role of CLN3.

Optimized CCA conditions were used to investigate SubC and globotriaosylceramide (Gb3) storage in CLN3 deficient ARPE-19 cells. SubC, as well as Gb3 were found to accumulate in lysosomes of CLN3-KO ARPE-19 cells. Increased levels of Gb3 have been recently published in ARPE-19 cells, fibroblasts and murine models of CLN3 and CLN7 diseases<sup>59</sup>. Gb3 is a known deposit in Fabry's disease, caused by mutations in the lysosomal enzyme  $\alpha$ -galactosidase A<sup>74</sup>. Why Gb3 accumulates in CLN3 deficient cells remains elusive. A degradation problem due to impaired enzyme

function would be as conceivable as an altered trafficking of Gb3 in CLN3 deficient cells.

Additionally, we found decreased levels of several bis(monoacylglycerol)phosphates (BMPs), also known as lysobisphosphatic acids (LBPA) in ARPE-19 CLN3-KO compared to WT cells. The reduced BMP/LBPA levels were only detected in cell lysates, not in the supernatant. This finding is consistent with a study in CLN3 deficient patient fibroblasts<sup>60</sup>. Reduced BMP levels in CLN3 defective cells are hypothesized to be caused by an impaired BMP synthesis<sup>60</sup>. The BMP synthesis is not yet fully understood, but it is believed to be synthesized in late endocytic compartments from the phospholipid precursor phosphatidyl glycerol (PG)<sup>79</sup>. PG in turn is synthesized and localized to mitochondria, most probably reaching lysosomes via mitophagy and being converted to BMP by a complex series of enzymatic reactions<sup>79</sup>. Hence, the reduced BMP levels observed in ARPE-19 CLN3-KO cells might be explained by altered mitophagy, impaired lysosomal enzymatic activity and/or a direct contribution of CLN3 to BMP synthesis.

In the acidic environment of the lysosome, BMP is negatively charged and present on the surfaces of inner membranes, where several positively charged lipids and enzymes are suggested to use BMP as a platform for degradation<sup>78</sup>. Therefore, it is hypothesized that the reduced BMP levels might contribute to an impaired lysosomal degradation capacity of CLN3 deficient cells.

In previous experiments, lysosomes were observed to accumulate in ARPE-19 CLN3-KO cells. To confirm, that not only LAMP1 is enriched in these cells, lysosomal membrane proteins as well as the pH sensitive dye LysoTracker were investigated with/without CCA. LAMP1, LAMP2, NPC1, as well as LysoTracker levels were found to be significantly elevated, demonstrating indeed an accumulation of lysosomes in CLN3 deficient ARPE-19 cells. With immunofluorescence analysis it was not possible to resolve if lysosomal number or size is altered. To elucidate this, electron microscopy images of cells under cell cycle arrest were quantified, showing increased number and also size of lysosomes in CLN3-KO cells. Expression analysis of several lysosomal genes (LAMP1, LAMP2, NPC1, CathB and D and TPP1) revealed no significant alterations between WT and CLN3-KO cells. Elevated LAMP1 levels were also observed in other neurodegenerative diseases, such as Alzheimer's disease, in the lysosomal storage disorder Pompe disease, and different types of

cancer. However, in contrast to results in ARPE-19 cells, mRNA expression of LAMP1 was upregulated in the mentioned studies<sup>102,103,104,105</sup>. Comparable mRNA expression levels of lysosomal markers between CLN3 deficient and WT cells suggest that not lysosomal biogenesis, but rather degradation of lysosomes is impaired in CLN3 defective cells. In line with this, LAMP1 was lately hypothesized not only to be a marker for degradative lysosomes, but also to be present on lysosomes lacking major hydrolyzing enzymes<sup>106</sup>, which could be the case in CLN3 deficient cells. Recently, elevated levels of LAMP1 protein have been detected in blood and urine samples from CLN3 patients, offering it as a potential biomarker for JNCL<sup>107,108</sup>.

Several studies have shown autophagy defects in CLN3 deficient cells, with increased LC3-II levels often interpreted to be a result of defects in autophagosome-lysosome fusion<sup>52,57</sup>. In ARPE-19 CLN3-KO cells also slightly increased basal LC3-II levels were found. These could result from increased autophagosome formation, deficiencies in autophagosome-lysosome fusion, or caused by defective lysosomal degradation. LC3-LAMP1 colocalizing structures/cell were found to be comparable in both cell lines and under both CCA conditions, which points towards a still functional autophagosome-lysosome fusion in CLN3 deficient ARPE-19 cells. Furthermore, several results suggest that autophagy induction is not altered in ARPE-19 CLN3-KO cells. The inhibition of autophagy with Bafilomycin A1 and Chloroquine further increased LC3(-II) levels in both genotypes, showing that CLN3-KO cells are constantly able to produce new autophagosomes. mRNA expression analysis of LC3 showed no differences between WT and CLN3 deficient cells, indicating that autophagy induction on expression level is not altered in CLN3-KO cells. TFEB, the master transcription factor for lysosomal and autophagosomal genes<sup>92</sup> was neither on expression, nor on protein level found to be changed in CLN3-KO cells. The energy and nutrient sensing complex mTORC1 is an upstream regulator of TFEB, as well as autophagy and is located in its activated status to the lysosomal surface<sup>84,85</sup>. By investigating mTOR amounts and colocalization with lysosomes no distinct difference between WT and CLN3-KO cells was found. However, immunoblots of direct mTORC1 downstream targets point towards an elevated mTORC1 activity in CLN3 deficient cells. The literature provides controversial data on mTORC1. In CLN3 fibroblasts, results indicate an increased mTORC1 activity<sup>55</sup>, whereas a decreased mTORC1 activity was concluded in mouse brain extracts and cerebellar cells carrying

a homozygous CLN3 $\Delta$ ex7/8 mutation<sup>57</sup>. mTORC1 regulates by various upstream signals like growth factors, energy status, oxygen and amino acids<sup>17</sup> several downstream processes including autophagy, mRNA translation, ribosome biogenesis and lipid synthesis<sup>5</sup>. Varying nutrient supplies in the studies might have led to differently measured mTORC1 activities. Also, depending on the cell type nutrient and energy needs as well as the resulting mTORC1 regulation might be different and therefore not comparable. Especially, in brain cell lysates from mouse models the effect of the diet on the nutrient status of different cell types is hard to control. Due to the complex interplay of mTORC1 with many cellular mechanisms, measured activities should be treated with caution.

Taken together, these data indicate a functional regulation and induction of autophagy, as well as an intact autophagosome-lysosome fusion. The elevated LC3-II levels found in ARPE-19 CLN3-KO cells might therefore be caused by an impaired lysosomal degradation, leading to an accumulation of lysosomes and storage material.

The processing of lysosomal enzymes was investigated using cathepsin B, D und TPP1. Expression levels of all three enzymes were not altered in ARPE-19 CLN3-KO cells, as seen in previous experiments. Using immunoblotting, mature active enzymes were visualized. Processing of inactive pre-, to intermediate and mature active enzymes is accompanied by differences in protein size, which can be separated on SDS gels. Without CCA, increased levels of pre/intermediate forms, but equal levels of mature active enzymes were found. However, under CCA and with taking the lysosomal number and size into account by normalization to LAMP1, especially the mature active enzyme forms of CathD and TPP1 were significantly reduced in CLN3 deficient cells. Both enzymes are known to be involved SubC degradation<sup>86,87</sup>. Decreased TPP1 and CathD protein levels were also found in previous studies investigating CLN3 deficient cells<sup>55,51,98</sup> and might therefore be an explanation for lysosomal storage material in JNCL. Increased lysosomal pH, altered protein transport or processing and impaired trafficking of lysosomal sorting receptors in CLN3-KO cells could lead to reduced enzyme levels<sup>53,55,109</sup>.

### **4.3 Increased TRPML1 activity in ARPE-19 CLN3-KO cells**

TRPML1 expression was similar in WT and CLN3 deficient cells, while TRPML1 activity was increased in ARPE-19 CLN3-KO cells. Controversial to these results, one study has shown impaired TRPML1 mediated calcium signaling in lipid accumulating lysosomes of RPE cells<sup>110</sup>. Reports studying TRPML1 in other lysosomal storage disorders have also shown reduced lysosomal TRPML1 activity<sup>89,111</sup>. Dysfunctional lysosomes and elevated lysosomal pH, both being hallmarks of various lysosomal storage disorders, are often hypothesized to inhibit TRPML1 expression and function<sup>89,111</sup>. Still, TRPML1 activity was increased in the ARPE-19 CLN3-KO cells investigated here. One potential mechanism underlying the increased activity of TRPML1 in CLN3 deficient cells might be reactive oxygen species (ROS), which are proposed to activate TRPML1<sup>90,14,16</sup>. ROS were found to accumulate in JNCL fibroblasts, probably due to oxidatively damaged mitochondria<sup>55</sup>. Mitochondria, being the source of ROS, are dysfunctional in JNCL. They were reported to be abnormally elongated in cerebellar cells harboring a CLN3 mutation<sup>51</sup>. Hence, the mitochondrial impairments of CLN3 deficient cells might be an explanation for the increased TRPML1 activity found in ARPE-19 CLN3-KO cells. Additional studies of mitochondrial function in ARPE-19 CLN3 deficient cells could give further insights into its effects on TRPML1 activity.

There are, however, other possible explanations for increased TRPML1 currents in CLN3 deficient ARPE-19 cells. An impaired turnover of TRPML1 may lead to a higher number of channels in lysosomal membranes. Recently, it was proposed that TRPML1 recycling is mediated by the endosomal sorting complex required for transport I (ESCRT-I)<sup>112</sup>. Furthermore, CLN3 was suggested to play a role in endosome-to-trans-golgi network (TGN) trafficking<sup>53</sup>. If cargo sorting, regulated by ESCRT complexes and/or subsequent trafficking back to the TGN is altered in CLN3 disease, this might possibly lead to elevated levels of TRPML1 as well as other lysosomal membrane proteins.

### **4.4 TRPML1 activation ameliorates lysosomal phenotypes in ARPE-19 CLN3-KO cells**

Activation of TRPML1 was shown to be beneficial in several neurodegenerative diseases<sup>24,25,26,27</sup>, but was not studied in CLN3 deficient cells so far. Upon TRPML1 activation in ARPE-19 CLN3-KO cells, lysosomal storage of SubC and Gb3

decreased significantly. This is in line with studies in Niemann-Pick type C disease cells, where activation of TRPML1 enhanced the clearance of lysosomal storage material including cholesterol accumulations<sup>26</sup>.

These novel results, that show the reduction of two unrelated accumulation products in CLN3 deficient cells upon TRPML1 activation, represent TRPML1 a promising therapeutic target for JNCL.

However, BMP/LBPA levels were not altered upon TRPML1 activation. This finding points towards a direct role of CLN3 in BMP synthesis, which could not be compensated by activation of TRPML1.

#### **4.5 Potential mechanisms involved in lysosomal phenotype reduction**

Potential mechanisms by which TRPML1 activity leads to the reduction of accumulation products in CLN3 deficient cells were investigated. TRPML1 has several calcium-dependent functions within the cell, which might be involved in aggregate reduction. One of them could be the translocation of TFEB. TRPML1 activation is leading to Ca<sup>2+</sup> release from lysosomes, which activates calcineurin, followed by dephosphorylation of TFEB and thereby induction of its translocation into the nucleus<sup>83</sup>. In ARPE-19 CLN3-KO cells, TFEB translocation was induced and mRNA expression of lysosomal genes such as LAMP1, CathD or TPP1 was increased upon TRPML1 activation. Increased expression only partially resulted in increased protein levels of lysosomal enzymes. Whereas LAMP1 protein, pre- and intermediate protein forms of CathD and TPP1 increased significantly, mature forms of CathD and TPP1 did not alter upon TRPML1 activation in CLN3-KO cells. These data indicate a processing defect of lysosomal enzymes in CLN3-KO cells, which could not be rescued by TRPML1 activation.

TFEB is a transcription factor for a variety of lysosomal and autophagosomal genes<sup>92</sup>. Translocation of TFEB, shown to be induced by TRPML1 activation in CLN3 deficient cells is therefore directly influencing autophagic flux and lysosomal processes. A TFEB knockdown was supposed to show the TFEB dependency of TRPML1 mediated accumulation material reduction. After knocking down TFEB using siRNA, TRPML1 activation was still leading to SubC reduction in ARPE-19 CLN3-KO

cells. These results suggest that TRPML1 mediated accumulation material reduction is a TFEB independent process.

A second possible cellular mechanism by which TRPML1 activation could lead to amelioration of lysosomal phenotypes in CLN3 deficient cells might be the induction of autophagy. A direct link between TRPML1 activation and autophagy induction has been proposed. TRPML1-dependent autophagy induction requires the calcium-dependent kinase CaMKK $\beta$  as well as AMPK and was reported to be independent of TFEB<sup>19</sup>. In ARPE-19 WT and CLN3-KO cells, treatment with the TRPML1 agonist ML-SA5 increased LC3-II levels in immunoblots and LC3 structures/cell in immunofluorescence analysis to same degrees. In addition, ML-SA5 significantly elevated autophagosome-lysosome colocalizing structures in WT and CLN3 deficient cells. Taken together, not only the autophagy inducing effect of TRPML1 activation was reproduced, also increased levels of autophagosome-lysosome colocalizing structures were found upon TRPML1 activation, indicating a functional autophagosome-lysosome fusion in CLN3 deficient cells. Basal differences in LC3-II levels found in CLN3 deficient cells are therefore hypothesized to be caused by a degradation deficiency of lysosomes.

Lysosomal exocytosis could be another calcium-related process potentially involved in reducing accumulation material. To measure lysosomal exocytosis the number of cells showing a positive LAMP1 signal on the cell surface (LAMP1-PM) were analyzed, indicating a fusion of lysosomes with the plasma membrane<sup>94</sup>. ML-SA5 treatment induced a concentration-dependent increase of LAMP1-PM positive cells in both genotypes, with CLN3-KO cells showing more exocytosis than WT cells. There are at least two likely explanations for these observations. Investigating lysosomes, an elevated LAMP1 protein expression was found in CLN3 deficient cells, potentially resulting in increased exocytosis due to more and bigger lysosomes present. Furthermore, CLN3-KO cells showed increased TRPML1 currents, which might lead to a higher number of exocytosis events. To my knowledge, this is the first time lysosomal exocytosis was observed in CLN3 deficient cells upon TRPML1 activation. Having TFEB excluded from being responsible for CLN3 phenotype reduction offers lysosomal exocytosis as a promising key mechanism here. Future investigations by knocking down proteins involved in lysosome-plasma membrane fusion, like Syt-VII

or STX4<sup>113</sup>, followed by a treatment with TRPML1 agonists and an analysis of accumulation material could give insights into the contribution of lysosomal exocytosis.

In addition to the three investigated TRPML1 dependent pathways, several others could play a role and a crosstalk of pathways might occur. To elucidate additional potential pathways activated by TRPML1, a transcription analysis using RNA sequencing of cells treated with TRPML1 agonists is planned.

Collectively, this study not only presents ARPE-19 CLN3-KO as a suitable model to study JNCL, it also supports TRPML1 as a potential therapeutic target for the disease. Additional analysis of the mechanisms underlying TRPML1 mediated amelioration of CLN3 phenotypes could help identifying the responsible pathways. Follow up studies should focus on the effects of TRPML1 activation in other cell types and also in animal models to strengthen the role of TRPML1 as potential therapeutic target for JNCL and potentially other lysosomal diseases.

## 5. Summary/Zusammenfassung

### 5.1 Summary

Juvenile neuronal ceroid lipofuscinosis (JNCL) is caused by mutations in the lysosomal membrane protein CLN3. CLN3 disease is characterized by accumulation of lysosomal storage material composed of lipofuscin, the mitochondrial ATPase subunit C (SubC), globotriaosylceramide (Gb3) and a defective autophagic pathway.

Here, different CLN3 deficient cell lines including HeLa, ARPE-19 and iPSC derived RPE (retinal pigment epithelial) cells were compared to study the cellular role of CLN3 in the lysosomal-autophagosomal system. Investigation of several processes such as endocytic uptake, lysosomal enzyme activity, lysosomal quantity, storage material accumulation and autophagy presented the ARPE-19 CLN3 knockout (CLN3-KO) cells as the most appropriate cellular model to study JNCL disease.

A detailed analysis revealed in addition to SubC, the accumulation of Gb3 and an elevated number and size of lysosomes in ARPE-19 CLN3-KO cells under cell cycle arrest. Observing autophagic processes more closely suggests that autophagy induction and autophagosome-lysosome fusion are functional in CLN3-KO cells. However, several results indicate that the observed autophagy defects and the increased number and size of lysosomes are caused by an impaired functionality of lysosomes.

Pharmacological activation of the lysosomal ion channel TRPML1 has previously been shown to be beneficial in several models of neurodegenerative diseases. Here, ARPE-19 cells were used to examine, if the activation of TRPML1 reduces CLN3 disease-associated phenotypes. Upon activation of TRPML1, accumulation of lysosomes as well as storage of SubC and Gb3 were significantly reduced in CLN3-KO cells. The TRPML1 dependent induction of autophagy and activation of lysosomal exocytosis suggests an involvement of both mechanisms in lysosomal phenotype amelioration in ARPE-19 CLN3-KO cells.

This study presents ARPE-19 CLN3-KO cells as a novel model to study cytopathological processes underlying JNCL and strongly supports TRPML1 as a potential therapeutic target for the disease for the first time.

## 5.2 Zusammenfassung

Die Juvenile Neuronale Ceroid Lipofuszinose (JNCL) entsteht durch Mutationen im lysosomalen Membranprotein CLN3. Charakterisiert wird die CLN3 Erkrankung durch die Akkumulation von lysosomalem Speichermaterial, bestehend aus Lipofuscin, der mitochondrialen ATPase Untereinheit C (SubC), Globotriaosylceramid (Gb3) und einem defekten Autophagie Verlauf.

Um die zelluläre Rolle von CLN3 im lysosomalen-autophagosomalen System zu untersuchen, wurden hier verschiedene CLN3 defiziente Zelllinien, HeLa, ARPE-19 und aus iPSC differenzierte RPE (retinale pigment Epithelien) Zellen verglichen. Bei der Betrachtung verschiedener Prozesse wie der Endozytose, der lysosomalen Enzymaktivität, der lysosomalen Menge, dem Akkumulieren von lysosomalem Speichermaterial und der Autophagie zeigten sich die ARPE-19 CLN3 knockout (CLN3-KO) Zellen als das am Besten geeignete Modell, um JNCL genauer zu untersuchen.

Eine detaillierte Analyse der ARPE-19 CLN3-KO Zellen unter Zellzyklusarrest zeigte zusätzlich zu SubC eine Akkumulation von Gb3 und eine erhöhte Anzahl, sowie Größe der Lysosomen. Die genauere Betrachtung des Autophagie Prozesses deutet auf eine funktionsfähige Induktion der Autophagie und Fusion von Autophagosomen mit Lysosomen in CLN3-KO Zellen hin. Zudem weisen mehrere Ergebnisse darauf hin, dass die gefundenen Autophagie-Defekte und die erhöhte Anzahl und Größe der Lysosomen durch eine beeinträchtigte Funktion von Lysosomen ausgelöst werden.

Bei der pharmakologischen Aktivierung des lysosomalen Ionenkanals TRPML1 konnten kürzlich vorteilhafte Effekte in mehreren neurodegenerativen Krankheitsmodellen gezeigt werden. Ob die Aktivierung von TRPML1 auch CLN3 Phänotypen reduziert, wurde hier in den ARPE-19 CLN3-KO Zellen untersucht. Lysosomale Ansammlungen, sowie die Akkumulation von SubC und Gb3 wurden durch die Aktivierung von TRPML1 signifikant verringert. Die TRPML1 abhängige Induktion von Autophagie, sowie die Aktivierung der lysosomalen Exozytose deuten auf eine Beteiligung beider Mechanismen an der Verringerung lysosomaler Phänotypen in ARPE-19 CLN3-KO Zellen hin.

Diese Studie präsentiert die ARPE-19 CLN3-KO Zellen als neues zytopathologisches JNCL Zellmodell und stellt zum ersten Mal TRPML1 als mögliches therapeutisches Ziel im Kampf gegen die CLN3 Erkrankung vor.

## 6. Abbreviations

ARPE-19 – Immortalized spontaneously arising retinal pigment epithelium cell line from a 19 year old donor

AU – Autophagosome

BMP – Bis(monoacylglycerol)phosphate

CathB/D – Cathepsin B or Cathepsin D

CCA – Cell cycle arrest

CLN3 – Ceroid lipofuscinosis, neuronal 3

CMA – Chaperone-mediated autophagy

DQ-BSA – Double quenched BSA

EE – Early endosome

EM – Electron microscopy

ER – Endoplasmic reticulum

Gb3 – Globotriaosylceramide

ILV – Intralysosomal vesicles

iPSC – induced pluripotent stem cells

JNCL – Juvenile neuronal ceroid lipofuscinosis

KO – Knockout

L – Lysosome

LAMP – Lysosomal associated membrane protein

LBPA - Lysobisphosphatic acid

LC3 – microtubule-associated light chain protein

LE – Late endosome

LIMP – Lysosomal integral membrane protein

M6PR – Mannose-6-phosphate receptor

mTORC1 - mechanistic target of rapamycin complex 1

PE – phosphoethanolamine

Rap. – Rapamycin

RPE – Retinal pigment epithelial cells

RT – Room temperature

RTqPCR – Real time quantitative polymerase chain reaction

STV - Starvation

SubC – Mitochondrial ATPase subunit C

TER – Trans-epithelial resistance

TFEB – Transcription factor EB

TGN – Trans golgi network

TPP1 – Tripeptidyl Peptidase 1

TRPML1 – Transient receptor potential mucolipin 1

UPS – Ubiquitin-proteasome system

WT – Wild type

## 7. References

1. de Duve, C., Pressman, B. C., Gianetto, R., Wattiaux, R. & Appelmans, F. Tissue fractionation studies. 6. Intracellular distribution patterns of enzymes in rat-liver tissue. *Biochem. J.* 60, 604–617 (1955).
2. Inpanathan, S. & Botelho, R. J. The lysosome signaling platform: Adapting with the Times. *Front. Cell Dev. Biol.* 7, 1–22 (2019).
3. Ballabio, A. & Bonifacino, J. S. Lysosomes as dynamic regulators of cell and organismal homeostasis. *Nat. Rev. Mol. Cell Biol.* (2019) doi:10.1038/s41580-019-0185-4.
4. Gowrishankar, S. & Ferguson, S. M. Lysosomes relax in the cellular suburbs. *J. Cell Biol.* 212, 617–619 (2016).
5. Lim, C. Y. & Zoncu, R. The lysosome as a command-and-control center for cellular metabolism. *J. Cell Biol.* 214, 653–664 (2016).
6. Saftig, P. & Klumperman, J. Lysosome biogenesis and lysosomal membrane proteins: Trafficking meets function. *Nat. Rev. Mol. Cell Biol.* 10, 623–635 (2009).
7. L. Bajaj, P. Lotfi, R. Pal, A. d. Ronza, J. Sharma, M. S. Lysosome biogenesis in health and disease. *J. Neurochem.* 148, 573–589 (2019).
8. Braulke, T. & Bonifacino, J. S. Sorting of lysosomal proteins. *Biochim. Biophys. Acta - Mol. Cell Res.* 1793, 605–614 (2009).
9. Luzio, J. P., Pryor, P. R. & Bright, N. A. Lysosomes: Fusion and function. *Nat. Rev. Mol. Cell Biol.* 8, 622–632 (2007).
10. Langemeyer, L., Fröhlich, F. & Ungermann, C. Rab GTPase Function in Endosome and Lysosome Biogenesis. *Trends Cell Biol.* 28, 957–970 (2018).
11. Li, X. *et al.* A molecular mechanism to regulate lysosome motility for lysosome positioning and tubulation. *Nat. Cell Biol.* 18, 404–417 (2016).
12. Oyarzún, J. E. *et al.* Lysosome motility and distribution: Relevance in health and disease. *Biochim. Biophys. Acta - Mol. Basis Dis.* 1865, 1076–1087 (2019).
13. Friedman, J. R., DiBenedetto, J. R., West, M., Rowland, A. A. & Voeltz, G. K. Endoplasmic reticulum-endosome contact increases as endosomes traffic and mature. *Mol. Biol. Cell* 24, 1030–1040 (2013).
14. Peng, W., Wong, Y. C. & Krainc, D. Mitochondria-lysosome contacts regulate mitochondrial Ca<sup>2+</sup> dynamics via lysosomal TRPML1. *Proc. Natl. Acad. Sci. U. S. A.* (2020) doi:10.1073/pnas.2003236117.
15. Napolitano, G. *et al.* mTOR-dependent phosphorylation controls TFEB nuclear export. *Nat. Commun.* 9, (2018).
16. Zhang, X. *et al.* MCOLN1 is a ROS sensor in lysosomes that regulates autophagy. *Nat. Commun.* 7, (2016).
17. Laplante, M. & Sabatini, D. M. mTOR signaling at a glance. *J. Cell Sci.* 122, 3589–3594 (2009).
18. Sarkar, S. Regulation of autophagy by mTOR-dependent and mTOR-independent pathways: Autophagy dysfunction in neurodegenerative diseases and therapeutic application of autophagy enhancers. *Biochem. Soc. Trans.* 41, 1103–1130 (2013).
19. Scotto Rosato, A. *et al.* TRPML1 links lysosomal calcium to autophagosome biogenesis through the activation of the CaMKK $\beta$ /VPS34 pathway. *Nat. Commun.* 10, (2019).
20. Onyenwoke, R. U. *et al.* The mucopolidosis IV Ca<sup>2+</sup> channel TRPML1 (MCOLN1) is regulated by the TOR kinase. *Biochem. J.* 470, 331–342 (2015).
21. Hesketh, G. G., Wartosch, L., Davis, L. J., Bright, N. A. & Luzio, J. P. The Lysosome and Intracellular Signalling. *Prog. Mol. Subcell. Biol.* 57, 151–180 (2018).
22. Huang, P., Xu, M., Wu, Y., Rizvi Syeda, A. K. & Dong, X. P. Multiple facets of TRPML1 in

- autophagy. *Cell Calcium* 88, 10–12 (2020).
23. Sun, X. *et al.* A negative feedback regulation of MTORC1 activity by the lysosomal Ca<sup>2+</sup> channel MCOLN1 (mucolipin 1) using a CALM (calmodulin)-dependent mechanism. *Autophagy* 14, 38–52 (2018).
  24. Tedeschi, V. *et al.* The activation of Mucolipin TRP channel 1 (TRPML1) protects motor neurons from L-BMAA neurotoxicity by promoting autophagic clearance. *Sci. Rep.* 9, 1–11 (2019).
  25. Cao, Q. *et al.* BK Channels Alleviate Lysosomal Storage Diseases by Providing Positive Feedback Regulation of Lysosomal Ca<sup>2+</sup> Release. *Dev. Cell* 33, 427–441 (2015).
  26. Wang, W. *et al.* Up-regulation of lysosomal TRPML1 channels is essential for lysosomal adaptation to nutrient starvation. *Proc. Natl. Acad. Sci. U. S. A.* 112, E1373–E1381 (2015).
  27. Yu, L. *et al.* Small-molecule activation of lysosomal TRP channels ameliorates Duchenne muscular dystrophy in mouse models. *Sci. Adv.* 6, (2020).
  28. Kaur, J. & Debnath, J. Autophagy at the crossroads of catabolism and anabolism. *Nat. Rev. Mol. Cell Biol.* 16, 461–472 (2015).
  29. García-Arencibia, M., Hochfeld, W. E., Toh, P. P. C. & Rubinsztein, D. C. Autophagy, a guardian against neurodegeneration. *Semin. Cell Dev. Biol.* 21, 691–698 (2010).
  30. Lamb, C. A., Yoshimori, T. & Tooze, S. A. The autophagosome: Origins unknown, biogenesis complex. *Nat. Rev. Mol. Cell Biol.* 14, 759–774 (2013).
  31. Schaaf, M. B. E., Keulers, T. G., Vooijs, M. A. & Rouschop, K. M. A. LC3/GABARAP family proteins: Autophagy-(un)related functions. *FASEB J.* 30, 3961–3978 (2016).
  32. Klionsky, D. J. *et al.* Guidelines for the use and interpretation of assays for monitoring autophagy (3rd edition). *Autophagy* 12, 1–222 (2016).
  33. Wild, P., McEwan, D. G. & Dikic, I. The LC3 interactome at a glance. *J. Cell Sci.* 127, 3–9 (2014).
  34. Yim, W. W. Y. & Mizushima, N. Lysosome biology in autophagy. *Cell Discov.* 6, (2020).
  35. Marques, A. R. A. & Saftig, P. Lysosomal storage disorders – challenges, concepts and avenues for therapy: Beyond rare diseases. *J. Cell Sci.* 132, (2019).
  36. F. M. Platt, A. d’Azzo, B. L. Davidson, E. F. Neufeld, C. J. T. Lysosomal storage diseases. *Metab. Dis. Found. Clin. Manag. Genet. Pathol.* 367–440 (2017) doi:10.3233/978-1-61499-718-4-367.
  37. Platt, F. M. Emptying the stores: Lysosomal diseases and therapeutic strategies. *Nat. Rev. Drug Discov.* 17, 133–150 (2018).
  38. Cárceles-Trullols, J., Kovács, A. D. & Pearce, D. A. Cell biology of the NCL proteins: What they do and don’t do. *Biochim. Biophys. Acta - Mol. Basis Dis.* 1852, 2242–2255 (2015).
  39. Mole, S. E. *et al.* Clinical challenges and future therapeutic approaches for neuronal ceroid lipofuscinosis. *Lancet Neurol.* 18, 107–116 (2019).
  40. Johnson, T. B. *et al.* Therapeutic landscape for Batten disease: current treatments and future prospects. *Nat. Rev. Neurol.* 15, 161–178 (2019).
  41. Seehafer, S. S. & Pearce, D. A. You say lipofuscin, we say ceroid: Defining autofluorescent storage material. *Neurobiol. Aging* 27, 576–588 (2006).
  42. Cotman, S. L. & Staropoli, J. F. The juvenile Batten disease protein, CLN3, and its role in regulating anterograde and retrograde post-Golgi trafficking. *Clin. Lipidol.* 7, 79–91 (2012).
  43. Mirza, M. *et al.* The CLN3 gene and protein: What we know. *Mol. Genet. Genomic Med.* 7, 1–41 (2019).
  44. Kyttälä, Aija; Ihrke, Gudrun; Vesa, Jouni; Schell, Michael J.; Luzio, J. P. Two Motifs Target Batten Disease Protein CLN3 to Lysosomes of Transfected Nonneuronal and Neuronal Cells. *Mol. Biol. Cell* 15, 1313–1323 (2004).

45. Nugent, T., Mole, S. E. & Jones, D. T. The transmembrane topology of Batten disease protein CLN3 determined by consensus computational prediction constrained by experimental data. *FEBS Lett.* 582, 1019–1024 (2008).
46. Ratajczak, E., Petcherski, A., Ramos-Moreno, J. & Ruonala, M. O. FRET-assisted determination of CLN3 membrane topology. *PLoS One* 9, 21–23 (2014).
47. Kmoch, S., Stránecký, V., Emes, R. D. & Mitchison, H. M. Bioinformatic perspectives in the neuronal ceroid lipofuscinoses. *Biochim. Biophys. Acta - Mol. Basis Dis.* 1832, 1831–1841 (2013).
48. Mitchison, H. M. *et al.* Targeted disruption of the Cln3 gene provides a mouse model for Batten disease. *Neurobiol. Dis.* 6, 321–334 (1999).
49. Katz, M. L. *et al.* A mouse gene knockout model for juvenile ceroid-lipofuscinosis (Batten disease). *J. Neurosci. Res.* 57, 551–556 (1999).
50. Cotman, S. L. Cln3 Deltaex7/8 knock-in mice with the common JNCL mutation exhibit progressive neurologic disease that begins before birth. *Hum. Mol. Genet.* 11, 2709–2721 (2002).
51. Fossale, E. *et al.* Membrane trafficking and mitochondrial abnormalities precede subunit c deposition in a cerebellar cell model of juvenile neuronal ceroid lipofuscinosis. *BMC Neurosci.* 5, 1–13 (2004).
52. Lojewski, X. *et al.* Human iPSC models of neuronal ceroid lipofuscinosis capture distinct effects of TPP1 and CLN3 mutations on the endocytic pathway. *Hum. Mol. Genet.* 23, 2005–2022 (2014).
53. Yasa, S. *et al.* CLN3 regulates endosomal function by modulating Rab7A-effector interactions. *J. Cell Sci.* 133, 1–14 (2020).
54. Getty, A. L., Benedict, J. W. & Pearce, D. A. A novel interaction of CLN3 with nonmuscle myosin-IIb and defects in cell motility of Cln3<sup>-/-</sup> cells. *Exp. Cell Res.* 317, 51–69 (2011).
55. Vidal-Donet, J. M., Cárcel-Trullols, J., Casanova, B., Aguado, C. & Knecht, E. Alterations in ROS Activity and Lysosomal pH Account for Distinct Patterns of Macroautophagy in LINCL and JNCL Fibroblasts. *PLoS One* 8, (2013).
56. Luiro, K., Yliannala, K., Ahtainen, L., Maunu, H. & Ja, I. Interconnections of CLN3, Hook1 and Rab proteins link Batten disease to defects in the endocytic pathway. *PLoS One* 13, 3017–3027 (2018).
57. Cao, Y. *et al.* Autophagy is disrupted in a knock-in mouse model of juvenile neuronal ceroid lipofuscinosis. *J. Biol. Chem.* 281, 20483–20493 (2006).
58. Uusi-Rauva, K. *et al.* Neuronal ceroid lipofuscinosis protein CLN3 interacts with motor proteins and modifies location of late endosomal compartments. *Cell. Mol. Life Sci.* 69, 2075–2089 (2012).
59. Soldati, C. *et al.* Repurposing of tamoxifen ameliorates CLN 3 and CLN 7 disease phenotype. *PLoS One* 16, 1–19 (2021).
60. Hobert, J. A. & Dawson, G. A novel role of the Batten disease gene CLN3: Association with BMP synthesis. *Biochem. Biophys. Res. Commun.* 358, 111–116 (2007).
61. Zhu, Y. *et al.* Three-Dimensional Neuroepithelial Culture from Human Embryonic Stem Cells and Its Use for Quantitative Conversion to Retinal Pigment Epithelium. *PLoS One* 8, (2013).
62. Livak, K. J. & Schmittgen, T. D. Analysis of relative gene expression data using real-time quantitative PCR and the 2- $\Delta\Delta$ CT method. *Methods* 25, 402–408 (2001).
63. Rahbari, R., Sheahan, T., Modes, V., Collier, P. & Macfarlane, C. A novel L1 retrotransposon marker for HeLa cell line identification. *Biotechniques* 46, 277–284 (2009).
64. Dunn, K. C., Aotaki-Keen, A. E., Putkey, F. R. & Hjelmeland, L. M. ARPE-19, a human retinal pigment epithelial cell line with differentiated properties. *Exp. Eye Res.* 62, 155–170 (1996).
65. Guo, X. L. & Chen, J. S. Research on induced pluripotent stem cells and the application in ocular tissues. *Int. J. Ophthalmol.* 8, 818–825 (2015).

66. den Dunnen, J. T. *et al.* HGVS Recommendations for the Description of Sequence Variants: 2016 Update. *Hum. Mutat.* 37, 564–569 (2016).
67. Brogna, S. & Wen, J. Nonsense-mediated mRNA decay (NMD) mechanisms. *Nat. Struct. Mol. Biol.* 16, 107–113 (2009).
68. Mauvezin, C. & Neufeld, T. P. Bafilomycin A1 disrupts autophagic flux by inhibiting both V-ATPase-dependent acidification and Ca-P60A/SERCA-dependent autophagosome-lysosome fusion. *Autophagy* 11, 1437–1438 (2015).
69. Tanida, I., Ueno, T. & Kominami, E. LC3 conjugation system in mammalian autophagy. *Int. J. Biochem. Cell Biol.* 36, 2503–2518 (2004).
70. Zhou, C. *et al.* Monitoring autophagic flux by an improved tandem fluorescent-tagged LC3 (mTagRFP-mWasabi-LC3) reveals that high-dose rapamycin impairs autophagic flux in cancer cells. *Autophagy* 8, 1215–1226 (2012).
71. Mauthe, M. *et al.* Chloroquine inhibits autophagic flux by decreasing autophagosome-lysosome fusion. *Autophagy* 14, 1435–1455 (2018).
72. Abraham, L. M., Selva, D., Casson, R. & Leibovitch, I. Mitomycin: Clinical applications in ophthalmic practice. *Drugs* 66, 321–340 (2006).
73. Nazaretyan, Samvel A.; Savic, Neda; Sade, Michael; Hackert, Brandy J.; Courcelle, Justin; Courcelle, C. T. Replication Rapidly Recovers and Continues in the Presence of Hydroxyurea in Escherichia coli. *J. Bacteriol.* 200, 1–16 (2018).
74. Hongo, K. *et al.* Massive accumulation of globotriaosylceramide in various tissues from a Fabry patient with a high antibody titer against alpha-galactosidase A after 6 years of enzyme replacement therapy. *Mol. Genet. Metab. Reports* 24, 100623 (2020).
75. Gallegos, K. M. *et al.* Shiga toxin binding to glycolipids and glycans. *PLoS One* 7, (2012).
76. Kobayashi, T. *et al.* A lipid associated with the antiphospholipid syndrome regulates endosome structure and function. *Nature* 392, 193–197 (1998).
77. Brotherus, J. & Renkonen, O. Subcellular distributions of lipids in cultured BHK cells: evidence for the enrichment of lysobisphosphatidic acid and neutral lipids in lysosomes. *J. Lipid Res.* 18, 191–202 (1977).
78. Gallala, H. D. & Sandhoff, K. Biological function of the cellular lipid BMP-BMP as a key activator for cholesterol sorting and membrane digestion. *Neurochem. Res.* 36, 1594–1600 (2011).
79. Gruenberg, J. Life in the lumen: The multivesicular endosome. *Traffic* 21, 76–93 (2020).
80. Ilnytska, O. *et al.* Enrichment of NPC1-deficient cells with the lipid LBPA stimulates autophagy, improves lysosomal function, and reduces cholesterol storage. *J. Biol. Chem.* 297, 100813 (2021).
81. Moreau, D. *et al.* Drug-induced increase in lysobisphosphatidic acid reduces the cholesterol overload in Niemann–Pick type C cells and mice. *EMBO Rep.* 20, 1–15 (2019).
82. Aman, Y. *et al.* Autophagy in healthy aging and disease. *Nat. Aging* 1, 634–650 (2021).
83. Medina, D. L. *et al.* Lysosomal calcium signalling regulates autophagy through calcineurin and TFEB. *Nat. Cell Biol.* 17, 288–299 (2015).
84. He, C. & Klionsky, D. J. Regulation mechanisms and signaling pathways of autophagy. *Annu. Rev. Genet.* 43, 67–93 (2009).
85. Alers, S., Löffler, A. S., Wesselborg, S. & Stork, B. Role of AMPK-mTOR-Ulk1/2 in the Regulation of Autophagy: Cross Talk, Shortcuts, and Feedbacks. *Mol. Cell. Biol.* 32, 2–11 (2012).
86. Ezaki, J., Takeda-Ezaki, M. & Kominami, E. Tripeptidyl peptidase I, the late infantile neuronal ceroid lipofuscinosis gene product, initiates the lysosomal degradation of subunit c of ATP synthase. *J. Biochem.* 128, 509–516 (2000).
87. Vella, F. Is There an Answer? What are the requirements for lysosomal degradation of subunit

- C mitochondrial ATPase? *IUBMB Life (International Union Biochem. Mol. Biol. Life)* 56, 281–283 (2004).
88. Cao, Q., Yang, Y., Zhong, X. Z. & Dong, X. P. The lysosomal Ca<sup>2+</sup> release channel TRPML1 regulates lysosome size by activating calmodulin. *J. Biol. Chem.* 292, 8424–8435 (2017).
  89. Shen, D. *et al.* Lipid storage disorders block lysosomal trafficking by inhibiting a TRP channel and lysosomal calcium release. *Nat. Commun.* 3, (2012).
  90. Wang, W. *et al.* Up-regulation of lysosomal TRPML1 channels is essential for lysosomal adaptation to nutrient starvation. *Proc. Natl. Acad. Sci. U. S. A.* 112, E1373–E1381 (2015).
  91. Samie, M. *et al.* A TRP Channel in the Lysosome Regulates Large Particle Phagocytosis via Focal Exocytosis. *NIH* 26, 511–524 (2014).
  92. Settembre, C. *et al.* TFEB Links Autophagy to Lysosomal Biogenesis. *Science (80- )*. 332, 1429–1433 (2011).
  93. Medina, D. L. *et al.* Transcriptional activation of lysosomal exocytosis promotes cellular clearance. *Dev. Cell* 21, 421–430 (2011).
  94. LaPlante, J. M. *et al.* Lysosomal exocytosis is impaired in mucopolipidosis type IV. *Mol. Genet. Metab.* 89, 339–348 (2006).
  95. Andrews, N. W. Detection of Lysosomal Exocytosis by Surface Exposure of Lamp1 luminal Epitopes. *Lysosomes Methods Protoc. Methods Mol. Biol.* 1594, 366–419 (2017).
  96. Chen, S., Einspanier, R. & Schoen, J. Transepithelial electrical resistance (TEER): a functional parameter to monitor the quality of oviduct epithelial cells cultured on filter supports. *Histochem. Cell Biol.* 144, 509–515 (2015).
  97. Tang, C. *et al.* A human model of Batten disease shows role of CLN3 in phagocytosis at the photoreceptor–RPE interface. *Commun. Biol.* 4, 1–18 (2021).
  98. Schmidtke, C. *et al.* Lysosomal proteome analysis reveals that CLN3-defective cells have multiple enzyme deficiencies associated with changes in intracellular trafficking. *J. Biol. Chem.* 294, 9592–9604 (2019).
  99. Wavre-Shapton, S. T. *et al.* Photoreceptor phagosome processing defects and disturbed autophagy in retinal pigment epithelium of Cln3 $\Delta$ ex1-6 mice modelling juvenile neuronal ceroid lipofuscinosis (Batten disease). *Hum. Mol. Genet.* 24, 7060–7074 (2015).
  100. Chandrachud, U. *et al.* Unbiased cell-based screening in a neuronal cell model of batten disease highlights an interaction between Ca<sup>2+</sup> homeostasis, autophagy, and CLN3 protein function. *J. Biol. Chem.* 290, 14361–14380 (2015).
  101. Mazzoni, F., Safa, H. & Finnemann, S. C. Understanding photoreceptor outer segment phagocytosis: Use and utility of RPE cells in culture. *Exp. Eye Res.* 126, 51–60 (2014).
  102. Armstrong, A. *et al.* Lysosomal network proteins as potential novel CSF biomarkers for Alzheimer's disease. *NeuroMolecular Med.* 16, 150–160 (2014).
  103. Karageorgos, L. E. *et al.* Lysosomal biogenesis in lysosomal storage disorders. *Exp. Cell Res.* 234, 85–97 (1997).
  104. Jensen, S. S., Aaberg-Jessen, C., Christensen, K. G. & Kristensen, B. Expression of the lysosomal-associated membrane protein-1 (LAMP-1) in astrocytomas. *Int. J. Clin. Exp. Pathol.* 6, 1294–1305 (2013).
  105. Wang, Q. *et al.* LAMP1 expression is associated with poor prognosis in breast cancer. *Oncol. Lett.* 14, 4729–4735 (2017).
  106. Cheng, X. T. *et al.* Characterization of LAMP1-labeled nondegradative lysosomal and endocytic compartments in neurons. *J. Cell Biol.* 217, 3127–3139 (2018).
  107. Iwan, K. *et al.* Urine proteomics analysis of patients with neuronal ceroid lipofuscinoses. *iScience* 24, 102020 (2021).
  108. Kuper, W. F. E. *et al.* Quantifying lymphocyte vacuolization serves as a measure of CLN3 disease severity. *JIMD Rep.* 54, 87–97 (2020).

109. Holopainen, J. M., Saarikoski, J., Kinnunen, P. K. J. & Järvelä, I. Elevated lysosomal pH in neuronal ceroid lipofuscinoses (NCLs). *Eur. J. Biochem.* 268, 5851–5856 (2001).
110. Gomez, N. M. *et al.* Robust lysosomal calcium signaling through channel TRPML1 is impaired by lysosomal lipid accumulation. *FASEB J.* 32, 782–794 (2018).
111. Santoni, G. *et al.* Pathophysiological Role of Transient Receptor Potential Mucolipin Channel 1 in Calcium-Mediated Stress-Induced Neurodegenerative Diseases. *Front. Physiol.* 11, 1–10 (2020).
112. Wróbel, Marta; Szymanska, Ewelina; Budick-Harmelin, Noga; Kolmus, Krzysztof; Goryca, Krzysztof; Dabrowska, Michalina; Paziewska, Agnieszka; Mikula, Michal; Cendrowski, Jaroslaw; Miaczynska, M. ESCRT-I controls lysosomal membrane protein homeostasis and restricts MCOLN1-dependent TFEB/TFE3 signaling. *bioRxiv* 753–754 (2021).
113. Trivedi, P. C., Bartlett, J. J. & Pulini, T. Lysosomal Biology and Function: Modern View of Cellular Debris Bin. *Cells* 9, 1–35 (2020).

## **8. Acknowledgements**

In the first place, I want to sincerely thank PD Dr. Guido Hermey for taking over the guidance of a project split up between different parties and not being fully under his supervision. Nevertheless, he was a dedicated advisor, supporting me always with his understanding and encouraging manner. I am grateful for all the scientific discussions we had and the experimental advices he gave. Also, many thanks to him for taking the time to proof read all the reports I wrote during this time.

I gratefully acknowledge the funding of this project by the NCL foundation Hamburg. Especially, I want to thank Dr. Frank Stehr for introducing me to the NCL research community and enabling me the participation in all associated conferences and meetings. I greatly appreciate the valuable discussions I had with PD Dr. Herman van der Putten. His broad expertise in the field of neurodegenerative diseases and particularly the NCL diseases helped me to develop scientifically and personally further. I am also very thankful for all the scientific relationships and cooperations he actively promoted.

Many thanks go to Dr. Rainer Kuhn and Dr. Doris Gruber-Schoffnegger for offering me the opportunity to conduct my studies at Evotec. In the various meetings we had they helped me to improve my presentation and discussion skills. My special thanks go to Dr. Doris Gruber-Schoffnegger and Dr. Sandra Markmann for taking over the role of directly supervising me. In the weekly appointments, they always had an open ear for my daily lab problems, came up with great suggestions and encouraged me to go on. I really appreciate the time they spend to support and push me forwards.

Further, a big thankyou goes to the best colleagues I can imagine. I would like to include everyone who accompanied me during this journey, but the list would get too long. So I will just name my current office members Kristin, Ela, Greta, Corinna, Remy, Rachel and Anja, who were always there for me. They went with me through my everyday ups and downs by simply listening, cheering me up with sweets, getting angry with me about failed experiments or rejoicing with my successes. Special thanks go to Stefan, for his constructive and supportive way of commenting and proof reading the whole thesis.

Finally, my heartfelt thank you goes to my friends and family. Thank you for always encouraging and motivating me! My warmest thanks go to my husband Julian Wünkhaus for always being by my side no matter if I was happy or sad, supporting me in all my decisions and encouraging me to follow my wishes.

## **9. Lebenslauf**

Entfällt aus datenschutzrechtlichen Gründen.

## 10. Eidesstattliche Versicherung

Ich versichere ausdrücklich, dass ich die Arbeit selbständig und ohne fremde Hilfe verfasst, andere als die von mir angegebenen Quellen und Hilfsmittel nicht benutzt und die aus den benutzten Werken wörtlich oder inhaltlich entnommenen Stellen einzeln nach Ausgabe (Auflage und Jahr des Erscheinens), Band und Seite des benutzten Werkes kenntlich gemacht habe.

Ferner versichere ich, dass ich die Dissertation bisher nicht einem Fachvertreter an einer anderen Hochschule zur Überprüfung vorgelegt oder mich anderweitig um Zulassung zur Promotion beworben habe.

Ich erkläre mich einverstanden, dass meine Dissertation vom Dekanat der Medizinischen Fakultät mit einer gängigen Software zur Erkennung von Plagiaten überprüft werden kann.

Unterschrift: .....